THE *IN VITRO* INVESTIGATION OF SARS-CoV-2 MAIN PROTEASE (M^{PRO}) EXPOSURE ON GLUCOSE HANDLING IN SKELETAL MUSCLE AND LIVER CELLS

A thesis submitted in fulfilment of the requirements for the degree of Master of Science (Pharmacy)

By

Praise Tatenda Nhau

January 2025

RHODES UNIVERSITY
Where leaders learn

Table of Contents

DEDICATION

I would like to dedicate this thesis to my late mother, Sandra Nhau. You were such an inspiration and you were my biggest supporter. If love could have saved you, you would have lived forever I hope you are smiling down from heaven.

I carry your legacy in everything I do and I will continue to strive to make you proud in every step of my journey. I love you endlessly and your memory will live on in my heart forever.

ACKNOWLEDGMENTS

Firstly, I would like to express my heartfelt gratitude to God for his unwavering guidance, strength and blessings in my life. Without His grace, none of this would have been possible.

I am deeply thankful to my supervisor Prof N Sibiya for his invaluable mentorship, encouragement and support throughout this journey. Your expertise and guidance have been instrumental in shaping my work. Your dedication pushed me to complete this degree in less than two years, a feat I would not have achieved without your guidance. I would also like thank my co-supervisor Dr N Gamede and Prof A Khathi for their guidance. I am truly grateful for your contributions throughout this process.

I would like to thank Rhodes University for the postgraduate scholarship, which has significantly contributed to the completion of my studies. This opportunity has been invaluable in my academic journey.

I would like to sincerely thank myself for the dedication, perseverance and hard work I put into this research. I am proud of this accomplishment.

To my family - especially my father Prosper Nhau, my sister Prudence Chinoingira, my brother Prosper Jr Nhau, my brother-in-law Tinashe Chinoingira, my aunt Brenda Bhunu and my nephew Ezra Chinoingira, thank you for your endless love, patience and belief in me. Your encouragement has been my anchor during the challenging moments.

To my friends, your companionship, humour and unwavering belief in me have been a constant source of strength. You made this journey not only bearable but enjoyable.

I also extend my appreciation to my colleagues especially Oyisa Katshaza and Charles Arineitwe, whose insights and camaraderie have enriched this experience.

I would also like to express my sincere thanks to my church, River of Life, for their prayers, support . Pastor and Mama Matepo, your spiritual guidance and church community has played an essential role in keeping me grounded throughout this journey.

To everyone who has played a role, no matter how small, in this journey—thank you.

LIST OF FIGURES

LIST OF TABLES

LIST OF ABBREVIATIONS

%	Percentage
3CLpro	3-Chymotrypsin-like Protease
ADA	Adenosine deaminase
ACE-2	Angiotensin-Converting Enzyme-2
ADP	Adenosine diphosphate
AKT	Protein kinase B
AMPK	AMP-Activated protein kinase
ATP	Adenosine triphosphate
C2C12	Myoblast cell line
cAMP	Cyclic adenosine monophosphate
ChREBP	Carbohydrate Response element binding protein
COVID-19	Coronavirus Disease 2019
CTLA4	Cytotoxic T-Lymphocyte Associated protein 4
CVB	Coxsackievirus B
DM	Diabetes mellitus
DENV	Dengue virus
DMEME	Dulbecco's Modified Eagle Medium
DPP4	Dipeptidyl peptidase-4
ECM	Extracellular matrix
ELISA	Enzyme-linked immunosorbent assay
EMEM	Eagle's minimum essential medium
GLP-1	Glucagon-like peptide-1
GLUT1	Glucose transporter 1
GLUT2	Glucose transporter 2

GLUT4	Glucose transporter 4
GSIS	Glucose-stimulated insulin secretion
GSVs	GLUT4 storage vesicles
HCMV	Human Cytomegalovirus
HepG2	Hepatic cell line
HFF	Human Foreskin Fibroblast
HIF-1alpha	Hypoxia-inducible factor 1-alpha
HLA	Human leukocyte antigen
IFN	Interferon
IL	Interleukin
IRF-1	Interferon regulatory factor-1
IL2Ra	Interleukin 2 receptor alpha
IR	Insulin Receptor
IRS	Insulin receptor substrate
IRS-1	Insulin receptor substrate -1
JAK-STAT	Janus kinase-signal transducer and activator of transcription
kDA	Kilodalton
MDA	Malonaldehyde
MERS-CoV	Middle East Respiratory Syndrome Coronavirus
Mm	Micromoles
M^{pro}	Main Protease
mTOR	Mammalian target of rapamycin
mRNA	Messenger Ribonucleic acid
Mu/ml	Milliunits per millilitre
NEMO	NF-KB Essential modulator
NF-KB	Nuclear factor Kappa-light-chain-enhancer of activated B

nmol/mL	Nanomole per millilitre
NSP	Non-Structural Proteins
ORF	Open reading frame
PBS	Phosphate-buffered saline
PDB	Protein Data Bank
PEPCK	Phosphoenolpyruvate Carboxykinase
PI3K	Phosphatidyl-Inositol-3-Kinase
PLpro	Papain-like protease
PPI	Protein-protein interaction
Pp1a/b	Polyprotein 1a/1b
RNA	Ribonucleic Acid
ROS	Reactive oxygen species
SDPP4	Soluble DPP4
SGLUT1	Sodium/Glucose Cotransporter 1
SARS-CoV-1	Severe Acute Respiratory Syndrome Corona Virus-1
SARS-CoV-2	Severe Acute Respiratory Syndrome Corona Virus-2
TBARS	Thiobarbituric acid reactive substances assay
TGF-β	Transforming Growth Factor Beta
TIMPS	Tissue Inhibitors of Metalloproteinases
TMPRSS2	Transmembrane Serine Protease 2
T1DM	Type 1 diabetes mellitus
T2DM	Type 2 diabetes mellitus
TMB	3, 3', 5, 5'- tetramethylbenzidine
TNF α	Tumour necrosis factor-α
WHO	World Health Organization

ABSTRACT

Despite evidence demonstrating risks of developing type 2 diabetes mellitus (T2DM) because of SARS-CoV-2, there is however insufficient scientific data available to elucidate the relationship between T2DM and COVID-19. The occurrence of multiple organ failure in COVID-19 patients highlights the importance of comprehending the cellular and molecular mechanisms of host cell factors exploited by SARS-CoV-2 to increase the risk of developing diabetes mellitus. Current literature associates obesity, inflammation and stress with insulin resistance, conditions that COVID-19 is known to induce suggesting a possible link to T2DM. Additionally, SARS-CoV-2 infection is associated with persistent organ damage due to systemic inflammation, which may contribute to long-term metabolic disruptions. Therefore, this *in vitro* study explored the perceived relationship between SARS-CoV-2 and diabetes mellitus by utilizing the SARS-CoV-2 Main protease (M^{pro}) to investigate its effects on key insulin-sensitive cells, C2C12(skeletal muscle) and HepG2(liver) cell lines. The aim was to uncover specific molecular mechanisms that may contribute to the development of the new-onset diabetes mellitus observed in patients post-COVID-19.

Methodology

This study was an *in vitro* laboratory-based experimental investigation that utilized C2C12 and HepG2 cell lines. This study was divided into seven distinct sections. The first part focused on examining how the viability of skeletal muscle and liver cell lines will be impacted by the exposure of SARS-CoV-2 M^{pro}. In the second section, the study investigated how M^{pro} affected the baseline glucose uptake and insulin-stimulated glucose uptake. The study further explored the expression and translocation of Glucose transporter type 4 (GLUT4) in the C2C12 cell line therefore assessing any potential insulin resistance. Next, the study focused on the expression of protein kinase B (AKT) in HepG2 and C2C12 cell lines. Thereafter, the study investigated the effect of M^{pro} on DPP4, MMP1 and IL-6 in C2C12 and HepG2 cells, including an assessment of the level of these proteins in cell culture medium. The sixth part of this study examined the reactive oxygen species (ROS) through the quantification of medium malonaldehyde (MDA) and an assessment of intracellular ROS . A solid-phase assay was conducted to assess any potential binding between

M^{pro} and insulin. Finally, in-silico studies were undertaken to assess the potential molecular binding between key proteins involved in the insulin signaling pathway.

Results

The baseline and insulin-stimulated glucose uptake was impaired in both HepG2 and C2C12 cell lines. M^{pro} also compromised GLUT4 translocation and expression in the C2C12 cell line. Insulin-stimulated AKT was also significantly reduced in the presence of M^{pro} for the HepG2 cell line. M^{pro} increased extracellular IL-6 levels and DPP4 shedding in the C2C12 cell line. An increase in ROS was observed in C2C12 cells, while MDA levels were elevated in both C2C12 and HepG2 cells, indicating increased oxidative stress. Lastly, our in-silico studies provided different models of the interaction between M^{pro} and various proteins involved in the insulin signaling pathway, with GLUT4 being the protein with the lowest binding energy.

Conclusion

These observations suggest that the SARS-CoV-2 M^{pro} may be inducing an insulin-resistant state, contributing to the dysregulation of glucose metabolism and therefore potentially being one of the contributors of new-onset diabetes mellitus seen in patients post-COVID-19. With the disturbances observed in glucose handling, GLUT4 translocation, and inflammatory markers, it is reasonable to propose that $M^{pro's}$ effect is predominantly indirect, likely disrupting intracellular signaling proteins and pathways critical for insulin signaling, rather than directly interacting with insulin itself. This hypothesis is supported by the minimal binding observed in the solid-phase analysis and the highest binding energy for molecular docking. Further studies are warranted to fully elucidate the mechanisms underlying the development of new-onset diabetes mellitus in patients with a history of COVID-19 since there is insufficient research to draw any definitive conclusions about whether M^{pro} is solely responsible.

ARRANGEMENT OF THESIS

Chapter 1: This chapter included the introduction, study rationale, aim and objectives of the research. Its purpose was to offer a brief overview of the research topic, provide a background on the problem being investigated and emphasize the significance of the study.

Chapter 2: This chapter presents the literature review, which aims to discuss the current information, situate the research study within the context of existing literature and provide a compelling rationale for the need for further research.

Chapter 3: This chapter outlines the study materials, equipment and methodology used to conduct the research. It provides a detailed explanation of how the study was designed, the tools and methods employed and the rationale behind the chosen approaches. The purpose of this chapter is to give the reader an understanding of how the research was carried out and to allow for replication of the study.

Chapter 4: This chapter presents the experimental results. This chapter aims to report the findings of the research study, highlighting the results using figures and tables. Additionally, it offers a clear interpretation of the findings, identifying trends and patterns that emerged during the experiments.

Chapter 5: This chapter consists of a discussion of the results. The purpose of this chapter is to interpret and elaborate on any new insights gained from the research and explore how the results contribute to the understanding of the topic. Additionally, this chapter examines any discrepancies between the findings and previous studies, providing possible explanations for these differences.

Chapter 6: This chapter includes the study conclusion, limitations and future recommendations. The purpose of this chapter is to summarize the conclusions drawn from the study's results, highlight potential limitations and offer recommendations for future research. It also suggests areas for further investigation to build upon the findings.

CHAPTER 1: INTRODUCTION

1.0 Background

The COVID-19 pandemic created a significant public health crisis, with long-term socioeconomic consequences including the exacerbated burden on public health systems due to increased incidences of other non-communicable diseases such as diabetes mellitus (DM) (1). With the prevalence of DM increasing worldwide, it is prudent to explore the pathophysiology involved in COVID-19-induced DM. Risk factors of DM such as sedentary lifestyles, high-fat diets, unbalanced diets and obesity contributing to insulin resistance and beta-cell failure have heightened during this COVID-19 era. However, the damage which the COVID-19 pandemic left on the metabolic systems and related diseases remain elusive.

Diabetes mellitus refers to a group of chronic endocrine metabolic disorders that are characterized by loss of glycaemic control, leading to elevated blood glucose concentration due to either insulin resistance or inadequate insulin production (2). The hallmark symptoms of DM include polydipsia, polyphagia, and polyuria (3). Studies indicate that DM is one of the primary causes of both morbidity and mortality in developing countries such as South Africa (4). Globally, it is projected that the prevalence of DM will increase from 415 million individuals in 2015 to 642 million individuals by the year 2040, indicating a significant rise in the burden of DM (5). DM is classified into different categories. The main two types are: Type 1 Diabetes Mellitus (T1DM) which is characterized by insulin dependence and Type 2 Diabetes Mellitus (T2DM) which is characterized by insulin resistance (6). According to the World Health Organisation (WHO), T2DM is projected to rank seventh among global causes of death by 2030 (7). This predicted rise is due to the increase in sedentary lifestyles and obesity (7). Globally T2DM accounts for the majority of cases, approximately 90-95% of cases (8). The other types of diabetes include Gestational diabetes, Maturity onset diabetes of the young, Neonatal diabetes and Latent Autoimmune diabetes in Adults (9).

However, a significant number of individuals may have undiagnosed prediabetes, a condition that is characterized by impaired fasting glucose and/or impaired glucose tolerance that is frequently

linked with low-level inflammation (10). Research conducted in the past thirty years has demonstrated that, in addition to pre-diabetes and DM, obesity can also contribute to low-grade inflammation, which increases the risk of systemic insulin resistance and the development of DM (2). Individuals with pre-diabetes and insulin resistance due to obesity can often maintain normal glucose tolerance for several years before transitioning abruptly to T2DM (11,12). Some researchers have suggested that viral infections may play a role in triggering this transition from pre-diabetes to T2DM (2,12).

Literature evidence has linked DM with susceptibility to SARS-CoV-2 and developing severe COVID-19 complications. On the other hand, COVID-19 has been associated with DM induction. In 2003, amidst the outbreak of SARS-CoV-1 which has been described by Pal and Banerjee et al. as "the cousin" of SARS-CoV-2, a study was conducted on 39 patients who had no previous history of DM (13,14). The results of this study showed that during their hospitalization, 20 of these patients developed DM. Despite glycaemic management during the three years of follow-up, 2 of those patients had persistent DM (13). Since this disruption in glycaemic management occurred due to the less virulent and less efficiently transmitted SARS-CoV-1, it is therefore not far-fetched to contend that the impact of SARS-CoV-2 will be far greater.

Indeed, COVID-19 has been associated with glycaemic aberrations, with reports of hospitalised patients demonstrating hyperglycaemia (15,16). Despite this knowledge, there is still a paucity of consensus on the mechanisms associated with SARS-CoV-2-induced glycaemic abnormalities. This *in vitro* study therefore aims to elucidate the mechanisms associated with SARS-CoV-2 in key insulin sensitive cell lines.

1.1 Research rationale

The relationship between DM and COVID-19 remains an ongoing area of research due to the limited amount of scientific data currently available. Although clinical evidence linking COVID-19 and DM is still emerging, current literature suggests that conditions such as obesity, chronic inflammation and metabolic stress are key contributors to insulin resistance, a precursor to T2DM. These conditions, which are exacerbated by COVID-19, could further heighten the risk of developing T2DM, particularly in individuals with underlying comorbidities. The SARS-CoV-2

virus triggers a systemic inflammatory response that may impair glucose metabolism, but the long-term effects of this inflammatory cascade on insulin sensitivity and glucose tolerance are not yet fully understood. Consequently, it is essential to consider these new factors when predicting the prevalence of DM in the future, especially since the incidence of DM was already on the rise before the pandemic. The envisaged impact of this research lies in its potential to uncover specific pathways through which SARS-CoV-2 induces insulin resistance or impairs glucose metabolism. If M^{pro} is found to be the culprit in this induction of new-onset DM, understanding the molecular mechanisms that this component of the virus utilizes could pave the way for developing targeted therapeutic strategies to prevent or mitigate DM in post-COVID-19 populations. Furthermore, these findings could provide a foundation for integrating COVID-19-related metabolic risks into broader public health strategies, addressing the rising incidence of DM with more informed, precise interventions.

1.2 Aim

The aim of this study was to investigate the impact of the SARS-CoV-2 protein, M^{pro} on glucose metabolism in C2C12 and HepG2 cell lines *in vitro*. This aim was achieved by the following objectives:

1.3 Objectives of the study

a. Perform *in vitro* cytotoxicity assay to evaluate the impact of M^{pro} on cell viability in:

- Skeletal muscle (C2C12) cell lines
- Hepatic (HepG2) cell lines

b. Investigate glucose utilization to assess how M^{pro} may influence glucose metabolism in:

- Skeletal muscle (C2C12) cell lines
- Hepatic (HepG2) cell lines

c. Investigate the effect of M^{pro} on insulin-stimulated glucose uptake in:

- Skeletal muscle(C2C12) cell lines
- Hepatic (HepG2) cell lines

d. Investigate the effect of M^{pro} on the expression of the key proteins, AKT and DPP4 that are involved in glucose metabolism and insulin signaling in:

- Skeletal muscle (C2C12) cell lines
- Hepatic (HepG2) cell lines

e. Investigate the effect of M^{pro} on the expression of MMP1 protein in:

- Skeletal muscle (C2C12) cell lines
- Hepatic (HepG2) cell lines

f. Investigate the effect of M^{pro} on the expression of the proinflammatory cytokine, interleukin-6 (IL-6) in:

- Skeletal muscle (C2C12) cell lines
- Hepatic (HepG2) cell lines

g. Investigate the effect of M^{pro} on GLUT4 expression and translocation in

- Skeletal muscle (C2C12) cell lines

h. Evaluate the effect of M^{pro} on oxidative stress status through a lipid peroxidation assay following exposure to M^{pro} in:

- Skeletal muscle (C2C12) cell lines
- Hepatic (HepG2) cell lines

i. Evaluate the effect of M^{pro} on reactive oxygen species levels in:

- Skeletal muscle (C2C12) cell lines

j. Perform in silico studies to assess for interactions of M^{pro} with human insulin, insulin receptor kinase domain, GLUT4 and PI3K using computational methodologies to assess any potential interactions.

CHAPTER 2: LITERATURE REVIEW

To ensure a comprehensive and well-structured review, a systematic literature search was conducted using databases and search engines such as PubMed, Scopus, Google scholar and Web of Science. The search focused on peer-reviewed articles published in English, covering the relationship between SARS-CoV-2 and diabetes mellitus, particularly its effects on insulin resistance and metabolic function. Keywords including "COVID-19," "SARS-CoV-2," "diabetes mellitus," "insulin resistance," "metabolic syndrome," and "inflammation" were used in various combinations with Boolean operators to refine results. Additional relevant studies were identified through reference mining of key articles.

2.0 SARS-CoV-2 infection

Since December 2019, millions of individuals worldwide have been impacted by the COVID-19 pandemic caused by SARS-CoV-2 (17). SARS-CoV-2 had such a profound global impact that millions of lives were lost. As of the 21st of June 2023, the World Health Organisation (WHO) reported 768,187,096 confirmed cases of COVID-19 globally and a staggering 6,945,714 deaths (18). Although these numbers are significantly high, they unfortunately do not account for unreported cases and deaths. The data available only inform us about recorded infections and deaths but provides no information on the long-term effects of COVID-19 such as “long COVID-19”. "Long COVID" refers to signs and symptoms that persist or develop after acute COVID-19 (19). Owing to this, we can safely say that the totality of the damage caused by the COVID-19 pandemic is still unknown. Coronaviruses have been responsible for three epidemics in the last 15 years. Approximately 26 countries were affected by the SARS-CoV-1 epidemic that occurred in 2003 in Guangdong, China (20). The largest outbreak is the most recent one which started in 2019.

SARS-CoV- 2 is a highly infectious novel coronavirus that emerged in 2019, causing a global pandemic of respiratory illness known as COVID-19 (17). Coronaviruses belong to a vast group of RNA viruses enclosed in a membrane envelope (20,21). This virus is also a single-stranded positive-sense RNA virus that infects both humans and animals such as bats (20,22). The transmission of this virus occurs when an infected person releases respiratory droplets that contain the virus and they enter the orifices such as the nose and mouth to ultimately reach the respiratory

tract. SARS-CoV-2 enters the host cell by binding to angiotensin-converting enzyme 2 (ACE-2) via the spike protein. ACE-2 is the functional receptor for Spike protein in SARS-CoV-2 that is found primarily in the upper respiratory tract, the heart, endothelial cells, pancreas, kidney tubular epithelium and enterocytes (22–24). This explains why the effects that SARS-CoV-2 has are widespread in the body. Research has shown that SARS-CoV-2 can infiltrate cells that possess ACE-2 receptors and it cannot enter cells that express different coronavirus receptors like aminopeptidase N and dipeptidyl peptidase 4 (DPP4) (25). Surface S (spike) proteins have a receptor-binding domain that initiates endocytosis of virions. Once the virus enters the host cell, it hijacks the host cell machinery to produce more virions. The translation of viral proteins and copying of the genome are both required to create new virions.

The genetic makeup of SARS-CoV-2 consists of a single-stranded RNA genome that spans a length of approximately 29.9 kilobases. The genetic assembly can be divided into two: structural proteins and non-structural proteins (NSP), with two-thirds of the genome encoding non-structural proteins (26). This genome is non-segmented and possesses 14 open reading frames (ORFs), that encode a total of 27 structural and 16 NSPs (27). In the host cell, structural proteins envelop the new viral genome and contribute to its morphology while NSPs constitute the genome replication complex and polymerase proteins that are involved in viral genome replication.

Within the first 20 kb of the genome's 5' end, there are two significant open reading frames (ORF1a and ORF1b) that give rise to two overlapping polyproteins known as polyprotein 1a and polyprotein 1b (pp1a and pp1b) (27–29). Proteases are then required to cleave the polyproteins into non-structural proteins. Within ORF1a, there are two viral cysteine proteases responsible for cleaving it at 14 specific sites, leading to the release of 16 NSPs. These are the papain-like protease (PLpro) and the 3C-like cysteine protease (3CLpro) (27,28,30). The generation of non-structural proteins occurs through the enzymatic action of these two. These NSP proteins are responsible for the formation of the viral replication complex, which is essential for viral genome replication and the production of new virus particles (31). Specific SARS-CoV-2 NSPs such as NSP12, the RNA-dependent RNA polymerase, NSP13 and helicase, combine to form an RNA replication complex (32).

Structurally, coronavirus is made up of four proteins, which are Spike (S), membrane (M), envelope (E) and nucleocapsid (N) that ensure the formation of mature virions (22,23). The Spike

protein, a transmembrane glycoprotein is responsible for host infection ability and recognition (26). The S protein, which is approximately 150 kDa in size exists as a monomer that can disintegrate to produce S1 and S2 subunits that have different functions (26,33). The S1 domain is responsible for binding the virus to ACE2 while the S2 domain allows the virus to fuse with the host cell receptor (26).

The M protein is a relatively small protein that is approximately 25-30 kDa. The M protein is composed of three transmembrane domains. It accounts for the highest proportion of protein in the virion and is believed to contribute to the virion's structural shape (33). Neuman et al reported that within the virion, the M protein can exist as a dimer as it has the ability to assume two distinct conformations. This property enables it to contribute to membrane curvature and also facilitates its binding to the nucleocapsid (34).

The E protein, which is relatively small in size (approximately 8-12 kDa), is present in limited quantities within the virion (33). The E protein ensures the progress of viral assembly and release of the virus. Within infected cells, E proteins are primarily found in the endoplasmic reticulum, Golgi apparatus and endoplasmic reticulum-Golgi intermediate compartments where several aspects of the viral life cycle take place (35). Lastly, the N protein is exclusively found in the nucleocapsid. This protein is divided into two distinct domains: the N-terminal domain and the C-terminal domain (33). The primary role of the N protein is to wrap the viral genomic RNA into helical structures within the cytoplasm. Additionally, it interacts with the M protein to guide the assembly and release of fully developed virions (33,35). Due to the devastating impact that COVID-19 has had, scientists have pursued various strategies with the aim of pinpointing medications that would provide optimum treatment. As of now, the treatments focus on three specific viral targets which are the spike glycoprotein, the RNA-dependent RNA polymerase and M^{pro} (36).

2.1 COVID-19 Main protease

A typical protease cleaves substrates based on various physical properties, with each protease requiring different substrate properties for cleavage to occur. The chymotrypsin-like cysteine protease of SARS-CoV-2 plays a vital role in allowing the virus to reproduce within host cells and

is therefore essential for the replication of the virus itself (21). The name "main protease" highlights its essential role in coronavirus gene expression and replicase processing (37). It is also referred to as "3C-like protease" due to its resemblance to 3C proteases found in picornaviruses, sharing similar substrate specificities and core structural features (37). Research has revealed that SARS-CoV-2 M^{pro}, is critical for the virus's replication process, making it an important target for drug development to treat SARS infections (38). M^{pro} is considered one of the most prominent drug target against the coronavirus that it is often referred to as the virus's "Achilles' Heel" (30).

Studies on SARS-CoV-1, the virus responsible for the 2003 SARS outbreak, have contributed significantly to our structural and enzymatic understanding of SARS-CoV-2 M^{pro} (39). Several researchers made a comparison between the sequences of SARS-CoV-1 and SARS-CoV-2 M^{pro} revealing only a difference of 12 amino acid residues (40–42). SARS-CoV-2 M^{pro}, however, exhibits greater structural flexibility and plasticity (40,42). According to literature, M^{pro} is approximately 34.21 kDa per monomer (43). The enzyme is a homodimer with three domains: domain I (residues 8-101), domain II (residues 102-184) and domain III (residues 201-306) in each monomer (44,45). The hydrolytic activity of $3CL^{pro}$ is dependent on the formation of 3CLpro dimers. A cleft exists between domain I and domain II where the active site can be found (27). A chymotrypsin-like fold resembling the picornavirus 3C proteinase is found at the active site of SARS-CoV-2 M^{pro}, which is composed of the catalytic dyad Cys145 and His41 as shown in Figure 2.1 (27,28,37). Accordingly, analysing the cellular factors that are used by the dimer should provide insight into the mechanism of action that might cause new-onset DM.

The COVID-19 $M^{pro's}$ main role is the cleavage of viral polyproteins required for viral replication. The enzyme identifies certain amino acid sequences (Leu, Phe, Met, Val)-Gln↓(Ser, Ala, Gly) (where the arrow is indicative of the cleavage site) inside viral polyproteins and cleaves them between the P1 and P1' locations, resulting in two smaller peptides (29,44). Researchers have noted that the expression of viral proteases can induce cellular toxicity in yeast and mammalian cells (36). Thus, it becomes prudent for us to assess whether M^{pro} is responsible for the alterations that are causing new-onset DM.

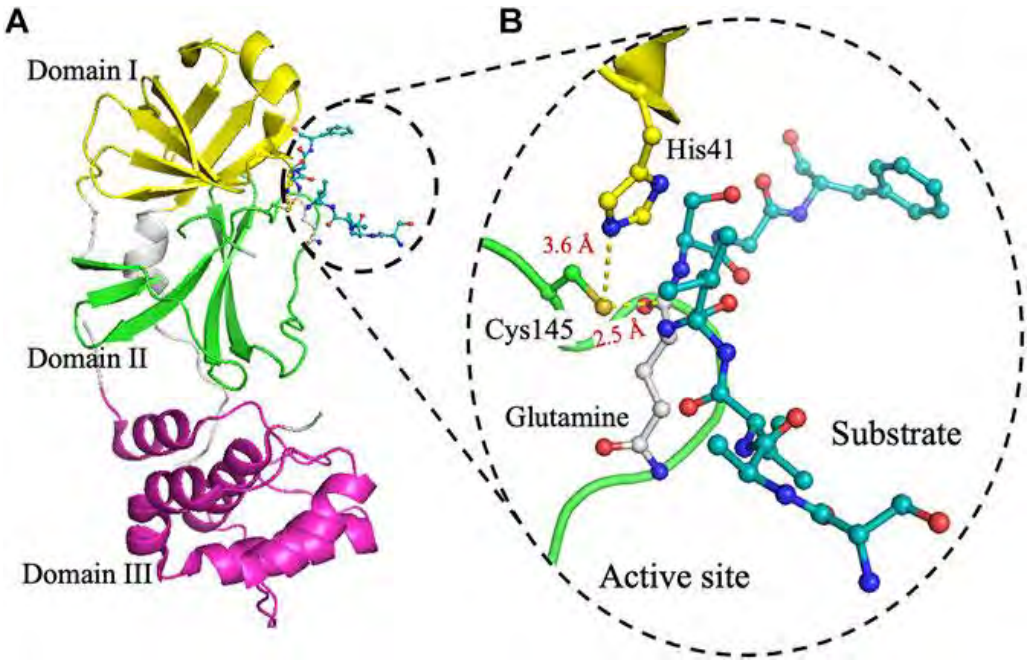

Figure 2.1: Structural representation of the COVID-19 main protease (M^{pro}), highlighting its active site, domains and key amino acid sequence The highlighted section represents the catalytic dyad and the amino-acid residues that form this dyad which are the cysteine residue (Cys145) and histidine residue (His41). Image adapted from Ferreira et al (27).

The M^{pro} of SARS-CoV-2 has been implicated in brain pathology. In a study conducted by Wenzel et al. the SARS-CoV-2 M^{pro} was stated to cause microvascular brain pathology. The SARS-CoV-2 M^{pro} does this by cleaving the nuclear factor (NF)-κB essential modulator (NEMO), the critical modulator of nuclear factor-B and by eliminating NEMO, M^{pro} causes the death of human brain endothelial cells (46). Several hypotheses have been suggested based on the available data, but the exact mechanisms underlying this phenomenon are still unclear. Wenzel et al also reported that M^{pro} induced apoptosis and oxidative stress in rat cortex neurons, resulting in neuronal damage (46). Observed neurological symptoms in COVID-19 patients may be caused by this neurotoxic effect. As of now, there are no studies that have reported on the potential hazards on M^{pro} of COVID-19 in DM predisposition. By this virtue, this is an area of research that is not fully understood and more research needs to be conducted so we can fully elucidate the effect that M^{pro} and other associated proteins on the possible development of poor glycaemic control. In this study, we intended to study the effect of M^{pro} on glucose metabolism and associated molecular pathways in insulin-responsive cell lines.

2.2 Diabetes mellitus and SARS-CoV-2 infection

Type 1 diabetes mellitus is a chronic autoimmune disorder that results in the destruction of pancreatic beta cells in the islets of Langerhans. This results in a deficiency of insulin production and subsequently, hyperglycaemia (2). The primary aetiology has been attributed to the infiltration of the pancreas by T-cells (47). An alternative model, however, states that beta cells may have a role in propagating the development of T1DM beyond merely being passive victims of an autoimmune attack (48). Children with T1DM are usually diagnosed when they are four or five years old or in their teens or early adulthood. Diagnosis of T1DM can be assessed by measuring the biomarkers of T1DM in the serum which are insulinoma-associated protein 2, zinc transporter 8 and 65 kDa glutamic acid decarboxylase (47). Environmental triggers may precipitate T1DM in genetically susceptible individuals and the currently implicated susceptible genes are HLA, insulin, CTLA4, PTPN22 and IL2Ra (47,49). Soon after the discovery of insulin in the early 1920s, it was viewed by patients and health workers as a potential cure for DM, despite being merely a replacement therapy with no curative effects on the chronic condition. Unfortunately, a perception that persists today is that insulin therapy is a temporary Band-Aid solution rather than a definitive treatment (50). The goal of treatment with insulin is to prevent complications by managing blood glucose levels through insulin administration, diet and lifestyle changes. For managing T1DM, insulin is the primary treatment option, while in T2DM, it becomes necessary when glycaemic control is not achieved through oral antidiabetic drugs (51). It is typically administered subcutaneously, with various types available for clinical use: short-acting insulin (regular), intermediate-acting insulin (isophane NPH), rapid-acting insulin analogues (aspart, lispro, glulisine), long-acting insulin analogues (glargine, detemir, degludec) for basal insulin replacement and premixed insulin, which combines basal and prandial components (52).The differences between the different types lie in their differences in pharmacokinetics, pharmacodynamics and clinical uses (53). The short, intermediate and rapid-acting insulins are categorized as bolus or prandial insulins, designed to manage post-meal glycaemic spikes. In contrast, long-acting insulin (basal insulin) helps maintain stable blood glucose levels during fasting by suppressing hepatic glucose production (53). The combination therapies aim to mimic

the body's natural insulin response more closely and provide more flexibility and control for individuals managing T1DM. However, a significant adverse effect of insulin therapy is hypoglycaemia and it remains the primary obstacle to achieving glycaemic targets in type 1 diabetes patients and patients on insulin for T2DM (53).

T2DM is a chronic metabolic disorder characterised by poor regulation of carbohydrate and lipid metabolism, beta cell dysfunction and insulin resistance leading to glucose intolerance (2). T2DM is generally prevalent in the older demographic although recently it has been reported to affect juveniles (6). It can be diagnosed by the elevated levels of glycosylated haemoglobin , fasting plasma glucose , or by measuring postprandial blood glucose level after 2 hours (3). T2DM is frequently related to obesity, inactivity and hereditary predisposition (2). Glycaemic control is initially maintained by compensatory hyperinsulinemia at the beginning of T2DM (54). Due to the desensitization of beta cells to insulin as the condition progresses, it unfortunately compromises glucose uptake in the target tissues such as adipose and skeletal muscle. Fazakerley et.al reported that these target tissues gradually become insensitive to insulin (55). The substantial increase in the incidence of T2DM can be attributed to the adoption of Westernized lifestyles that feature reduced physical activity due to sedentary habits and high-fat diets (11). These factors have been exacerbated by the emergence of SARS-CoV-2 (56). These changes in lifestyle result in an upsurge in insulin resistance, obesity, compensatory hyperinsulinemia and eventually beta-cell failure, all of which ultimately lead to the onset of T2DM (10).

T2DM poses significant risks to numerous individuals as it can affect the quality of life of an individual. Due to the potential consequences of this illness, such as the impact of medications on the quality of life referred to as glycaemic disutility, the prevention of T2DM becomes crucial (57). The management of T2DM is a bit more complex when compared to the management of T1DM. There are different classes of drugs therefore treatment agents should be selected to achieve glucose control, minimize treatment burden and reduce the risk of microvascular and macrovascular disease (58). Table 2.1 presents a summary of the different classes of drugs utilized for the management of T2DM.

Table 2.1: Antihyperglycaemic agents used clinically, with their mechanisms of action, examples and side effects (52,59–69).

Drug class	**Primary mechanism of action**	**Common side effects**
Biguanides (Metformin)	Decrease hepatic glucose production Increase glucose uptake in muscle	Weight loss
Sulphonylureas (Glimepiride)	Increase insulin secretion	Hypoglycaemia
Thiazolidinedione (Pioglitazone)	Increase glucose uptake in muscle and fat Decrease hepatic glucose production	Heart failure
Meglitinides (Nateglinide)	Promote pancreatic beta-cell insulin secretion	Hypoglycaemia
SGLT2 inhibitors (Dapagliflozin)	Increase urinary excretion of glucose	Urinary tract infection (UTI)
DPP4 inhibitors (Sitagliptin)	Increase glucose-dependent insulin secretion Decrease glucagon secretion	Headache
Alpha-glucosidase inhibitors (Acarbose)	Delay the absorption of glucose by delaying carbohydrate breakdown	Diarrhoea Flatulence

Insulin (glargine)	Promote glucose uptake	Hyperinsulinemia
GLP-1 receptor agonist (Liraglutide)	Increase glucose-dependent insulin secretion, slows gastric emptying	GIT disturbances

Various studies have reported enhanced fatality in diabetic subjects who have been infected with COVID-19 (17,70–72). Those with comorbidities such as DM have been demonstrated in studies to be more vulnerable to catastrophic COVID-19 results (17,71,72). Studies have also observed that elevated levels of glucose directly promote the replication of the SARS-CoV-2 virus in human monocytes (73). DM was linked to the first three deaths caused by COVID-19 in Hong Kong's initial wave (74). Wu et al. conducted a study on 52 individuals in intensive care and discovered that among the 32 individuals who did not survive, 22% had DM as a comorbidity (71). In a separate study conducted by Yang et al, the authors found that the incidence of DM among patients in intensive care was twice as high compared to both non-intensive care patients and those with COVID-19 (72). Similarly, in a study by Yang and colleagues (2020), 62% of ICU patients had DM, showing that diabetic patients predominate amongst ICU admissions (70). For heightened compression, in the next section, we are going to provide an overview of the key glucose-handling process, to contextualize SARS-CoV-2-induced hyperglycaemia or DM. Subsequently, we will explore cellular and molecular mechanisms linking SARS-CoV-2 infection with the risk of the development of DM.

Insulin was used to treat patients with T2DM during the COVID-19 era. Since then, there have been different retrospective studies conducted that have implicated insulin as the causative agent for the increase in mortality while others have disagreed. A retrospective study carried out by Yu et al presented findings that indicated a notable increase in mortality among individuals with both COVID-19 and T2DM who were undergoing insulin therapy. This association was observed regardless of the severity of the COVID-19 infection (75). Riahi et al also supported the aforementioned findings (76). The authors reported a significant association between inpatient mortality and peak insulin requirements. It was found that despite patients having comparable steroid doses and glycated haemoglobin levels, the hospitalized patients who died had used

significantly higher insulin doses (76). Furthermore, a meta-analysis of 6 studies conducted by Wang et al is supporting this hypothesis as the results unveiled a connection between insulin usage and higher mortality rates in individuals with both DM and COVID-19 (77). Yang et al also conducted a meta-analysis of eighteen articles and concluded three main things. Firstly, insulin treatment in COVID-19 patients resulted in a significantly higher mortality rate and COVID-19 complications. Furthermore, there was an observed trend that indicated an increased likelihood of hospital admission for patients with both COVID-19 and DM (78).

However, there has been resistance to this hypothesis as other authors have stated that confounding variables may be attributed to this noted trend. The findings by Sardu et al. contradict previous findings as the researchers reported that insulin infusions may improve patient outcomes and help them achieve their glycaemic targets (79). This comes after the patient group receiving insulin infusions experienced a significant reduction in plasma glucose after the treatment period compared to the patient group without the insulin infusion (79). By exploring the underlying mechanisms that insulin potentially uses to trigger mortality, the hypothesis can gain more credibility. This hypothesis also opens questions like : is new onset DM that post-COVID-19 patients are experiencing as a result of insulins deleterious effect on host cells? From our perspective, an increase in insulin in COVID-19 patients could allude to a state of insulin resistance, possibly instigated by the inflammatory state induced by SARS-CoV-2 infection. However, we also cannot rule out psychological stress which could also favour an insulin resistance state, therefore necessitating higher insulin dose requirements.

2.3 Virus-induced glucose homeostasis alteration

The primary energy source for most cells and the main substrate for many biochemical reactions is glucose. For glucose to be utilized by cells, it needs to cross the cell membrane and reach the cytoplasm (80). Glucose metabolism involves an intricate series of processes by which cells transform glucose into energy and various metabolic compounds. These processes include glycolysis, gluconeogenesis, glycogenolysis and glycogenesis (80). Glycolysis is the first step in this process that produces vital molecules that are required in cellular respiration. The molecules produced are either glycogen for storage or adenosine triphosphate (ATP), a source of cellular

energy and pyruvate (80,81). There are significant implications on health that come with disruptions to glucose metabolism.

Owing to its high molecular weight and polar nature, glucose cannot easily enter a cell through diffusion and thus relies on facilitated diffusion via glucose transporters (GLUTs) to facilitate cellular entry. GLUTs are categorized based on their affinity, structure and functions into different classes, resulting in the following: glucose transporters (GLUT1, GLUT2, GLUT3, GLUT4) and sodium/glucose cotransporter 1 (SGLUT1) (82). GLUT1 is found in all cells but is particularly abundant in endothelial cells that form protective barriers like the blood-brain barrier and human erythrocytes while GLUT4 is a glucose transporter that is stimulated by insulin and is present in the heart, skeletal muscle, adipose tissue and the brain. Insulin stimulation enhances the recycling of GLUT4 while slowing its endocytosis, leading to a net increase in GLUT4 accumulation at the plasma membrane (83).

Viruses activate host signaling pathways from the moment they attach to host cells. This marks the earliest interaction between the virus and the host (84). Viruses manipulate host metabolism by disrupting essential metabolic pathways and targeting key regulatory proteins. Metabolic signaling pathways serve as primary decision-making processes that coordinate cell signaling, gene transcription and precise modulation, all of which are crucial for organism survival. Viral adaptation has enabled viruses to target these pathways, modifying cellular metabolism to their advantage (81). To facilitate replication, the virus utilizes the host's metabolic activity, which explains why it induces a reprogramming of the cell's metabolism (85). Viruses have been shown to alter glucose metabolism in host cells through various mechanisms. Fontaine et al reported that a DENV infection in primary human foreskin fibroblast (HFF) cells results in an amplification of glycolysis and changes in the levels of glycolytic intermediates when compared to uninfected cells (86). Additionally, DENV infection causes an increase in GLUT1 protein levels and an elevation in both hexokinase 2 mRNA and protein levels (86). Cells infected with Human Cytomegalovirus (HCMV) have been reported to present a heightened reliance on glucose, leading to an upregulation of glycolysis and increased production of lactate (85). The infected cells also promote glycolysis by activating AMP-activated protein kinase. Additionally, it has also been observed that in HCMV-infected cells there is a substantial increase in the expression of carbohydrate response element binding protein (ChREBP), which results in the upregulation of GLUT4

expression (85). A substantial body of circumstantial evidence has implicated enteroviruses, specifically coxsackieviruses, as prime viral candidates responsible for precipitating T1DM (49). In 1967, an outbreak of the Coxsackie B4 virus hit a group of islands in the Bering Sea, thus providing an opportunity to assess whether contracting this virus might be linked to an increased likelihood of developing DM. Five years after the outbreak, the results revealed no signs of a higher prevalence of DM (87). Researchers, however, persisted in their exploration despite these results. Three years later, in 1978, it was shown by Yoon et al that certain inbred strains of mice can be infected by Coxsackie virus B4 and the virus can destroy the pancreatic beta cells thus precipitating hypoinsulinemia and subsequently lead to T1DM (88). In addition to coxsackievirus, rotavirus and cytomegalovirus have also been implicated in T1DM development (48,89,90). Dotta et al. provided compelling evidence that revealed the direct involvement of Coxsackie B4 enterovirus and pancreatic β cells of individuals with T1DM (90). This viral infection was shown to induce inflammation and functional impairment in type 1 diabetic patients. Support for the conclusions drawn in the previous study was reinforced by Honeyman et al. who reported that rotaviruses may exacerbate pancreatic islet autoimmunity and thus cause T1DM (89).

In pre-diabetic individuals, Sestan et al. highlighted a potential mechanism by which viral inflammation can lead to T2DM in a prediabetic mouse model (12). By exposing the pre-diabetic mice to different viral pathogens, the researchers reported that viral infections independently pose a risk for the onset of DM in pre-diabetic obese mice. Viral-induced Interferon-γ has been recognized as the culprit in the emergence of insulin resistance in skeletal muscle, especially in the context of obesity. Given the important role of skeletal muscles in maintaining normoglycemia and the widespread occurrence of insulin resistance in individuals with obesity, it becomes prudent to combat these effects in humans (12). Sestan et al. also reported that in humans, acute infections did not impact plasma glucose concentration but it only temporarily reduced systemic insulin sensitivity (12). Despite the virus-induced interferon- γ directly targeting skeletal muscles leading to the downregulation of the insulin receptor, glycaemic control was unaffected due to hyperinsulinemia. The same was also observed in the mice model that was not obese (12). With this background, we will now consider unpacking plausible mechanistic insights associated with SARS-CoV-2-induced glycaemic abnormalities.

2.4 Insulin secretion

Insulin is a peptide hormone that is secreted by the beta-cells in the Islets of Langerhans of the pancreas in response to an increase in post-prandial glucose levels in the blood. This process is referred to as glucose-stimulated insulin secretion (91,92). Insulin helps to regulate fasting glucose levels by blocking gluconeogenesis and glycogenolysis in the liver (93,94). This hormone also stimulates uptake of glucose by the adipose tissue, the liver and the skeletal muscles (92). Insulin further inhibits hepatic glucose production and release through promoting gluconeogenesis and glycogenolysis. Aside from glucose homeostasis, insulin promotes lipid metabolism, DNA synthesis, gene transcription, amino acid transport, protein synthesis and degradation (92). As a result, Duvnjak L et al. has described insulin as the most powerful anabolic hormone in our body since it plays a vital part in regulating glucose, protein and fat metabolism, endothelial function, differentiation and cellular growth (95).

In a healthy individual, a normal fasting serum insulin assay level should not exceed 25.0 mU/L, while maintaining a normal fasting euglycemic range of 3.60 to 5.99 mmol/L. Similarly plasma insulin levels should also remain below 25.0 mU/L within 3 hours after a meal and the normal 2-hour postprandial euglycemia should be below 7.8 mmol/L (96) . Normal serum insulin levels and plasma glucose levels must be observed in healthy individuals in both normal fasting and normal postprandial states (96). These values should fall within the standardised values as healthy individuals should have normal insulin sensitivity and fully functional beta cells.

Insulin biosynthesis and secretion is an intricate and multifactorial process that is triggered by an increase in plasma glucose concentration. Glucose is transported into beta cells facilitated by GLUT1 and GLUT2 transporters (97). Upon entry, glucose phosphorylation is then carried out by the glucokinase enzyme to produce glucose 6-phosphate and ultimately pyruvate, which is the end product of glycolysis (98). When extracellular glucose concentrations are low, the resting membrane potential of the beta cells is between −70 to −80 mV which is maintained by ATP-sensitive potassium (K_{ATP}) channels that are open (99). The oxidation of pyruvate in the mitochondria of the beta cells results in an increase in ATP which subsequently leads to the closure of these voltage-sensitive K_{ATP} channels. The closure of the voltage K_{ATP} channels triggers a gradual depolarization of the membrane potential. This comes about due to an accumulation of

potassium ions (K+) inside the cell, making the inside of the cell more positive than the outside. This difference leads to a depolarization of the plasma membrane due to the increase in the adenosine triphosphate/adenosine diphosphate (ATP/ADP) ratio in the mitochondria as shown in Figure 2.2 (97–99). When this depolarization reaches approximately −40 mV, it promotes the opening of voltage-dependent Na^+ and T-type Ca^{2+} channels. Subsequently, more Na^+ and Ca^{2+} enter the cells, leading to additional depolarization (97,98). The elevation of intracellular Ca^{2+} levels, coupled with the activation of protein motors and kinases, prompts the fusion of insulin vesicles with the plasma membrane. This fusion facilitates the exocytosis of the insulin-containing granules into the bloodstream (97).

Insulin secretion is also mediated by the two incretin hormones, glucagon-like peptide-1(GLP-1) and gastric inhibitory polypeptide (GIP) to give rise to GSIS via activation of cyclic adenosine monophosphate (cAMP) signaling in pancreatic beta cells (97). This phenomenon is estimated to be responsible for approximately 50 to 70% of the insulin response to glucose (100). GLP-1 and GIP are peptide hormones originating from the gut. They are secreted specifically from enteroendocrine L cells and K cells in the gastrointestinal tract, respectively (97,101). Interaction with their receptors on pancreatic beta cells leads to an increase in cAMP levels. This elevation causes an increase in the intracellular calcium concentration, ultimately potentiating the exocytosis of granules containing insulin (101). However, plasma levels of many gut hormones experience a rapid increase within minutes after nutrient intake, followed by a swift decline primarily attributed to renal clearance and enzymatic inactivation by DPP-4 therefore making incretin effects a secondary mechanism of insulin secretion. DPP4 is a serine protease that acts on various substrates throughout the body. It exists in two forms: a soluble form, found primarily in plasma and interstitial fluid and a membrane-bound form, present in vascular smooth muscle and endothelium, as well as in locations like the blood, kidneys and intestines (102–104). DPP4 inactivates different substrates, notably GLP-1 and GIP (105). Inhibiting DPP4 activity extends the half-life of GLP-1 and GIP, stimulating pancreatic insulin secretion, suppressing glucagon production and ultimately helps to improve glycaemic control (106). The main focus of the research on DPP4 has been in the context of T2DM treatment (105). However, there has been research that suggests that DPP4 is an adipokine (103,104,107). Alternatively, M^{pro} might also interfere with DPP4 glycosylation. The primary structure of DPP4 contains nine N-glycosylation sites and proper glycosylation is essential for its enzymatic activity, correct protein folding and accurate cellular trafficking (104). Research

has shown that the addition of a sugar molecule to murine DPP4 at the Thr330 position acts as a significant block to MERS-CoV infection, but without this sugar attachment, DPP4 can serve as a receptor, allowing the virus to enter the cell (108). A key question therefore arises whether hyperglycaemia and M^{pro} could affect the glycosylation of DPP4, potentially changing its activity. Research conducted by Sebastián-Martín et al on the role of DPP4 on COVID-19 pathophysiology showed that DPP4 interacts via protein-protein interactions with various partners such as fibronectin and collagen (104). It is therefore plausible to hypothesize that DPP4 might interact with M^{pro} potentially leading to functional interferences that influence disease progression. These hypotheses warrant more research to understand the exact mechanisms that M^{pro} potentially utilizes.

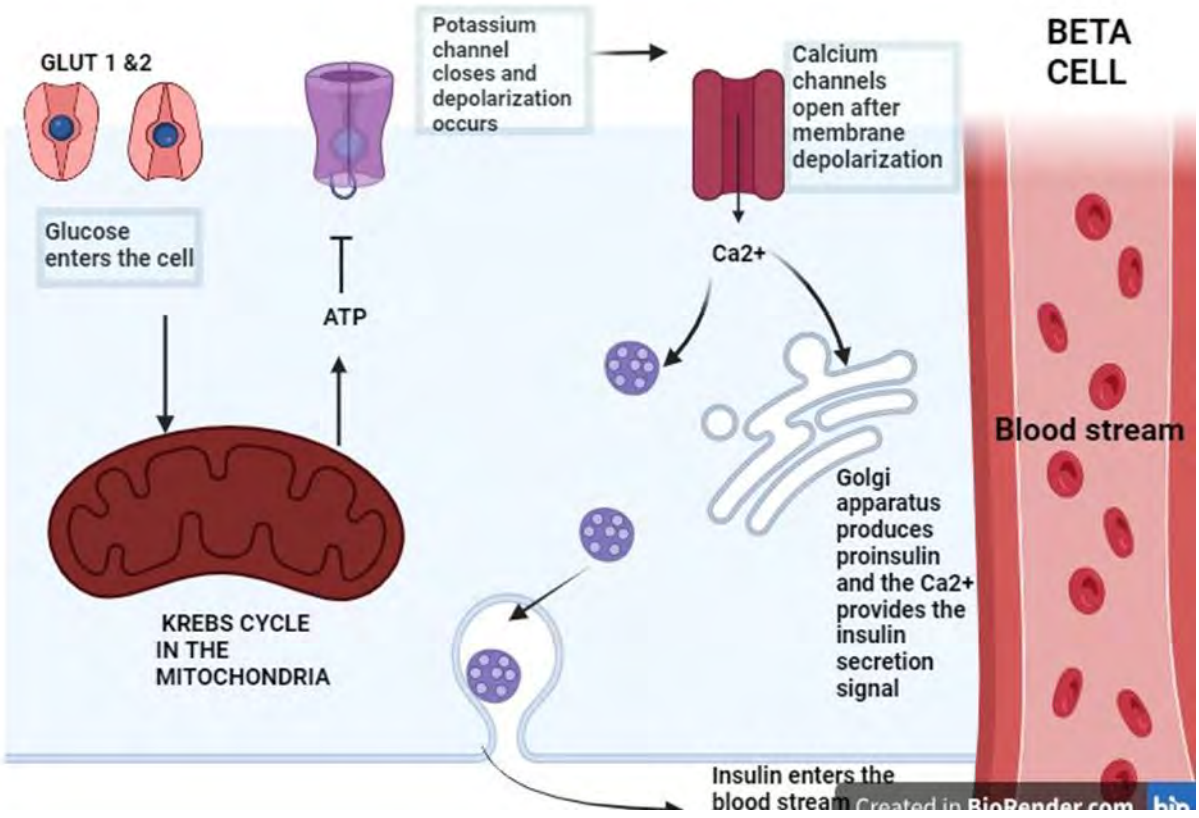

Figure 2.2: The beta cell takes in glucose through glucose transporters and the glucose undergoes metabolic processes in the Krebs cycle, resulting in elevated ATP levels (or a change in the ATP/ADP ratio). This increase leads to the closure of ATP-sensitive K+ channels which are open

to maintain a resting potential. This closure leads to membrane depolarization in the beta cell and the opening of voltage-dependent Ca^{2+} channels, enabling the entry of Ca^{2+}. Consequently, there is a surge in intracellular Ca^{2+} concentration which provides a signal to the Golgi apparatus and ultimately triggers the secretion of insulin into circulation (97–99).

EFFECT OF SARS-COV-2 ON INSULIN SECRETION

Although the respiratory system is the major target of SARS-CoV-2, there is accumulating evidence that the virus can also impact other organ systems, including the endocrine system (11). COVID-19 may directly or indirectly damage other systemic organs including the pancreas. This can be via direct invasion by SARS-CoV-2 via the ACE-2 receptor or indirect damage caused by the cytokine storm (109). Interestingly, clinical data established that normal individuals possess ACE2 in their pancreas, which was marginally higher compared to that in the lungs. Kelesidis et al. reported that SARS-CoV-2 can directly invade pancreatic endocrine cells and trigger indirect responses within the body such as autoimmune and inflammatory reactions which may contribute to additional harm to the endocrine cells (110). This was further supported by reports by Liu et al, where patients with severe COVID-19 presented with pancreatic injury (109,111). Valuable evidence suggests that SARS-CoV-2 infects and replicates in cells of the human endocrine and exocrine pancreas (112–114). A study conducted by Müller et al. revealed that SARS-CoV-2 induces changes in the morphology and function of human pancreatic cells such as the beta cells. This results in impaired glucose-stimulated insulin secretion and a reduction in the insulin-secretory granules (112). Similarly, Morris et al. also reported that SARS-CoV-2 replicates within the islets of Langerhans thus causing disruptions in insulin secretion (113). Qadir et al. provided additional evidence that potentially implicates SARS-CoV-2 infection and new-onset DM (114). The above literature evidence research suggest that SARS-CoV-2 may trigger both acute and chronic pancreatic dysfunction, directly through pancreatic invasion (114). Furthermore, emerging evidence associated COVID-19 with autoimmunity, as anti-pancreatic antibodies have been observed (109). The entirety of these findings suggests that SARS-CoV-2 can potentially contribute to the metabolic dysregulation observed in patients with COVID-19. The pancreatic damage particularly the beta cells is a plausible explanation linking COVID-19 with acute hyperglycaemia and DM.

T1DM has been studied in the past as far back as 1991 and indisputable evidence suggests viruses are etiologic agents. A study conducted by Wagenknecht et al. revealed that there was a statistically significant increase in the incidence of T1DM following an epidemic of Coxsackievirus B5 (115). The study explored several possible mechanisms through which T1DM could be precipitated by the presence of the virus and these were similar to what we are observing with COVID-19. The mechanisms observed all focused on the destruction of beta cells. The simplest of the three was via direct action on the cells, whereas the other two observed relied on either an immune recognition of altered beta cells or the virus acting as a trigger for genetically susceptible individuals (115). This study was conducted in Alabama and the researchers found that their results were consistent with findings from other regions such as the US Virgin Islands and Poland (115). A study more recently conducted in 2018, confirmed previous observations that enterovirus infections (including CVB) may increase diabetes type 1 islet autoimmunity (116). A significant proportion of type 1 diabetics had enterovirus in their pancreatic beta cells, suggesting a persistent viral infection in these individuals (116). This might be the case with COVID-19 and thus more research is warranted to elucidate the clinical significance of the involvement of the pancreas in COVID-19 patients.

2.5 Insulin signaling pathway

Insulin plays a pivotal role in promoting glucose uptake primarily by translocating GLUT4 from an intracellular storage reservoir to the cell's plasma membrane. Glucose uptake is stimulated by insulin in two ways: by promoting GLUT4 translocation to the plasma membrane and by altering glucose metabolism enzyme activities (117). GLUT4 translocation to the plasma membrane is mediated by insulin, increasing glucose uptake primarily in skeletal cells and adipocytes thus facilitating glucose uptake (117).

When insulin enters the bloodstream, insulin-receptor complexes are formed in a few target tissues such as adipose and skeletal muscle to elicit a biological response (118). When insulin binds to its tyrosine kinase receptor on the cell surface, it triggers a conformational change that results in autophosphorylation of the tyrosine residues in the intracellular domain of the receptor as summarised in Figure 2.4 below (94,119–121). Phosphorylated tyrosine residues on the receptor create a molecular interaction site for insulin receptor substrates (IRS) proteins. The IRS proteins

activate phosphatidylinositol-3-kinase (PI3K) (120). This enzymatic interaction stimulates the production of phosphatidylinositol (3,4,5)-trisphosphate (PIP3). The PIP3 subsequently activates AKT. When AKT is activated it promotes the translocation of GLUT4 to the plasma membrane which in turn facilitates insulin-driven glucose uptake and glycogen synthesis in the skeletal muscle and liver (121). Hepatic insulin signaling is primarily responsible for reducing gluconeogenesis, which occurs through AKT-induced phosphorylation of forkhead box O1 (FOXO1). This phosphorylation excludes FOXO1 from the nucleus, preventing the transcriptional activation of gluconeogenic genes like glucose-6-phosphatase and PEPCK enzyme (92,94). Insulin also enhances hepatic glycogen synthesis through its actions on the glycogen synthase enzyme (GYS2) and glycogen phosphorylase through GSK3 and PP1, similar to its effects on skeletal muscle (94).

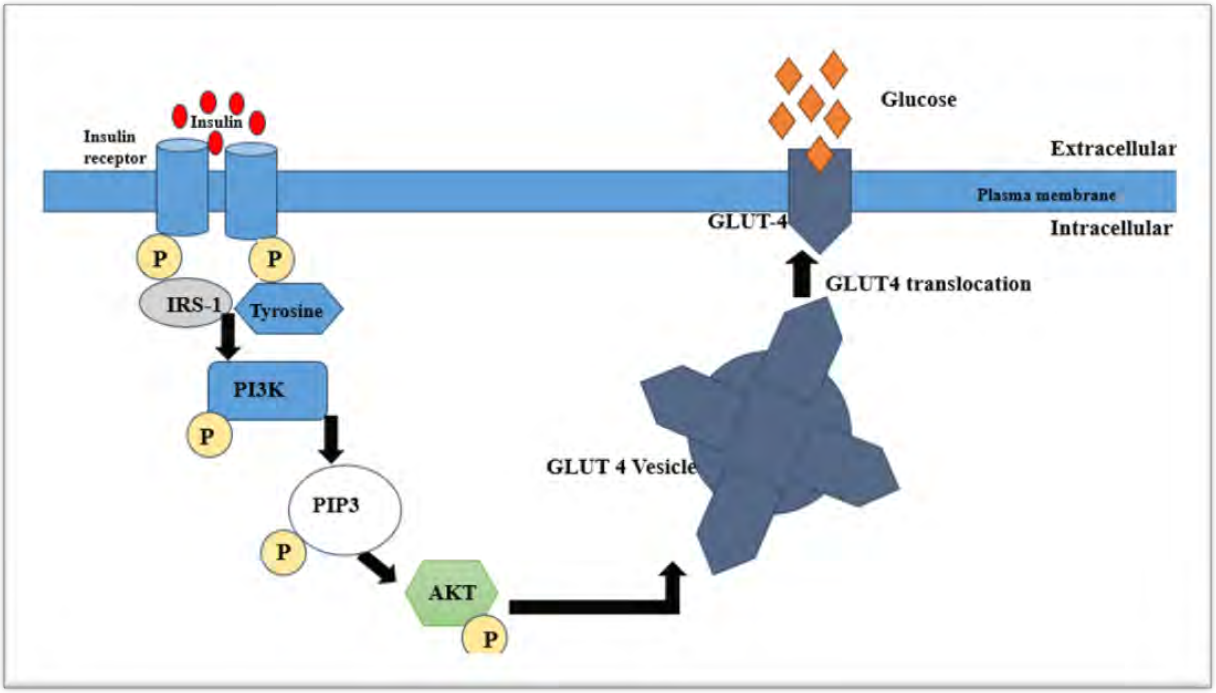

Figure 2.3: Upon insulin binding to the insulin receptor (IR), the receptor undergoes autophosphorylation at tyrosine residues, leading to the activation of insulin receptor substrate-1 (IRS-1). IRS-1 is then phosphorylated, which activates phosphoinositide 3-kinase (PI3K). PI3K catalyzes the conversion of phosphatidylinositol 4,5-bisphosphate (PIP2) into phosphatidylinositol 3,4,5-trisphosphate (PIP3), triggering the activation of protein kinase B (AKT). Phosphorylated

AKT promotes the translocation of glucose transporter type 4 (GLUT4) vesicles to the plasma membrane, enabling glucose uptake into the cell (119–121).

Insulin is also a potent activator of the PI3K/AKT signaling pathway in skeletal muscles and adipose tissue (122,123). Phospho-inositol kinase, AKT and GLUT4 proteins play essential roles in controlling glucose metabolism and insulin signaling pathways. Luo et al further identified that the deletion of Pik3r1 and Pik3r2, which encode isoforms of the PI3K subunit in the skeletal muscle of mice, inhibits insulin-stimulated glucose transport (124). Insulin signaling enhances glycogen synthase activity by prompting AKT to phosphorylate glycogen synthase kinase 3 (GSK3) (94). In cases such as obesity or insulinoma, there is a downregulation of insulin receptors, resulting in insulin resistance and, ultimately T2DM (125). Therefore, AKT expression was analyzed in this study using an enzyme-linked immunosorbent assay (ELISA) to identify potential disruptions in the insulin signaling pathway.

Studies have shown that SARS-CoV-2 proteins manipulate host signaling pathways, creating an environment favourable for viral replication (32). Approximately 100 human kinases involved in cellular physiology, metabolism and immune responses can be upregulated or downregulated by SARS-CoV-2 proteins (32). Shin et al. played a pivotal role in presenting one of the initial scientific findings that demonstrate how SARS-CoV-2 disrupts the insulin/insulin-like growth factor (IGF) signaling pathway in the respiratory tract as well as in metabolic and endocrine tissues such as the liver, adipose tissue and pancreas (126). As previously mentioned, the insulin signaling pathway is critical for glucose homeostasis. The authors reported that SARS-CoV-2 infection resulted in the downregulation of genes significantly associated with insulin signaling, mammalian target of rapamycin (mTOR) signaling and mitogen-activated protein kinase (MAPK) signaling (126). The authors also revealed that there was a diverse array of deficiencies in insulin/IGF signaling components, encompassing disruptions in IRS, PI3K, AKT and mTOR molecules. As also described in the insulin signaling pathway, these proteins are essential for the maintenance of cellular homeostasis.

2.6 Insulin resistance pathophysiology

Many studies have revealed that problems within the insulin signaling pathway at different stages result in reduced glucose uptake leading to insulin resistance (127–129). The exact mechanisms behind the development of insulin resistance remain unclear and may occur at different stages of insulin signaling. Teff et al. suggested that the main issue seems to be a significantly reduced capacity to phosphorylate the post-receptor insulin receptor substrate (130).

Studies have demonstrated that insulin resistance partially disrupts muscle glucose uptake by impairing the translocation of GLUT4 to the cell surface (94). Han and Bonen et al. reported that s changes in glucose transport have been directly linked to two main things; cell surface expression of GLUT4 and alterations in the accessibility of glucose to the GLUT4 transporter on the cell surface (131).When the insulin signaling pathway is disrupted, GLUT4 primarily stays in intracellular compartments known as GLUT4 storage vesicles (GSVs) (132). This impairment is particularly concerning because literature states that insulin resistance is associated with impaired insulin-stimulated GLUT4 translocation in key insulin-sensitive tissues like muscles, which is a major risk factor for metabolic diseases and T2DM (122). Given this critical role of GLUT4 in maintaining glucose homeostasis, we assessed GLUT4 expression and translocation using the ELISA assay in the C2C12 cell line.

DM and insulin resistance are associated with elevated glucose levels in the systemic circulation, which promote the formation of free radicals/ROS (reactive oxygen species). Free radicals and oxidative stress damage lipids, proteins and DNA in the body (133). Oxidative stress, which occurs when there is an imbalance between oxidant production and antioxidant defences within cells and the bloodstream, can play a role in the induction of insulin resistance in the body (134–136). Various studies have shown that oxidative stress inhibits insulin action on glucose transport (137,138). Research conducted by Ding et al. concluded that insulin-stimulated glucose uptake was inhibited by chronic oxygen stress resulting in ROS-induced insulin resistance in C2C12 myotubes (137). The same effect was observed in cultured rat L6 muscle cells that had undergone oxidative stress (138). Thus, we assessed the generation of intracellular ROS in C2C12 cells.

Research also indicates that disruptions in lipid metabolism lead to the buildup of lipotoxic compounds, which trigger oxidative stress in both skeletal muscle and the liver (139). Over time, it has become clear that increased levels of free fatty acids adversely impact insulin sensitivity and ultimately leads to T2DM (140). Research has shown that toxic intracellular fatty acid metabolites

such as ceramides and diacylglycerols are linked to the activation of TNF-α and several stress-related kinases, including NF-kB, c-Jun N-terminal kinases and atypical isoforms of protein kinase C in skeletal muscle. These enzymes disrupt the insulin signaling pathway by promoting serine/threonine phosphorylation of IRS1 (141–145). Ultimately, the generation of ROS disrupts the activation of the insulin signaling cascade.

Lipid peroxidation, which is the reaction between oxygen and unsaturated lipids, generates a diverse range of oxidation products (146). This process plays a critical role in cellular damage and contributes significantly to oxidative stress in biological systems. The primary products of lipid peroxidation are lipid hydroperoxides. Among the various aldehydes produced as secondary products, malondialdehyde (MDA) is one of the most notable (147). Lipid peroxidation assays are often used to assess oxidative status *in vitro* since lipids and lipoproteins are the primary targets of peroxidation in biological membranes. MDA, a key product of lipid oxidation, serves as an important and widely used biomarker for lipid peroxidation (136).

Hyperglycaemia is associated with massive production of ROS which exacerbates oxidative stress and promotes lipid peroxidation (148). Scientific evidence shows that SARS-CoV-2 infection causes ROS overproduction, oxidative stress and hyperinflammation, leading to endothelial layer damage and dysfunction. These effects can, in turn, impair insulin signaling and disrupt glucose metabolism (149). Endothelial dysfunction contributes to reduced glucose uptake by tissues, increased insulin resistance and chronic inflammation which are key factors in the development of T2DM. SARS-CoV-2 infection, by amplifying ROS production and endothelial dysfunction, emerges as a significant contributor to this cascade. The link between oxidative stress and SARS-CoV-2 infection establishes a critical connection in understanding metabolic dysregulation. Thus, there is a clear cause-and-effect relationship between the development of DM and oxidative stress. Individuals with a history of SARS-CoV-2 infection may face an increased risk of developing DM due to these interconnected metabolic disruptions. We therefore examined the production of MDA in response to SARS-CoV-2 M^{pro} in C2C12 and HepG2 cells.

EFFECT OF SARS-COV-2 ON THE INSULIN SIGNALLING PATHWAY

The mechanism of the impairment of the insulin/IGF signaling pathway was seen to be facilitated by heightened interferon responses, especially the upregulation of interferon regulatory factor-1 (IRF-1) (110,126). This was also an observation that Sestan et al. shared in their proposed model

of how viruses potentially trigger new-onset DM (12). IRF-1 can both activate and repress gene transcription to finely tune the immune response, ensuring an appropriate and controlled reaction to various stimuli. A SARS-CoV-2 infection was reported to cause an increase in the gene expression of IRF-1 and this mediated impairments in the insulin/IGF signaling pathway (126). The insulin/IGF signaling pathway is important in various biological processes, including energy metabolism and the preservation of cell viability. This dysfunction of the insulin/IGF signaling pathway in metabolic organs and tissues can lead to insulin resistance, cellular death and metabolic abnormalities. This, in turn, contributes to the development of various metabolic disorders, including hyperglycaemia, DM, hyperlipidaemia and obesity (126). Additional clinical research is imperative to address these aspects to prevent new-onset DM and other complications that may arise from future coronaviruses.

Yang et al. conducted a study comparing SARS patients without a history of T2DM. In their investigation over a 3-year follow-up, more than 50% of the patients' developed DM while in hospital for SARS-CoV-1 infection. However, after three years of recovery from the viral infection, only 5% of patients remained diabetic (72). Considering, the similarities between SARS-CoV-1 and SARS-CoV-2, it is highly likely that new-onset DM will also be a manifestation of long COVID-19.

2.7 SARS-CoV-2-induced glycolytic and hepatic gluconeogenic pathway

The liver is essential for metabolic balance, detoxification and immune function, but these roles make it susceptible to various stressors that can lead to cell damage and impaired function (150). Liver injury and regeneration are closely tied to intricate extracellular matrix (ECM) pathways (151). Post-mortem studies in patients infected by SARS-CoV-2 have revealed clues indicating traces of viral proteins, which could be indicative that SARS-CoV-2 can be classified as a hepatotropic virus (152). Indeed, *in vitro* studies have demonstrated hepatocytes express ACE-2 receptors and transmembrane serine protease which are crucial for viral entry. Interestingly, the entry and replication of SARS-CoV-2 is without cytopathic changes. In the hepatocytes, studies indicate the virus promotes hepatic-glucose production through the gluconeogenic pathway (153). This, therefore, can in part explain hyperglycaemia observed in COVID-19. Mechanistically,

molecular analysis suggests the virus promotes the activity of key gluconeogenic enzyme, phosphoenolpyruvate kinase (PEPCK) (154). PEPCK is a rate-limiting enzyme that is inhibited by insulin whilst stimulated by glucagon and other hormones including glucocorticoids and catecholamines. Studies report the activity of PEPCK was not associated with genetic transcription (153). This therefore suggests that SARS-CoV-2 may modulate this enzyme through acetylation, thus promoting its activity. In a COVID-19 context, the virus aims to promote its propagation and host weakness by ensuring glucose availability in infected immune cells (155,156). To efficiently utilize glucose to its benefit, SARS-CoV-2 has been reported to reprogram glucose metabolism, favouring the glycolytic pathway over oxidative phosphorylation (157). The reprogramming involves forcing the infected cells, particularly monocytes to oxidise glucose through glycolysis for immediate ATP generation to support cell proliferation and synthesis of molecules of pro-inflammatory cytokines (158). To ensure glycolytic oxidation dominates over the oxidative phosphorylation, the virus has been reported to induce mitochondrial oxidative damage. Furthermore, studies have reported increases in lactate dehydrogenase over pyruvate dehydrogenase, further supporting the metabolic shift toward hyper glycolysis (159). From a biochemical perspective, favouring hyper glycolytic pathways could ensure sustainable production of lactate (154). Lactate amongst other metabolic substrates including alanine and glutamate are the main precursors for glucose in gluconeogenesis. Hyper glycolysis could therefore afford the availability of substrates required for the hepatic gluconeogenic pathways, which is a major source of glucose. In a COVID-19 setting, the glycolytic pathway may also be induced by hypoxic conditions either due to limited ventilation or septic shock due to cytokine storm. The increases in gluconeogenesis could therefore be part of the mechanisms associated with SARS-CoV-2-induced hyperglycaemia. Furthermore, the overproduction of lactate could also be associated with the induction of an insulin resistance state. Studies have reported that direct exposure to lactate to insulin-sensitive cells induces insulin resistance (160). On the contrary to our argument, clinical studies analysing acid-base balance in COVID-19 reported a lack of plasma lactate accumulation (161). The possible explanation behind this observation was ascribed to the utilisation of lactate in the gluconeogenic pathway (158).

2.8 SARS-CoV-2 and inflammation

The SARS-CoV-2 infection elicits an immune response due to the damage in the respiratory system. This response calls upon specialized immune cells like macrophages and monocytes to combat the infection. These cells not only combat the virus but also release signaling molecules called cytokines, which in turn, prepare the body's immune system by activating T and B cells for a more tailored defence. During infection, the virus also triggers the activation of specific host Toll-like receptors, leading to the release of a wide range of proinflammatory cytokines. These include interleukin IL-7, IL-2, IL-6, interferon-gamma (IFN-γ) and TNF-α (32). However, this response can become dysregulated and will result in a phenomenon known as the cytokine storm that results in extensive inflammation in the lungs (162). The cytokine storm caused by COVID-19 is not only localized to the lungs but it causes widespread systemic inflammation which damages different organs including the insulin-producing organ, the pancreas (163).

A cytokine storm is an exaggerated and uncontrolled immune response that results in a large number of cytokines such as IL-6, IL-4 and TNF-α being released in a short period, resulting in widespread inflammation and tissue damage (164,165). According to Chen et al., COVID-19 patients who died had higher levels of IL-2 receptors, IL-10, TNF-α, IL-6 and IL-8, when compared to those who recovered (166). In a study conducted by Queiroz M et al, the findings indicated that a long COVID-19 cytokine profile appears to be characterized by high levels of IL-17 and IL-2, low levels of IL-4 and IL-10 (167). The take-home message is that elevated cytokine levels lead to multiple organ systems failure as endothelial dysfunction, metabolic dysregulation and vascular damage occur (164,165). Studies conducted both *in vitro* and *in vivo* have demonstrated that increased expression of TNF-α is linked to a reduction in insulin sensitivity in both skeletal muscle and adipose tissue (168–170). IL-6 enhances insulin-stimulated glucose disposal in humans and promotes glucose uptake and fatty acid oxidation in rat myotubes *in vitro* (165). This can be postulated to be a propagating agent in the development of new-onset DM.

Several authors have reported on the connection between insulin resistance and inflammation (171–173). Furthermore, increased levels of TNF-α have also been shown to cause conditions like septic shock and the failure of multiple organs (162). Steinberg et al. also reported that elevated TNF-α would cause insulin resistance via a decrease in insulin sensitivity in the skeletal muscles

and adipose tissue (169). Another study conducted on healthy human subjects by Ploomgaard et al. also confirmed that TNF-α induced skeletal muscle resistance (170). The clinical significance of this study's data was that even a small increase in TNF-α concentration can negatively affect peripheral insulin action and also affect the ability of skeletal muscle cells to store glucose in response to insulin (170). This phenomenon was observed because TNF-α decreases GLUT4 expression, which is essential for glucose transport in insulin-sensitive tissues (91). Since 1997, it has been hypothesized that chronic low-grade inflammation is closely linked to the aetiology of DM (163). Since that time over a dozen studies have revealed that pro-inflammatory cytokines are responsible for the body's acute-phase response and that IL-6, TNF-α and interferons present in the bloodstream can serve as reliable indicators for predicting the onset of T2DM (111,163,174). Another key cytokine that has also been implicated in long COVID-19 is IL-6. Several factors trigger the production of IL-6 including TNF-α, IL-1, bacterial products (LPS) and viral infections (175). IL-6 binds to either the membrane-bound IL-6 receptor or the soluble IL-6 receptor, forming a complex that acts on glycoprotein130. This complex regulates IL-6 levels through the Janus kinase-signal transducer and activator of transcription (JAK-STAT) pathway, thereby sustaining inflammatory processes (164,175). In insulin-resistant conditions like obesity and T2DM, circulating IL-6 levels are notably elevated (165).

T2DM is linked to chronic low-level inflammation and COVID-19 triggers an excessive inflammatory response, the interaction between these inflammatory conditions may amplify the harm caused by inflammatory agents (176). As the immune response plays a substantial role in the evolution of COVID-19, assessing the inflammatory mediators at a cellular level may provide better insight into how the host's response may be attributed to new-onset DM. Research has shown that inflammation in adipose tissue, especially within visceral fat depots, plays a significant role in the development of systemic insulin resistance, impaired glucose tolerance and T2DM (177). This additive effect would therefore increase the propensity of new-onset DM.

Chronic low-grade inflammation is thought to play a key role in DM aetiology (163). In various cell types, high glucose levels activate signaling pathways that disrupt the balance between the synthesis and breakdown of ECM (178). MMPs and their specific inhibitors, called tissue inhibitors of metalloproteinases (TIMPs), play a crucial role in maintaining ECM homeostasis in healthy livers (179). Normal ECM degradation plays a key role in tissue repair and remodelling,

but abnormal ECM turnover is associated with various liver diseases (180). A study conducted by Duarte et al revealed that MMP-1, MMP-2, MMP-3, MMP-11and MMP-13 are constitutively expressed in healthy livers, whereas other MMPs are typically associated with pathological conditions, including acute or chronic liver injury (180). Given the importance of MMP regulation in liver function, we aim to investigate whether the SARS-CoV-2 M^{pro} affects MMP production, potentially contributing to ECM imbalances in liver injury and disease. Besides their well-known functions in ECM protein degradation, MMPs also target non-ECM substrates, including cytokines and chemokines, playing key roles in regulating inflammation and immune responses (181). Many cell types do not exhibit continuous expression of MMPs; rather, they are stimulated by growth factors cytokines such as TNF-α (182). Research has shown that MMP expression and activity can be influenced by glucose levels in certain cell types, highlighting the potential role of glucose in regulating MMP-related processes within these cells (183,184). In 2003, Death and colleagues utilized hyperglycaemic culture for macrophages and endothelial cells and found that MMP1, MMP2 and MMP9 expression and activity were increased while MMP3 activity decreased (178). Additionally, various studies have reported that MMP1, MMP2, MMP9 and MMP14 are involved in shedding a wide range of substrates, highlighting that a single MMP can act on multiple substrates (106,185). Given the role of MMPs in both inflammation and ECM remodelling, we hypothesize that SARS-CoV-2 M^{pro} could influence MMP expression and activity, further modulating the inflammatory environment and potentially exacerbating the risk of new-onset DM. Figure 2.4 summarizes the potential mechanisms through which SARS-CoV-2 infection may induce metabolic disturbances and new-onset DM.

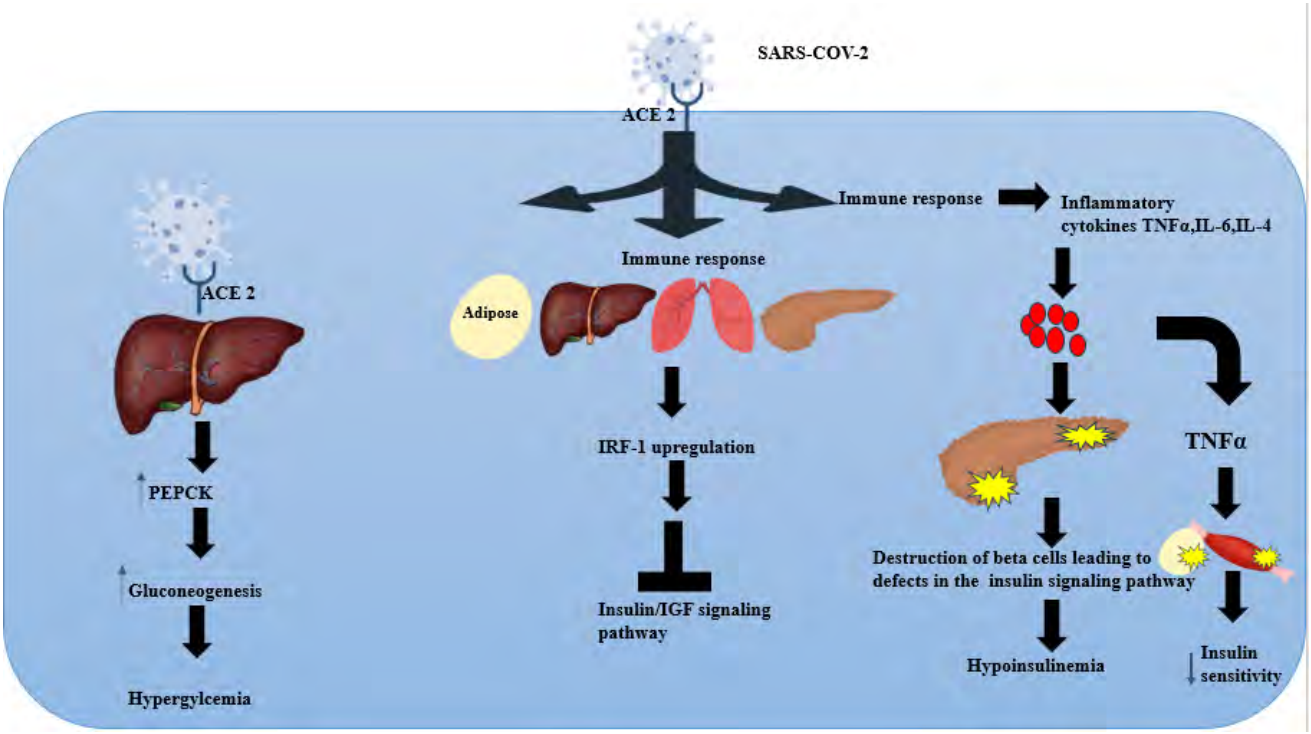

Figure 2.4: A depiction of the possible mechanisms of how viruses potentially result in new-onset DM. The possible mechanisms are pancreatic beta cell destruction, TNF-induced insulin resistance in the skeletal muscle and adipose tissue as well as sustained hyperglycaemia due to hepatic gluconeogenesis.SARS-CoV-2 binds to angiotensin-converting enzyme 2 (ACE2), triggering an immune response that upregulates interferon regulatory factor 1 (IRF-1) and inflammatory cytokines (TNF-α, IL-6, IL-4). This leads to beta-cell destruction, reduced insulin production (hypoinsulinemia), and decreased insulin sensitivity. In the liver, ACE2 interaction increases phosphoenolpyruvate carboxykinase (PEPCK) activity, promoting gluconeogenesis and hyperglycemia. (126,154,157,168,170).

2.9 COVID-19 and New-onset diabetes mellitus: Outcomes with new-onset hyperglycaemia with or without diabetes mellitus in people who have suffered from COVID-19

While the long-term effects of SARS-CoV-2 virus are still being studied, there is growing evidence suggesting a bidirectional relationship between COVID-19 and DM (13,14,112,186,187). Several

studies have reported a potential link between SARS-CoV-2 infection and disturbances in glucose metabolism. However, not all research supports this relationship and some have failed to demonstrate a clear link between COVID-19 infection and new-onset DM (188,190,191). Despite these discrepancies, understanding this potential connection is critical, particularly given the rising prevalence of DM worldwide. Table 2.1 below summarises key findings form studies exploring this relationship, highlighting the effects of COVID-19 on DM incidence and progression.

Table 2.2: A summary of the key findings on the relationship between COVID-19 and new-onset diabetes mellitus

Study Reference	**Study Design and Data**	**Key Findings**	**Associated Effect and Remarks**
Unsworth et al. 2020 (186)	Multi-centre regional study: data on new-onset T1DM for 30 children aged 23 months to 16.8 years that developed new-onset T1DM.	The first report to outline a noticeable rise in the occurrence of new-onset T1DM among children during the COVID-19 pandemic, with indications of SARS-CoV-2 infection or exposure identified in a portion of the individuals tested.	The study supports the bidirectional relationship between COVID-19 and new-onset DM.
Müller et al. 2021 (112)	ACE2 pancreatic islet cells	SARS CoV-2 infects and replicates in cultured human islets	Supports the bidirectional relationship between COVID-19 and new-onset DM

Coppelli et al. (15)	Cohort study of 271 hospitalized COVID-19 patients with DM and no DM.	COVID-19 patients who developed hyperglycaemia without having preexisting DM had a higher mortality rate when compared to those with normoglycemia.	Hyperglycaemia- indicative of a link between COVID-19 and DM.
Iacobellis et al. (16)	85 COVID-19 patients (27 of the sample population had DM).	Hyperglycaemia on admission serves as the most reliable indicator for detecting radiographic signs of SARS-CoV-2 infection, irrespective of an individual's prior history of DM.	Hyperglycaemia- indicative of a link between COVID-19 and DM.
Fadini et al. (187)	Retrospective study:21 COVID-19 patients with new-onset DM.	A higher rate of ICU admission and mortality among COVID-19 patients with new-onset DM than among those with preexisting DM and normoglycemia. New-onset DM had the worst prognosis out of the three.	New onset DM- Supports the bidirectional relationship between COVID-19 and new-onset DM.
Singh and Khunti et al. (188)	Literature review	New-onset hyperglycaemia and new-onset DM have been increasingly recognized in the context of COVID-19.	There is no conclusive evidence of SARS-CoV-2 directly infecting pancreatic islets

Bode et al. (189)	Retrospective observational study	Individuals with new-onset hyperglycaemia have poorer outcomes than those with pre-existing DM.	New-onset hyperglycaemia without DM had poorer outcomes than pre-existing DM.
Drucker et al.(190)	Mass literature review	No significant increase in T1DM incidence rates between 2020 and before COVID-19.	There was no evidence to support the association between increased T1DM cases during the COVID-19 pandemic.
Ibrahim et al. 2021 (191)	Mass literature review	There is no direct link between COVID-19 beta cell injury being the direct cause of new-onset DM.	Long-term follow-up research is needed, since damage to the beta cells may prolong DM or autoimmunity over time.

In the following sections, we will focus on the use of cell lines as experimental models, such as C2C12 and HepG2, which are pivotal in studying insulin sensitivity and glucose uptake under controlled conditions. Additionally, we will discuss the role of protein-protein interactions, particularly in disrupting cellular processes that regulate glucose metabolism. By examining these aspects, we can gain valuable insights into the molecular mechanisms by which SARS-CoV-2 may contribute to insulin resistance and the development of DM.

2.10 Skeletal muscle cell line

The skeletal muscle system makes up about 40% of the body weight of a young man, which makes it the largest organ system in the body (192). Skeletal muscle cells play an important role in maintaining glucose homeostasis, storage of essential molecules, such as amino acids, glycogen and generation of heat to help regulate body temperature (193). Additionally, myokines are released by the skeletal muscle, making it an active endocrine organ (107). Approximately 80% of postprandial glucose utilization from the circulation is attributed to skeletal muscle (192,194). Consequently, insulin resistance can be brought on by skeletal muscle cell defects. However, in the case where insulin resistance has been brought on primarily by skeletal muscles, whole-body insulin resistance can be reversed by reversing skeletal muscle insulin resistance (192). Skeletal muscles are also susceptible to immune cell invasion in both human and murine models. These immune cells such as T cells and macrophages exert a pro-inflammatory effect in T2DM and obesity (192). Considerable attention has been devoted to understanding the impact of COVID-19 on the respiratory system which has left a knowledge gap on how COVID-19 affects other body systems such as the skeletal system. For studying metabolic diseases, the C2C12 cell line has been extensively used as an *in vitro* model (133). This cell line is derived from mice and is regarded as a valuable model for studying metabolic conditions such as DM, obesity, growth disorders and hyperlipidaemia (133,192). C2C12 cells start as mononucleated, spindle-shaped myoblasts. As they grow, these cells fuse together to form multinucleated structures and then rapidly differentiate into long, fibre-like myotubes within 3–5 days, once the culture reaches confluence and is supplied with a differentiation medium (133). In a review article by Wong et al., the authors reported that there is well-documented evidence that using the C2C12 cell line model one can effectively explore various factors such as glucose metabolism, insulin signaling pathways, insulin resistance, oxidative stress, reactive oxygen species and glucose transporters both at a cellular and molecular level (133). This cell line also expresses GLUT4 transporter proteins, similar to human skeletal muscles which are essential in insulin-stimulated glucose uptake. As a result, our study utilized this cell line to assess any possible up or down-regulation of these transporter proteins. This therefore rationalized the choice of this cell line model in exploring the mechanistic insights that M^{pro} may be utilising in causing new-onset diabetes mellitus.

2.11 Hepatic (HepG2) cell line

The liver has a regenerative ability and carries out a wide range of complex functions such as replenishing and storing easily accessible energy in the form of glycogen, regulating carbohydrate metabolism and detoxifying and eliminating metabolic byproducts from the body (195). Additionally, the liver regulates blood glucose concentration in humans by controlling glycogen breakdown (glycogenolysis) and de novo glucose production (gluconeogenesis) (196). This organ plays a key role in storing energy as glycogen and triglycerides, while also exporting glucose when energy levels are depleted. In 1975, HepG2 cells were the first to exhibit the characteristics of hepatocytes and were described as hepatocellular carcinomas (195). The HepG2 cell line was derived from human hepatoma, specifically from the liver tissue of a 15-year-old Caucasian male with well-differentiated hepatocellular carcinoma (195). Despite their cancerous origin, HepG2 cells retain several key characteristics of differentiated hepatocytes, including albumin secretion, insulin-stimulated glycogen synthesis and glutathione-based detoxification (197,198). Additionally, they have a stable phenotype, normal liver cell genetic characteristics, high glucose consumption and active energy metabolism (199). These features make them a widely used model for studying liver functions. However, it is important to note that HepG2 cell lines have an extremely low expression of the relevant human CYP450 enzymes involved in phase 1 and 2 metabolism such as CYP3A4, CYP2A6 and CYP2C9 (197,198). Research showed that by culturing HepG2 cell lines in EMEM compared to DMEM, there was upregulation of the expression of CYP1A and CYP2B therefore EMEM was the medium of choice (200).

Due to its broad applications in scientific research such as in pharmacological and toxicological studies, the HepG2 cell line is highly popular (198). HepG2 cell lines are widely utilized not only in cancer research but also in the study of hepatitis B, drug-induced liver injury, hepatitis D viral infections (195,197). Pancreatic beta cells release insulin after a meal in response to an increase in blood glucose levels. Insulin then acts directly and indirectly on the liver (196). A disruption in hepatic glucose production has been shown to exacerbate T2DM hyperglycaemia (196). Therefore, using this cell line will be crucial in the assessment of the impact of M^{pro} on insulin resistance and glucose metabolism.

2.12 Protein-protein interaction

Proteins are essential in cellular functions, encompassing metabolism, information processing, decision-making, transport and structural organization (201). They interact with other proteins and a range of molecules, including nucleic acids, lipids and metabolites. When performing their functions *in vivo*, most proteins rarely act as isolated species. This is based on research conducted in the past that has shown that more than 80% of proteins don't function independently; instead, they often form protein complexes (202). The environment in which proteins are found typically has an abundance of potential binding partners, each possessing different potential binding sites and surface properties (203).

Protein folding, protein assembly and subsequently the protein-protein interactions (PPI) are all dependent on the non-covalent connections formed between the side chains residues (202). While physical protein interactions were recognized early on, going as far back as 1838, as well as antibodies and antigens interactions, the early 1900s saw relatively little exploration of them (204). As increasing numbers of protein interactions became apparent in the 1940s, there was a gradual recognition of the importance of PPIs as well as an improved understanding of their significance (201). Because protein interactions are so crucial, it is essential to assess the interactions if any, that M^{pro} has with other proteins in the host cell. A variety of biological functions are made possible by PPIs. These include facilitating communication between cells and regulation of metabolic and developmental processes (202).

PPIs play different roles in biology depending on various factors such as permanent or transient connections, affinity and their composition (203). There are various ways that PPIs can be classified owing to their contrasting structural and functional characteristics. The stability that the PPIs possess can categorize them as either obligate or non-obligate, while their duration of the complex labels them as transient or permanent (202,203). They can also be further classified based on the surfaces involved during the interactions since PPIs can occur on both identical and non-identical chains which result in homo-oligomeric or heterooligomeric interactions (202,203). Nevertheless, numerous protein-protein interactions do not neatly fit into distinct categories. Often, a single PPI may exhibit a combination of these characteristics, with stability being dependent on the prevailing physiological conditions and environmental factors (202,203).

Therefore, analysis at a molecular level becomes prudent to enable a deeper understanding of how the M^{pro} might interact with other proteins pertinent to glucose homeostasis.

The only computational approach that models physical interactions between proteins directly is protein-protein docking. A signaling pathway's interactions, for example, the insulin signaling pathway, are expected to be transient since their functionality is not permanent. Insulin binds to the extracellular domain of insulin receptor tyrosine kinase (IRTK), triggering a conformational change that results in the autophosphorylation of IRTK tyrosine residues and activation of phosphotyrosine-binding proteins such as IRS (94). IRTK-induced phosphorylation of IRS is primarily responsible for insulin's effects on glucose and lipid metabolism. As such it becomes prudent to assess whether M^{pro} binds to both insulin and the insulin receptor substrate.

Kinetic experiments undertaken by Northrup et al. gave evidence that when proteins collide, they don't disperse immediately but rather loosely adhere to one another, rolling on each other's surfaces (205). This enables the two proteins to cover a significantly larger surface area than they would through a single elastic collision. This extended interaction time allows for reorientation and reshaping on the surface, facilitating a tighter fit between the proteins as shown by Figure 2.5 below.

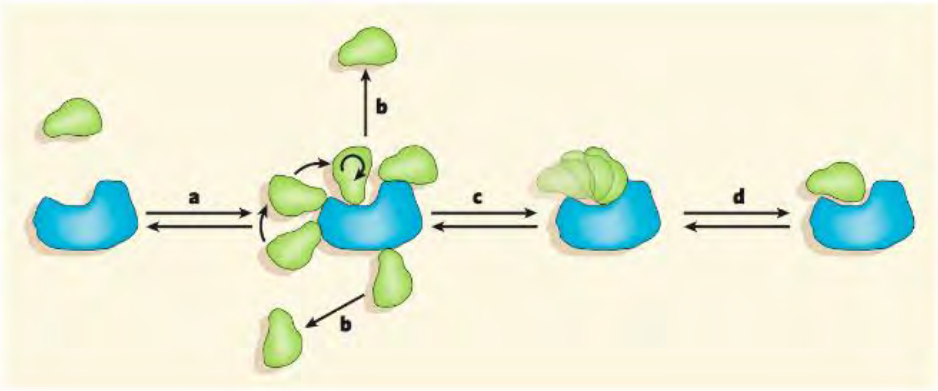

Figure 2.5: This figure illustrates the stages of interaction between two proteins (blue and green). (a) The initial encounter complex forms as the two proteins approach each other. (b) Multiple reversible associations occur facilitating complex stabilization. (c) The proteins bind to each other with the most stable conformation (d) A stable protein-protein complex is formed, completing the interaction process. The arrows indicate the reversibility of certain interaction steps, reflecting the dynamic nature of protein-protein binding. Adapted from Northrup et al. (205).

Protein-protein docking has emerged as a crucial computational approach to predict and analyze molecular interactions, providing insights into complex biological processes such as signal transduction. Protein-protein docking can be accomplished using the ClusPro server which requires just two PDB files in the Protein Data Bank (PDB) format (206). The ClusPro docking server has been reported to be a consistently top-performing server in the Critical Assessment of Predicted Interactions, a double-blinded protein-protein docking experiment (207,208). The server operates through three main computational steps which are rigid body docking, clustering and refinement. Rigid-body docking involves the sampling of billions of conformations to explore the possible protein-protein interactions. Clustering involves using root-mean-square deviation to group the 1000 lowest-energy structures into clusters, with the largest clusters representing the most likely models of the complex. Lastly, energy minimization is used to refine the selected structures (207). ClusPro utilizes fast Fourier transforms, which allow for the rapid calculation of energy functions. This therefore enables an efficient and exhaustive sampling of billions of conformations by evaluating interaction energies at each grid point, facilitating protein docking without requiring prior structural information about the complex (207). This is possible as a negative binding energy means there is a spontaneous reaction and high affinity between the two proteins for binding. In contrast, a positive binging energy means there is a lower probability of bond formation. With and without experimental data, Jones et al. demonstrated that ClusPro can predict high-accurate protein complex structures (207). Protein-protein docking using ClusPro was performed to investigate potential interactions between M^{pro} and key proteins involved in insulin signaling and glucose metabolism. This computational approach helps identify high-affinity binding partners and predicts mechanistic insights into how M^{pro} might disrupt these pathways that may potentially contribute to new-onset DM observed in post-COVID-19 cases. By modelling these interactions, molecular docking complements experimental findings and provides a framework for understanding the molecular basis of metabolic dysfunction induced by M^{pro}. However, it is vital to validate the outcomes we derive from computer-based simulations by conducting real-world experiments.

The solid-phase protein-binding assay was designed as an alternative approach to evaluate the binding and release dynamics of protein-protein interactions. This method requires only minimal amounts of protein and eliminates the need for specialized equipment, making it a more accessible and efficient option (209). Mould et al. described the solid-phase assay as a straightforward, quick

and reliable approach to studying protein-protein interactions, such as whether protein X interacts with protein Z (210). In this method, protein X, referred to as the "receptor," is immobilized on the wells of a high-binding ELISA plate, creating a solid phase. The wells are then blocked with bovine serum albumin (BSA) to prevent nonspecific binding. Next, biotin-labelled protein Z, termed the "ligand," is added to the wells. After washing away any unbound ligand, the bound ligand is detected using a conjugate, followed by a colorimetric reaction for visualization (210). The solid-phase protein-binding assay is based on ELISA methodology, leveraging its foundation in measuring antibody-antigen interactions, which are fundamentally protein-protein interactions (209). Building on this established methodology, we conducted a solid-phase analysis using high-binding plates to assess the binding interactions between insulin and the SARS-CoV-2 M^{pro}. The findings will not only corroborate docking results but also provide a foundation for further investigations into the molecular mechanisms underlying $M^{pro's}$ contribution to metabolic disturbances observed in post-COVID-19 patients.

2.13 Justification of the study

This study is justified by the urgent need to address the potential long-term health impacts of COVID-19, particularly those with pre-existing comorbidities such as DM. With the rising prevalence of DM even before the pandemic, understanding how SARS-CoV-2 exacerbates conditions like chronic inflammation, metabolic stress and insulin resistance is crucial for predicting and mitigating future public health challenges. Given the complex interactions between SARS-CoV-2 and metabolic pathways, understanding how the virus impacts glucose metabolism and insulin sensitivity is of paramount importance. The importance of this study also lies in its potential to uncover new insights into the molecular interactions between SARS-CoV-2 and glucose metabolism. Identifying these pathways could lead to the development of more targeted therapies aimed at preventing or managing DM in individuals affected by COVID-19. Additionally, these findings would fill a critical gap, inform public health strategies, providing a foundation for more effective and tailored interventions to address the rising global incidence of DM, especially in the wake of the pandemic. By integrating COVID-19-related metabolic risks into broader healthcare strategies, this research could help reduce the long-term burden of DM on

individuals and healthcare systems alike. The findings could offer insights into targeted interventions to mitigate the risk of DM in post-COVID-19 populations, advancing both clinical care and public health strategies (209).

CHAPTER 3: MATERIALS AND METHODOLOGY

3.0 Chemicals

All chemicals and reagents utilized in this study were of analytical grade and purchased from Sigma Aldrich Chemical Corporation ,St Louis, USA: Dulbecco's modified eagle's medium (DMEM), Eagles minimum essential medium (EMEM), fetal bovine serum (FBS), COVID-19 M^{pro}, murine anti-insulin primary antibody, anti-mouse secondary antibody,anti-GLUT-4 primary antibody, penicillin-streptomycin, Fluorometric Intracellular ROS Kit, Sodium chloride (NaOH), hydrochloric acid (HCL), dimethyl sulfoxide (DMSO), Triton X-100, potassium chloride, sodium phosphate dibasic (Na_2HPO_4), Monopotassium phosphate (KH_2PO_4) hydrogen peroxide, phosphate-buffered saline (PBS), Horseradish peroxidase (HRP), Hydrogen peroxide (H_2O_2), bovine serum albumin (BSA), 3,3',5,5'-tetramethylbenzidine (TMB), paraformaldehyde, Tween-20, Anti-Akt antibody produced in rabbit, Rabbit polyclonal anti-IL-6, Anti-Rabbit polyclonal anti-GLUT4 antibody, Rabbit polyclonal anti-DPP4 antibody,anti-PITRM1, Citric acid, Phosphoric acid (H_3PO_4), Thiobarbituric acid (TBA), butylated hydroxyl toluene (BHT), butanol. Insulin was purchased from NoVo Rapid®, Johannesburg, South Africa.

3.1 Equipment

Incubator (FSOH4)(220/240V 50Hz, 0.5kW; Labcon (pty) ltd 15 Aschenberg street Chamdor Krugersdorp Transvaal); SpectraMax M3 multi-mode microplate reader (100 – 240V~3.5A 50 – 60Hz; manufactured in China, designed in California, USA); BV1000 vortex mixer (230VAC 50Hz, 0.75amps; Benchmark Scientific Inc. PO BOX 709, Edison, NJ 08818, USA; made in Taiwan), Varioskan LUX type spectrophotometer 3020 100-240VAC 50/60Hz 200VA (Thermo Scientific, Waltham, MA, USA), Multi-channel pipet; Microplate shaker Intl plug(888610242),150-1000rpm, AC100-240V.50/60Hz,71VA, L9CF61024008,(Fisher brand), Assembled in China; Inverted microscope BS-2092,200-240V 50/60HZ,0.8A Lasec,(BIO38RAD)TC20; Automated cell counter (508BR09575, 30W, made in Singapore); Centrifuge,166145,1-14, Made in Germany(SIGMA); Labotec Ecobath model 207 40 Litre reciprocal shaking bath 230V~50Hz,1600W, Accu-Check Performa glucometer and contour plus test stipes.

3.2 M^{pro} preparation for *in vitro* testing

Covid-19 M^{pro} (CAE0172-200UG) was purchased from Sigma-Aldrich St Louise, USA. The vial contained 0.2 mg of M^{pro} in powder form. To prepare the working solutions, the concentration was calculated using the molar mass of M^{pro}. Since 1 mole of M^{pro} is equivalent to 34,000 g (or 34 kDa), the concentration was determined to be 5,900 nmol/mL. The stock solution was prepared by dissolving M^{pro} in DMSO (1 mL). Using the dilution formula ($C_1V_1=C_2V_2$), we prepared various concentrations of M^{pro}: 2.5, 5, 10, 20, 40, 80 and 160 nmol/mL. The solution was filtered through a 0.22 µm membrane filter and stored at -20ºC until use. Several precautionary measures were taken in preparing the working solution of COVID-19 M^{pro} for the cell-based assay. Personal protective equipment such as a lab coat, gloves, a face mask and safety goggles were always worn. Sterile techniques were employed, including using a biosafety cabinet (BSC) to maintain a sterile environment and prevent contamination. Sterile pipette tips, tubes and other consumables were used and work surfaces were disinfected before and after the experiment.

3.3 Insulin preparation

A vial of insulin from NovoRapid® was obtained with a known concentration of 100 units/mL where 1 unit of insulin aspart corresponds to 6 nanomoles. Before use, the insulin vial was gently shaken to ensure homogeneity. Thereafter, 10 mL of DMEM was placed into a 15 mL sterile container. Using a sterile syringe and appropriate pipetting techniques, 5µL of insulin solution was carefully withdrawn and placed into the 15 mL container. The solution was then mixed thoroughly using the Vortex that induced agitation and inversion to ensure uniform distribution of insulin throughout the media. The final concentration of the stock solution was estimated to be 0.05 units/mL. The solution was filtered using a 0.22 µm membrane filter and properly stored at 2°C to 8°C.

3.4 Cell culture

The two cell lines used in this study were C2C12 and HepG2 cell lines which were kindly donated by Dr Mlungisi Ngcobo at Traditional Medicine, Howard Campus, University of KwaZulu Natal.

To culture the skeletal (C2C12) muscle and hepatocarcinoma (HepG2) cell lines, their respective media DMEM AND EMEM were supplemented with 10% fetal bovine serum (FBS), L-glutamine (1%) and penicillin-streptomycin (1%). The frozen cell lines were then transferred into sterile 25cm^3 flasks for growth and incubated at 37 ºC in an incubator in the presence of CO_2 (5%). The cells were cultured over a brief period until they became confluent in their respective flasks. The cells were washed three times with a phosphate buffer solution (PBS) before being trypsinized with 1 mL of trypsin (for detachment from the bottom of the flask) and sub-cultured into new flasks. Subsequently, the cell lines were plated into 24-well and 96-well plates depending on the experiment to be performed.

3.5 Skeletal muscle differentiation

For the C2C12 cell line, a differentiation process was conducted for the estimation of media glucose uptake assays. C2C12 myoblasts were seeded in 24-well plates at a seeding density of 3.5 × 105 at 37°C in a 5% CO2 atmosphere. The C2C12 myoblasts were cultured in high glucose-containing DMEM. When the myoblasts reached 80% confluence, the cells were rinsed with PBS (250 µL) and the growth medium was replaced with differentiation medium [DMEM supplemented with FBS (2%) and penicillin/streptomycin (1%)]. For 3-4 days following differentiation induction, the differentiation medium was replaced every 24 hours to allow for myotube growth. The differentiation progress was monitored under a microscope by checking for the presence of elongated multinucleated cells.

3.6 Cell Viability Assay: MTT Assay

Principle

The MTT assay is a colourimetric assay used to assess cell viability and proliferation. It measures the metabolic activity of living cells, which is an indirect indicator of cell health. The cytotoxic assay was performed using the MTT protocol. The MTT assay was firstly described by Mosmann in 1983 as a rapid quantitative colorimetric assay that assesses the cell's survival and proliferation (211). This assay relies on the mitochondrial dehydrogenase found in viable cells that break down the tetrazolium rings of the light yellow MTT reagent. This process produces purple formazan crystals that cannot pass through cell membranes. The quantity of metabolically active cells correlates directly with the amount of formazan produced (deep purple colour) and this can be measured using a spectrophotometric method. Simply put, the

deeper the intensity of the purple, the more viable and metabolically active cells are. In this study, the MTT assay was used to assess the viability of both the C2C12 cells and HepG2 cells when exposed to varying concentrations of M^{pro} and inherently assess whether M^{pro} is cytotoxic on C2C12 and HepG2 cell lines. The reaction responsible for the colour formation of the MTT assay is shown in Figure 3.1 below.

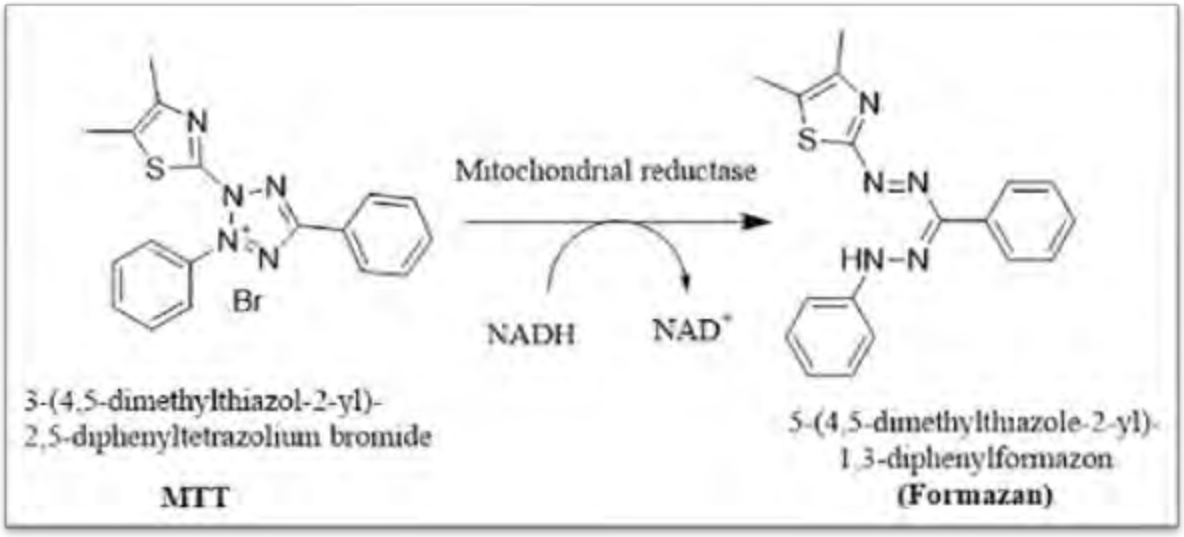

Figure 3.1: MTT is converted into formazan crystals by the mitochondrial reductase enzyme. The chemical reaction illustrates the reduction of MTT (3-(4,5-dimethylthiazol-2-yl)-2,5-diphenyltetrazolium bromide) to Formazan (5-(4,5-dimethylthiazol-2-yl)-1,3-diphenylformazon) by mitochondrial reductase. The reduction process involves the conversion of NADH to NAD+, which facilitates the formation of the coloured formazan product, commonly used in cell viability assays.(Adapted from Farooq et al.) (212).

Protocol

C2C12 and HepG2 cells were plated in the 96 well plates at a density of (4.55×10^4) cells/mL and (4.15×10^4) cells/mL, respectively until they reached approximately 80% confluence. Cells were then treated with the different concentrations of M^{pro} (2.5,5 ,10 ,20 ,40 ,80 and 160 nmol/mL). Some wells containing cells were left untreated and contained media only to serve as the control group. The cells were incubated for 24 hours at 37°C. After the treatment with the different concentrations of M^{pro}, the culture medium was gently removed and the MTT solution was prepared by dissolving 1mg of MTT powder in PBS (10%) and FBS-free media (90%).

Filter-sterilization was conducted followed by the addition of (1 mg/mL, 100 µL) of the MTT solution to each well. The plates were incubated for 3 hours at 37°C in the dark. Thereafter, the MTT solution was discarded from each well followed by the addition of DMSO (100 µL/well) to dissolve the formazan crystals formed by the MTT solution. Subsequently, the cells were incubated for 10 minutes and the absorbance of the purple-coloured crystals was read using a spectrophotometer at a wavelength of 570nm. The assay was performed in duplicate and each concentration was tested in sextuplicate. An overview of the methodology is summarized in Figure 3.2 below. Cell viability was calculated as a percentage of the absorbance of the control group using the following equation:

$$\text{Percentage cell viability} = \left(\frac{\text{Average absorbance of treated wells}}{\text{Average absorbance of control}}\right) \times 100$$

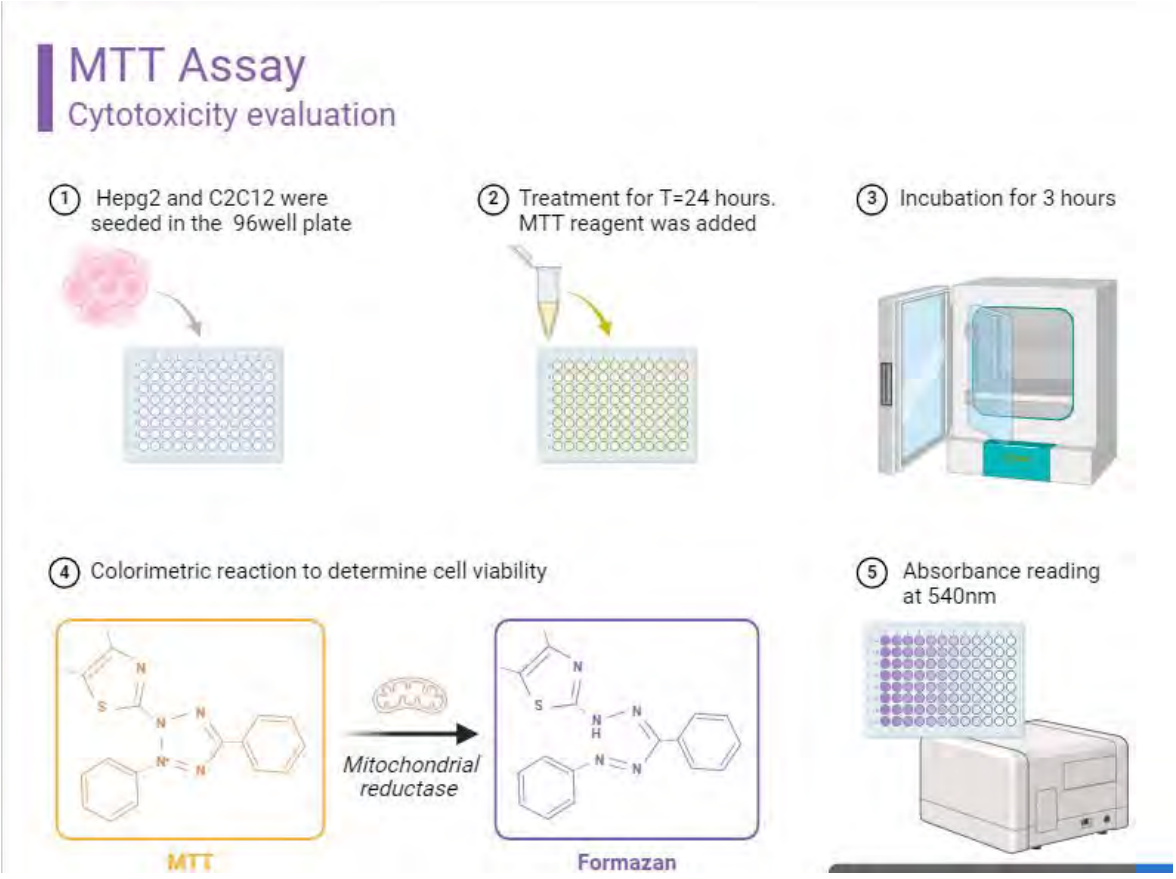

Figure 3.2: Schematic overview of cell viability assay. Figure 3.2 illustrates the principle of the MTT assay, which measures cell viability by quantifying the conversion of the yellow MTT dye

to a purple formazan product by living cells. The absorbance of the solubilized formazan is measured spectrophotometrically, providing an indirect assessment of cell viability and metabolic activity. (Created by Bio Render)

3.7 Estimated glucose utilization assay

Accu-Check Performa glucometer appraisal and validation for glucose uptake measurement

The Accu-Chek Performa glucometer is a widely used robust device for monitoring blood glucose levels in clinical and home settings. When considering its application for glucose uptake measurements in research, especially in *in vitro* or *ex vivo* studies, it is crucial to assess its accuracy, precision and suitability to provide accurate readings in the specific experimental context. A validation experimental procedure was carried out to ensure accurate glucose measurement in cell culture medium using glucometers and glucose strips. The glucose concentration of the cell culture medium was determined by assessing its composition, after which the values were converted to mmol/L, the unit used by the glucometer. A 4ml of medium was diluted to obtain theoretical concentrations of 24.97, 12.48, 6.24, 3.12 and 1.56 mmol/L. The glucometer was then employed to measure the actual glucose concentrations in the diluted samples, as shown in Figure 3.3. Each sample underwent triplicate testing for consistency.

The graph illustrates the correlation between theoretical glucose values (mmol/L) and the glucometer readings obtained during the validation assay. The linear regression equation was $y=0.8263x + 0.6393$ with an R^2 value of 0.9972. The high R^2 value indicates a strong linear relationship between the theoretical and measured glucose values, suggesting that the glucometer

provides consistent readings across the tested range.

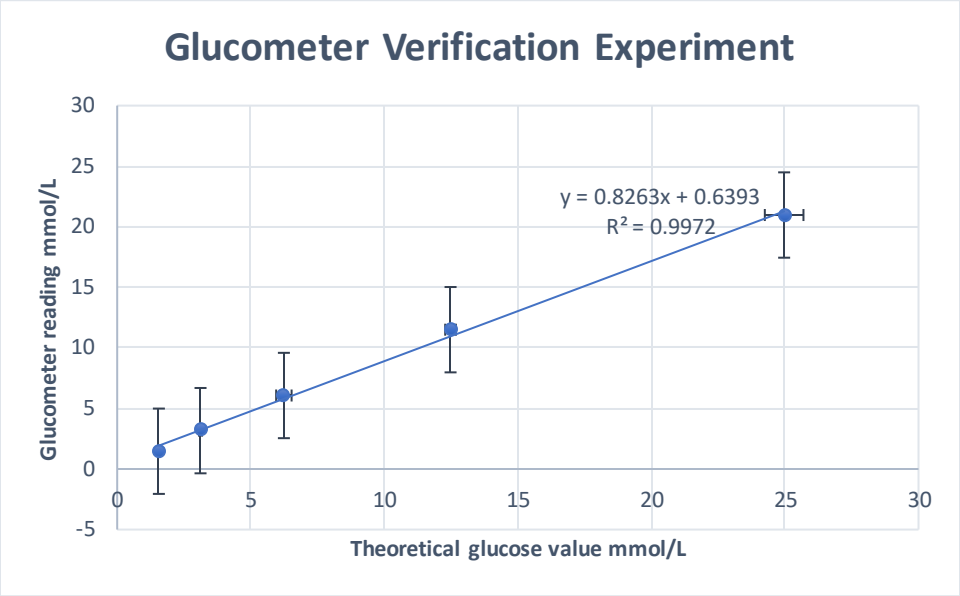

Figure 3.3: The graph depicts the relationship between theoretical glucose concentrations (mmol/L) and glucometer readings. Error bars represent the standard deviation of glucometer readings at each glucose concentration, highlighting variability across the tested range.

Principle

Glucose uptake measurement is an assay used to evaluate the ability of cells to transport glucose from the extracellular environment. When the cells are metabolically active, they utilize glucose for energy. Measuring media glucose is one way that we can estimate glucose uptake in cells, i.e. as the cells absorb and utilize glucose, media glucose concentration decreases. In this study, the Accu-Check Performa glucometer and contour plus strips were used to measure media glucose uptake. Therefore, this experiment aimed to assess whether M^{pro} would induce a shift in glucose handling in the cell lines.

Protocol

The glucose utilization assay was carried out following the methodology outlined by Ventera et al with some modifications (213). C2C12 (3.92×10^4) cells/mL and HepG2 cells (3.79×10^4) cells/mL were separately seeded and placed into 24 well plates, cultured and allowed to attach and obtain confluency of about 80% in an incubator at 37ºC and 5% CO_2. The cells were incubated in their respective culturing media which were DMEM AND EMEM respectively.

After cell preparations were ready for experimentation, the old cell media was discarded and 250 µL of M^{pro} (2.5, 5, 10, 20, 40, 80 and 160 nmol/mL) was placed into the wells. A control group of cells was incubated with media only. The initial glucose readings were measured at time = 0 hours. After an incubation time of 24 hours, media glucose concentrations were recorded, again. To assess the effect of M^{pro} exposure on insulin sensitivity and its effect on the cell lines, the cells were incubated with M^{pro} for 24 hours. Thereafter, the cells were treated with media containing insulin (250µL, 0.05 units/mL). Subsequently, a glucometer was used to read the media glucose measurements at t=0 and 24 hours. Each concentration was tested in quadruplicate and the assay was repeated three times.

The estimation of glucose uptake was determined using the following equation:

$$\text{Glucose uptake (\%)} = \left(\frac{\text{Medium glucose(T0)} - \text{Medium glucose (T24)}}{\text{Medium glucose (T0)}}\right) \times 100$$

3.8 In cell ELISA: Semi-Quantitative expression of GLUT4, AKT, IL-6, DPP4 and MMP1

Principle

ELISA is a sensitive biochemical technique used to detect and quantify specific proteins, antigens or antibodies in a sample through antigen-antibody interactions and enzyme-mediated signal amplification. Enzyme immunoassays operate by utilizing an antigen-primary antibody, enzyme-conjugated secondary antibody, an appropriate substrate and chromogen which leads to a detectable colour change, observable both visually and spectrophotometrically. The primary antibodies selectively bind to specific antigenic epitopes found on proteins through non-covalent interactions like hydrogen bonds and electrostatic forces. Secondary antibodies, often anti-immunoglobulin antibodies such as IgG, are utilized in immunoassays as labelled or conjugated entities thus facilitating the detection of antigen-primary antibody interactions. The binding of the antigen and antibody is detected because of the enzyme-linked to a secondary antibody, which turns the antigen-antibody complex into a coloured product when the enzyme substrate is added.

There are various methodologies which have been utilized to measure cytokines and glucose transporters and presently, immunoassays are the most frequently used. Notably, the solid-phase ELISA owing to its heightened specificity and sensitivity was employed for these biochemical assays.

Protocol

All solutions were freshly prepared and used immediately for each assay. C2C12 and HepG2 cells were seeded in a 96-well plate and cultured in their respective media DMEM AND EMEM for each ELISA experiment. After 24 hours, the cells were treated with 100 µL of the different concentrations of M^{pro} (40, 80and 160 nmol/mL) and incubated overnight. The following day, the media was aspirated and placed in vials for storage at 4°C.

The control wells were set up to have a blank and negative control. The blank consisted of growth medium only and no cells and the M^{pro}. The negative control consisted of cells that had the primary antibody and secondary antibody, but without the addition of M^{pro}. While both controls aim to measure non-specific binding, the blank control assesses the background signal from the growth medium or any potential contaminants in the reagents used, without the influence of cells or M^{pro}, while the negative control evaluates any potential background noise from the interaction of antibodies with cells in the absence of M^{pro}.

For the in-cell ELISA, paraformaldehyde (8%, 100 µL) solution was used to fix and cross-link the cells to the microplate for 15 minutes at room temperature whilst shaking with a microplate shaker at 300 rpm. The paraformaldehyde was aspirated and following this, a wash step was performed to eliminate any residual solution using 1XPBS (200 mL). The wash step was conducted by placing 200 µL per well of wash buffer and repeated three times. After the final wash, the plates were blotted dry on a paper towel. The next step was the permeabilization of the cells using a permeabilization buffer (250 µL Triton X-100 in 24.75 mL 1XPBS) for 30 minutes at room temperature on the plate shaker. After 30 mins, the permeabilization buffer was aspirated from the wells and a blocking buffer (200 mL, prepared by adding 2g of bovine serum albumin in 20 mL of 1XPBS) was added and incubated at room temperature for 2 hours whilst shaking the plate at 300rpm. After aspirating the blocking buffer, 100 µL of the primary antibody (AKT, GLUT4, IL-6, MMP1 and DPP4) diluted at 1:5000 was added to each well separately. The plate was then

incubated overnight at 4ºC. Following incubation, the primary antibody was aspirated and the wells were washed three times with 250 µL of wash buffer (prepared by adding 625 µL Tween-20 to 250 mL of 1XPBS) to remove excess and unbound antibody.

Next, 100 µL of a secondary antibody (anti-rabbit IgG, diluted 1:5000) specific to the primary antibody was added to each well. The plate was incubated at room temperature for 2 hours with gentle shaking. After the incubation, the wells were washed four times with 250 µL of wash buffer, followed by the addition of 100 µL of TMB horseradish peroxidase substrate. The plate was incubated in the dark for 30 minutes. To stop the reaction, 100 µL of 0.1M HCl was added, resulting in a colour change from blue to yellow. The absorbance was then measured at 450 nm using a UV-VIS spectrophotometer. The assay was performed in duplicates, with each concentration tested in triplicate. For GLUT4 translocation, the same procedure was used, except the cell permeabilization step was omitted to detect only GLUT4 found across the membrane. GLUT4 expression and translocation were studied exclusively in C2C12 cells.

The relative expression of each protein was calculated as follows:

$$\text{Relative percentage expression} = \left(\frac{\text{Average absorbance of treated wells}}{\text{Average absorbance of control}}\right) \times 100$$

The schematic diagram of ELISA is presented in Figure 3.4 .

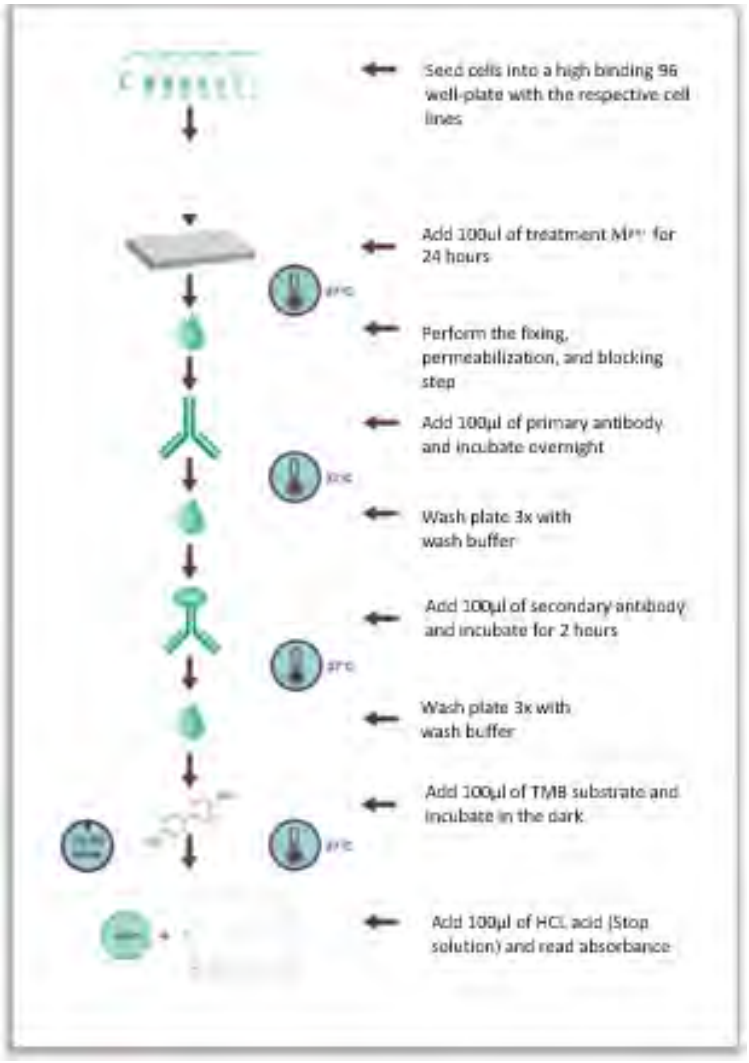

Figure 3.4: Stepwise workflow of an ELISA assay to assess protein expression in treated cell lines. Cells are seeded, treated, fixed and incubated with primary and secondary antibodies. The assay concludes with substrate addition, reaction termination and absorbance measurement to quantify protein levels. Adopted from AssayGenie.com and modified.

3.9 Cell culture medium ELISA for IL-6, DPP4 and MMP1

The harvested media was used for extracellular assessment of DPP4, MMP1 and IL-6. The samples were centrifuged at a low speed of 300-500 xg and the supernatant was collected. A high-binding 96-well plate was prepared by adding 50 µL of DMEM and EMEM aspirated from the C2C12 and HepG2 cell lines, followed by incubation at room temperature for 6 hours. After the incubation period, the media was removed and the plate was blotted dry. No fixation or permeabilization steps were performed; however, the subsequent steps followed the same procedure as previously described in the in-cell ELISA above. The percentage expression of each protein was also calculated using the previously mentioned formula.

3.10 Computational prediction of M^{pro} -protein interactions

Principle

In silico protein docking experiments serve as invaluable tools in predicting and understanding molecular interactions that might occur between different proteins. This computational assay aims to explore the binding affinities and potential structural conformations of the key proteins whose interaction with M^{pro} could lead to insulin resistance. In silico protein docking offers a cost-effective and efficient means to predict protein-protein binding which may be challenging to achieve experimentally. ClusPro is a web-based server for the direct docking of two interacting proteins. By simulating the docking process computationally, we can potentially identify the interactions with the highest likelihood of biological relevance and thus perform experimental assays such as solid-phase binding to validate these interactions.

Protocol

After the identification of 4 proteins of interest through the literature review, the 3D structures were retrieved from the RCSB Protein Data Bank. These were M^{pro} (PDB ID:7CAM), insulin receptor kinase domain (PDB ID:1IRK), Human insulin PDB ID (3I40), PI3K (PDB ID:4JPS) and GLUT4 (PDB ID:7WSM). The first step involved the preparation of the proteins using Auto Dock software. This involved the elimination of native ligands such as co-crystallized waters and hetero atoms. The next step involved the addition of solvation parameters such as polar hydrogen atoms and Kollman charges by utilizing the Auto Dock software tool. ClusPro was utilized for the

docking simulations therefore the outcomes of the protein preparation were saved as a PDB file format to ensure compatibility with ClusPro. Each protein of interest underwent a docking experiment with M^{pro}, with each ligand being rotated 70,000 times. Based on the protein size, M^{pro} was designated as either the receptor or the ligand. M^{pro} was larger than GLUT4, insulin receptor and PI3K and was the ligand. For the docking of M^{pro} and human insulin, M^{pro} was the receptor. For each rotation, ClusPro translated the ligand in x, y and z relative to the receptor on a grid to ultimately give the translations with the best score from each rotation. We assessed the results based on binding free energies. ClusPro produced 30 clusters ranked according to the number of members in each cluster. Next, we ranked the protein-protein complexes according to their docking energies. ClusPro provides the ligand-receptor binding energy based the sum of the van der Waals, desolvation energy and electrostatic interaction energies. Since we have no prior knowledge of the nature of the interaction of the proteins, we used the balanced coefficient models. We selected the cluster with the greatest number of members as this represents the near-native structure and would therefore be the most biologically relevant structure. The next step involved visualization and analysis with PyMOL software. This was achieved by importing the protein-protein complex structure into PyMOL, followed by utilizing PyMOLs and visualization tools to highlight the key residues that are directly involved in binding to the ligand. The images that illustrated the binding interactions between the ligand and receptor were exported to Microsoft Word to report the results.

3.11 Solid phase binding analysis: Detection of M^{pro} -insulin- M^{pro} interactions

Principle

Solid-phase assays are used in the detection of biomolecular interactions through the assessment of binding affinity. The assay utilizes a solid support such as the high-binding ELISA plate to immobilize one interaction partner on its surface followed by the capture of the second interaction partner from the solution as depicted in Figure 3.5 below. The interacting partners can be identified by performing assays such as the Western blot or by quantitative detection such as enzyme-linked immunosorbent assay (ELISA). Molecular docking software (ClusPro) provided computational models that predicted binding interactions and potential conformations that may result from insulin

and M^{pro}. In this experiment, the aim was to experimentally validate the docking results by analyzing solid-phase interactions between insulin and M^{pro}.

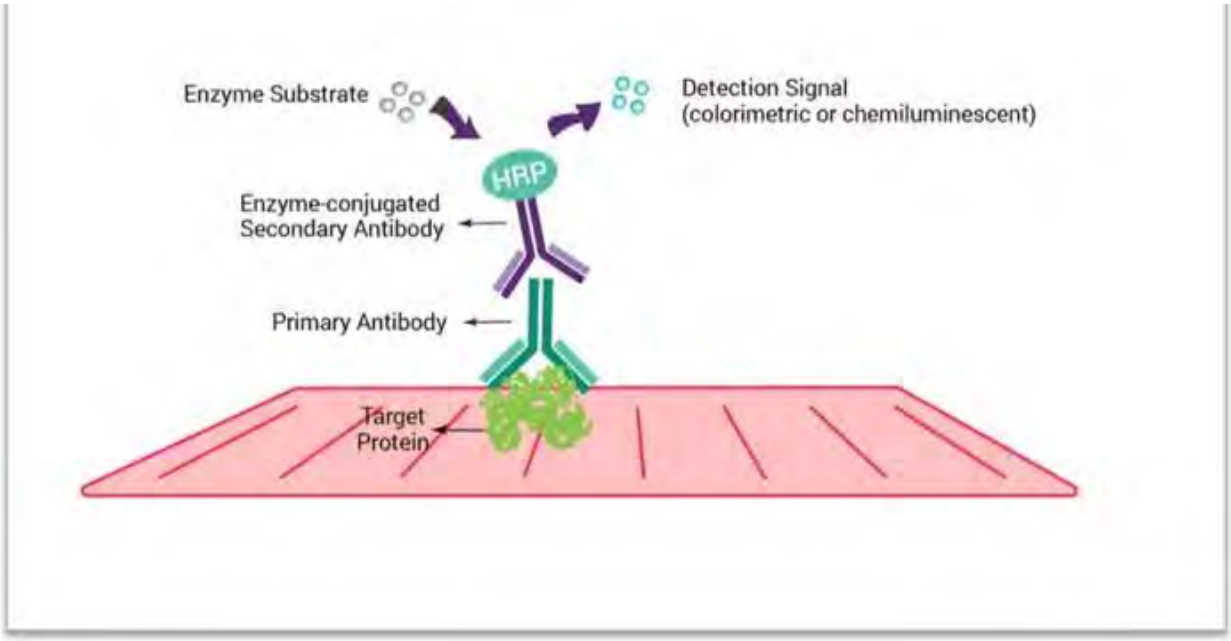

Figure 3.5: Overview of the principle of the detection of any potential insulin and M^{pro} interaction. The primary antibody binds to the target protein, followed by an enzyme-conjugated secondary antibody. The addition of a substrate generates a detectable colorimetric signal proportional to the protein quantity. (adapted from AssayGenie.com)

Protocol

The different concentrations (40, 80 and 160 nmol/mL) of the M^{pro} were immobilized by placing them into a high-binding 96-well plate at a volume of 50 µL/well. The plate was incubated for 6 hours at 25°C to allow for coating of the plate with the protein. After the 6 hours lapsed, the media containing the M^{pro} was discarded. The next step involved the blocking step which was accomplished by adding the blocking solution (100 µL/well). This step was essential to obstruct the non-specific binding sites left on the plate. After two hours of incubation, the remaining blocking solution was discarded as before. The plates were blotted dry on a sterilized paper towel. The next step involved incubation with the second protein, insulin (50 µL/well, 0.05 units/mL). Two different control groups were incubated comprising wells with no insulin added but only the M^{pro} and wells with only the media and no M^{pro} and insulin. The wash buffer (250 mL/well) was

utilized 3 times to remove any unbound antigen. After the final wash, the plates were blotted dry on a sterilized paper towel. The plate was then incubated with anti-insulin primary antibody solution (100 mL/well) overnight stored at 4°C. After 12 hours, the plate was then rewashed four times using the wash buffer to remove any unbound primary antibody. After the final wash, the plates were blotted dry on a sterilized paper towel. The HRP-conjugated secondary antibody was then added and the plate was incubated at room temperature on a plate shaker for 2 hours. Following a final wash step to remove any unbound secondary antibody, the HRP substrate, TMB (100 mL/well) was added and after a few minutes, a colour change was observed from colourless to blue. A stop reagent of 0.1M HCL (100 mL/well) was added to halt the reaction. Lastly, ELISA plates were read at 450 nm using the UV-VIS Spectrophotometer reader.

3.12 Reactive oxygen species by a fluorometric assay

Principle

The intracellular ROS assay is a highly sensitive and rapid one-step cell-based assay designed for the detection of reactive oxygen species such as superoxide and hydroxyl radicals in viable cells. Detecting intracellular reactive oxygen species (ROS) is accomplished by using cell-permeable fluorescent probes or dyes that react with ROS to produce a measurable signal. To detect ROS, the assay utilizes a cell-permeable, reduced form of the Mito Tracker Red CM-H2XROS dye. This dye remains non-fluorescent until it is oxidized by ROS, at which point it becomes fluorescent, allowing the direct measurement of ROS activity. Upon oxidation, the dye produces a fluorescence signal that can be measured. The strength of the fluorescence is directly proportional to the concentration of ROS present, providing a quantitative measure of intracellular oxidative stress.

Protocol

The intracellular ROS fluorescence assay followed the manufacturer's instructions (Fluorometric Intracellular ROS Kit, CN: MAK143-1KT, Saint Louis, USA), with some modifications. C2C12 cells were seeded at a density of 4.67×10^4 cells/mL in a solid black 96-well plate and incubated for 24 hours to allow for them to be confluent. Cells were treated with M^{pro} (40, 80 and 160 nmol/mL) for 24 hours, while untreated wells served as controls. After treatment, 50 mL of the master reaction mix containing the ROS detection reagent was added to each well. The plate was then placed in the incubator (5% CO^2, 37 °C) for one hour. Absorbance was measured using the

Varioskan Lux Microplate Reader, with excitation set at 490 nm and emission at 525 nm. The assay was conducted in duplicate. The relative fluorescence was expressed as a percentage of the control. There was no measurement of ROS conducted in the HepG2 cell line, due to assay kit reagents being limiting.

3.13 Lipid peroxidation: Media malondialdehyde concentration

TBARS Method

Principle

Oxidative stress arises when there is an imbalance between the production of reactive oxygen species (ROS) and the cell's ability to detoxify them, leading to damage to lipids, proteins and DNA. The ROS levels were measured following the technique outlined by Nagiah et al, which uses lipid peroxidation to indicate oxidative stress specifically, extracellular malondialdehyde (MDA), a byproduct of lipid peroxidation (214). The Thiobarbituric Acid Reactive Substances (TBARS) assay is a well-established method for quantifying MDA, making it an indirect but reliable indicator of oxidative stress. The assay works by reacting MDA with thiobarbituric acid (TBA) under acidic and high-temperature conditions to form an MDA-TBA adduct, which produces a coloured complex as outlined in Figure 3.6 below. The amount of MDA in a sample and therefore the degree of lipid peroxidation can be assessed through spectrophotometric analysis at 532 nm. By measuring MDA in this way, the TBARS assay measures oxidative stress.

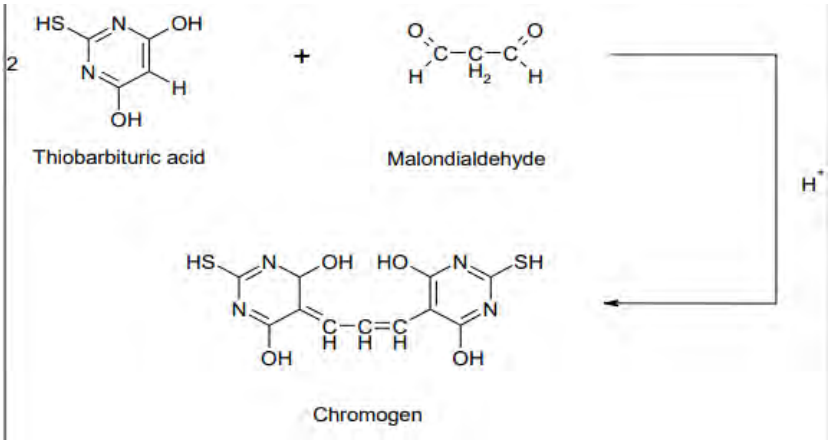

2-Thiobarbituric Acid + MDA ⟶ MDA-TBA adduct (λ_{max} =532nm)

Figure 3.6: Formation of a TBA-MDA Chromogen: This figure illustrates the reaction between TBA and MDA to form a chromogen, which is commonly used to measure lipid peroxidation levels. The resulting chromogen emits a characteristic colour that can be quantified spectrophotometrically.

The absorbance from these wavelengths was used to calculate the concentration of MDA using the Beer-Lambert law as follows:

$$\text{MDA concentration} = \left(\frac{\text{Final absorbance} - \text{Blank}}{\text{MDA coefficient } (156\text{mmol}^{-1})}\right)$$

Protocol

C2C12 and HepG2 cell lines were seeded in the 24 well plates at a density of 3.62×10^4 cells/well and 4.54×10^4 cells/well respectively and treated using the same protocol (time of incubation and concentrations) used for the ELISA. Following each treatment, 250 µL of supernatant was aspirated and used for the TBARS assay. The working solutions consisted of 2% H_3PO_4, 7% H_3PO_4, 1M HCl, 20mmol BHT solution and 50mL of the TBA/BHT solution (0.1g of NaOH,0.5g of TBA,250 µL of the 20Mm BHT solution and deionized water up to 50mL) were prepared. After preparing working solutions, 13 graduated plastic tubes were taken and labelled as control,160, 80,40 and blank in triplicates for each concentration. In each test tube, the following solutions were added as displayed in Table 3.1 below:

Table 3.1: The experimental setup and composition of each test solution

Test tube 1-12 (Treatment test tubes)	Test tube 13 (blank)
100 µL of samples/supernatant from the 250 µL sample	100 µL of DMEM and EMEM
200 µL of 2% of H_3PO_4	200 µL of 2% of H_3PO_4
400 µL of 7% of H_3PO_4	400 µL of 7% of H_3PO_4

400 µL of TBA/BHT	200 µL of 1M HCl
200 µL of 1M HCl	

All test tubes were boiled at 100˚C for 15 minutes using the Labotec shaking Eco Bath water bath. They were then left to cool to room temperature for 10 minutes. After cooling, 1.5 mL of butanol was added to each test tube, which was then vortexed for 10 seconds. The test tubes were left to stand until the butanol phase (the top layer) became visible. Then, 200 mL of the butanol phase was added in triplicate to a 96-well plate. The optical density of the samples was measured spectrophotometrically at 532 nm, with a reference wavelength of 600 nm, using the Varioskan Lux microplate reader. MDA concentrations (Mm) were calculated by dividing the average absorbance of the samples by the absorption coefficient (156 Mm^{-1}).

3.14 Statistical analysis

The data were expressed as the mean ± SD of three replicates. Graphs were generated using GraphPad Prism software (Version 8, GraphPad Software, San Diego, CA, Canada, 2019). Firstly, a normality test was conducted on the data using normality and log-normality tests in GraphPad Prism. Depending on the results, if the data adhered to a normal distribution, a one-way ANOVA followed by Tukey's multiple comparison test for comparing the different concentrations of M^{pro} with the control was performed. For data that did not follow a normal distribution, the Kruskal-Wallis test was utilized. Subsequently, statistical significance was evaluated using the one-way ANOVA or the Kruskal-Wallis test. Despite the use of a non-parametric test for non-normally distributed data, mean and standard deviation were reported for consistency across all datasets. While median and interquartile range (IQR) are typically preferred for non-parametric data, mean ± SD was retained as a descriptive measure due to the small sample size (n=3), where individual variation within replicates is still relevant for interpretation. However, all statistical conclusions were based on the appropriate tests (ANOVA or Kruskal-Wallis) to ensure robust analysis.Subsequently,significant differences between the treatment and control are indicated by asterisks (*). The significance levels were predetermined as follows: (*) $p < 0.05$, (**) $p < 0.01$, (***) $p < 0.001$ and (****) $p < 0.0001$.

CHAPTER 4: RESULTS

4.0 Cytotoxic assay

A cytotoxicity study was conducted on C2C12 and HepG2 cell lines using various concentrations of 2. 5, 5,10, 20,40, 80 and 160 nmol/mL of M^{pro}, as depicted in Figures 4.1 A and B, respectively. All concentrations generally demonstrated a decrease in cell viability by comparison to the control. For C2C12, there was no concentration-dependent decrease observed however, the highest concentration of M^{pro} showed a statistically significant decrease by comparison to the control. For the HepG2 cells, the first four concentrations (2.5-20 nmol/mL) showed a decrease in cell viability, however, there was no significant statistical difference from the control. The concentrations of 40 nmol/mL and 80 nmol/mL exhibited a decrease in cell viability which was of statistical significance compared to the control(untreated cells).

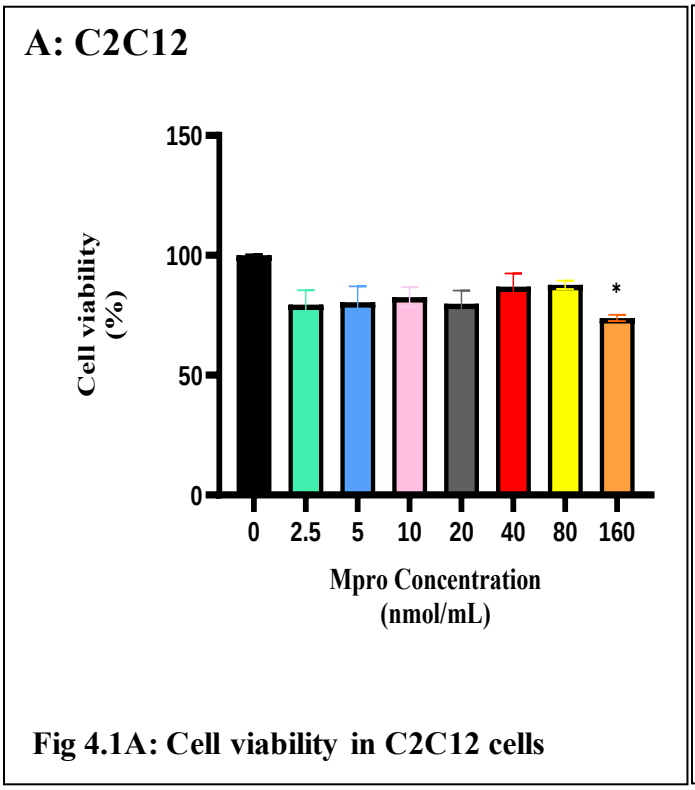

Fig 4.1A: Cell viability in C2C12 cells

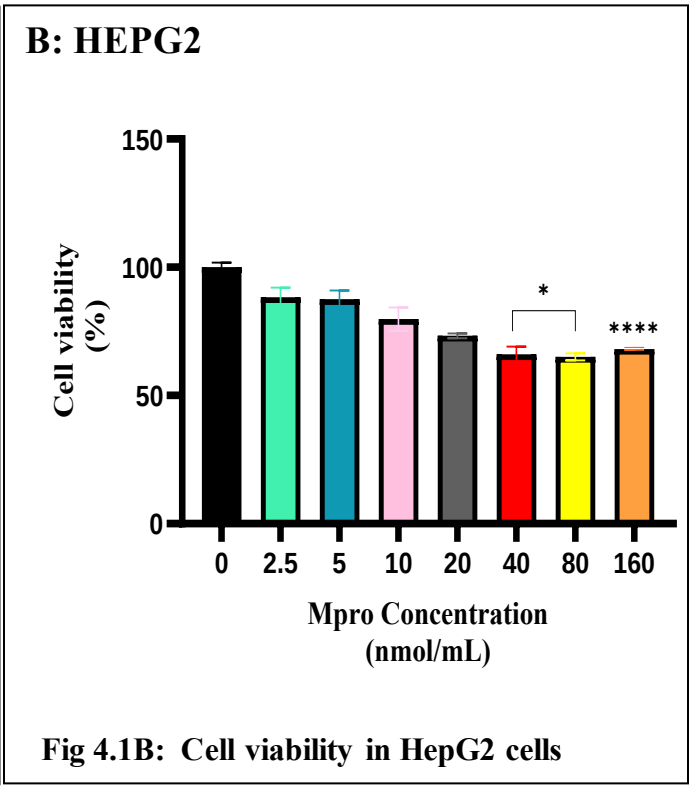

Fig 4.1B: Cell viability in HepG2 cells

Figure 4.1: Cell viability was assessed after treating C2C12 and HepG2 cell lines with M^{pro} (2.5,5,10 ,20,40, 80 and 160 nmol/mL) for 24 hours at different concentrations. Results are expressed as a percentage of viable cell count. Untreated cells were used as the control group. The

values are expressed as mean ± standard deviation represented with error bars, (n = 3). The asterisk (*) represents the statistical difference between the test compounds and the control at * ($p < 0.05$), (***) $p < 0.001$, (****) $p < 0.0001$.

4.1 Effect of M^{pro} on non-insulin stimulated glucose uptake

The relative glucose uptake was measured after treating C2C12 and HepG2 cell lines with different concentrations of M^{pro} (2.5,5,10 ,20,40,80 and 160 nmol/mL) for 24 hours. The results are presented in Figures 4.2 A and B, respectively. The insulin-treated control exhibited higher glucose uptake compared to the untreated control in both C2C12 and HepG2 cells, indicating that the insulin was effectively stimulating glucose uptake as expected. This response is consistent with insulin's known role in promoting glucose transport into cells, thereby validating the experimental conditions and the responsiveness of the cell lines to insulin treatment.

In C2C12 cells, there was a significant statistical difference from the control (untreated) cells observed for all the concentrations of M^{pro}. The control (untreated) cells exhibit baseline glucose uptake, with no interference from M^{pro}. Insulin-treated cells show significantly enhanced glucose uptake compared to the control (untreated) cells, indicating insulin sensitivity and promoting glucose uptake. M^{pro} treatments at increasing concentrations (from 2.5 to 160 nmol/mL) caused a progressive reduction in glucose uptake compared to the insulin-treated and control groups. There is a dose-dependent decrease in glucose uptake with an increase in M^{pro} concentration, with the most significant reduction observed at 160 nmol/mL.

In HepG2 cells, a significant statistical difference from the control (untreated) cells was observed only for insulin treated cells, 80 nmol/mL and 160 nmol/mL concentrations of M^{pro}. The glucose uptake results show a similar trend as in C2C12 cells, with a concentration-dependent reduction in glucose uptake across the different concentrations tested (2.5 to 160 nmol/mL) except that the inhibitory effect of M^{pro} is not as pronounced as in the C2C12 cell line. As the concentration of M^{pro} increases from 2.5 to 160 nmol/mL, glucose uptake progressively declines, with the most substantial reduction observed at the highest concentrations (80 and 160 nmol/mL). Overall, the results suggest that M^{pro} impairs glucose uptake in skeletal muscle and hepatic cells.

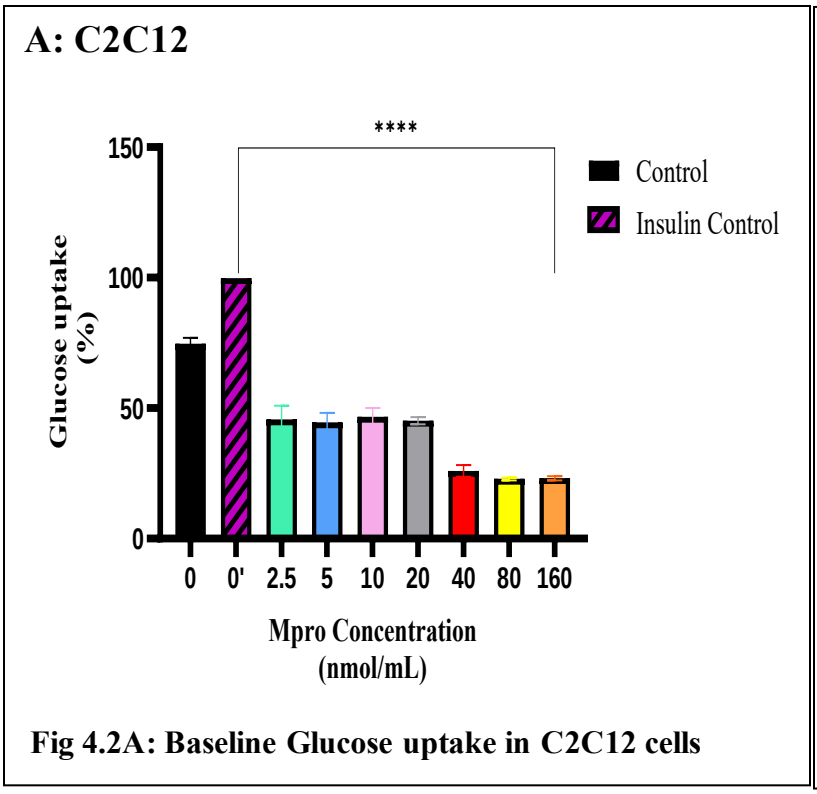

Fig 4.2A: Baseline Glucose uptake in C2C12 cells

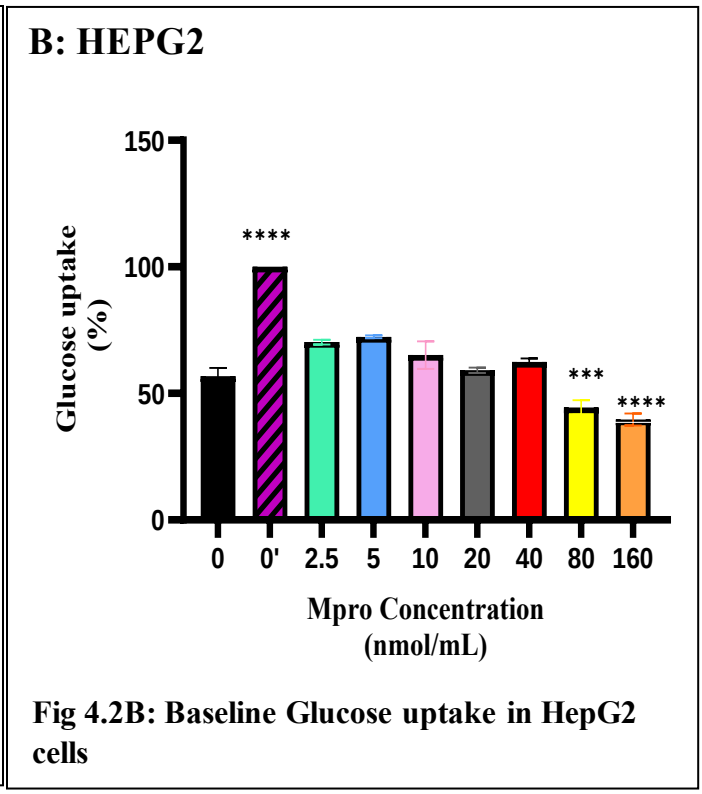

Fig 4.2B: Baseline Glucose uptake in HepG2 cells

Figure 4.2: The relative glucose uptake was estimated after treating C2C12 and HepG2 cell lines with the different concentrations of M^{pro} (2.5,5,10 ,20,40,80 and 160 nmol/mL) for 24 hours. Results are expressed as a percentage. Untreated cells are presented as 0 while 0' represents insulin-treated cells. Untreated cells were used as the control group. The values are expressed as mean ± standard deviation represented with error bars, (n = 3). The asterisk (*) represents the statistical difference between the test compounds and the control at (***) $p < 0.001$ and (****) $p < 0.0001$.

4.2 Effect of M^{pro} on insulin-stimulated glucose uptake

The effect of M^{pro} on insulin-stimulated glucose uptake was also performed. Different concentrations of M^{pro} (2.5 nmol/mL- 160 nmol/mL) for the C2C12 and HepG2 cell lines. Graphs 4.3A and 4.3B below illustrate the effects of the co-administration of insulin and M^{pro} on glucose uptake thus insulin is the relative control to assess for statistical differences. The data indicates that insulin significantly stimulates glucose uptake at low concentrations M^{pro} for both cell lines compared to the normal control. However, as the concentrations of M^{pro} increase, there is a noticeable decrease in glucose uptake. For the C2C12 cell line, there was a gradual decrease in insulin-stimulated glucose uptake from 2.5 to 160 nmol/mL. Insulin-stimulated glucose uptake remains high for the 2.5 to 20 nmol/mL M^{pro} concentrations although slightly reduced compared to insulin alone (statistically significant at 10 nmol/mL). Glucose uptake decreases further, with the most significant reduction observed at 160 nmol/mL. The HepG2 cell line, the results show a similar trend to C2C12 cells, with higher concentrations of M^{pro} (40 to 160 nmol/mL) causing a significant decrease in glucose uptake (statistically significant from 40 to 160 nmol/mL), except that the overall effect is less pronounced compared to C2C12. Lastly, the results suggest that while low levels of M^{pro} do not seem to affect the efficacy of insulin in stimulating glucose uptake, higher concentrations may inhibit this effect.

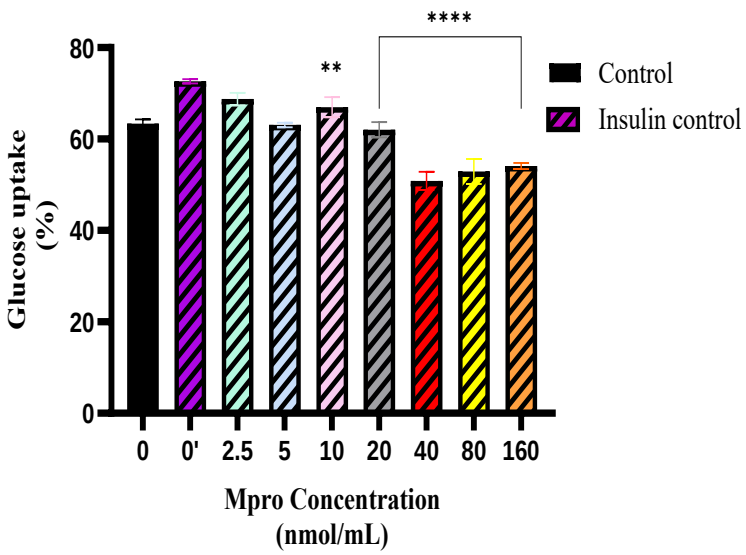

Fig 4.3A: Insulin-stimulated glucose uptake in C2C12 cells

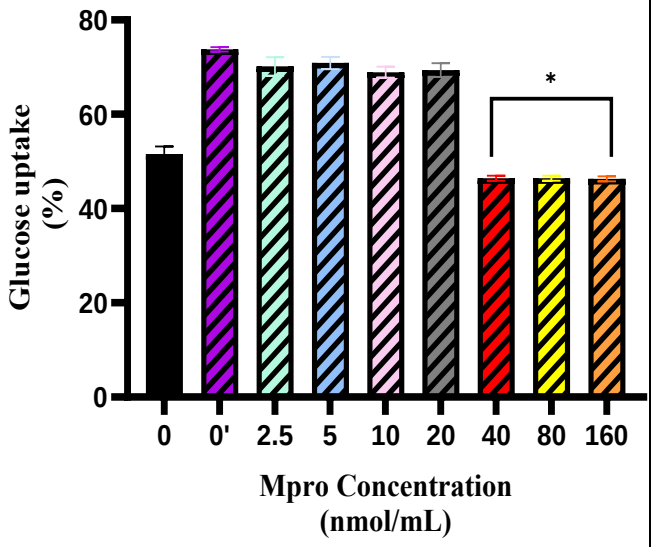

Fig 4.3B: Insulin-stimulated glucose in HepG2 cells

Figure 4.3: The relative glucose uptake was estimated after treating C2C12 and HepG2 cell lines with M^{pro} (2.5,5,10 ,20,40,80 and 160 nmol/mL) for 24 hours at the different concentrations. Untreated cells are presented as 0 while 0' represents insulin-treated cells. Insulin-treated cells were used as the control group. The values are expressed as mean ± standard deviation represented with error bars, (n = 3). The asterisk (*) represents the statistical difference between the test compounds and the control at (*) $p < 0.05$, (**) $p < 0.01$ and (****) $p < 0.0001$.

N.B: There is a decrease in the number of concentrations of M^{pro} being used for the subsequent assays to increase optimization and efficiency. The subsequently used concentrations induced a notable response in the cell lines with a statistically significant difference and therefore were more likely to reflect the threshold at which cellular pathways are activated or modulated. Furthermore, these concentrations (40, 80 and 160 nmol/mL) demonstrated noticeable responses in prior assays.

4.3 In-cell and medium ELISA

4.3.1 Relative GLUT4 expression

To investigate GLUT4 expression in C2C12 cells, we analyzed relative GLUT4 levels after M^{pro} treatment of concentrations of 40 to 160 nmol/mL under both baseline and insulin-treated conditions. Figure 4.4 illustrates GLUT4 expression in C2C12 cells under baseline conditions (M^{pro} treatment only-no insulin activation). The insulin treatment showed a significant increase in GLUT4 expression compared to the control(untreated) cells, indicating that insulin upregulates GLUT4 expression in skeletal muscle cells. For M^{pro} treatment, GLUT4 expression is comparable to the control (untreated), except for 80 nmol/mL where we observed a slight decrease in GLUT4 expression. No statistically significant difference was observed relative to the control (untreated cells). There was a statistically significant difference between insulin and the control (untreated cells).

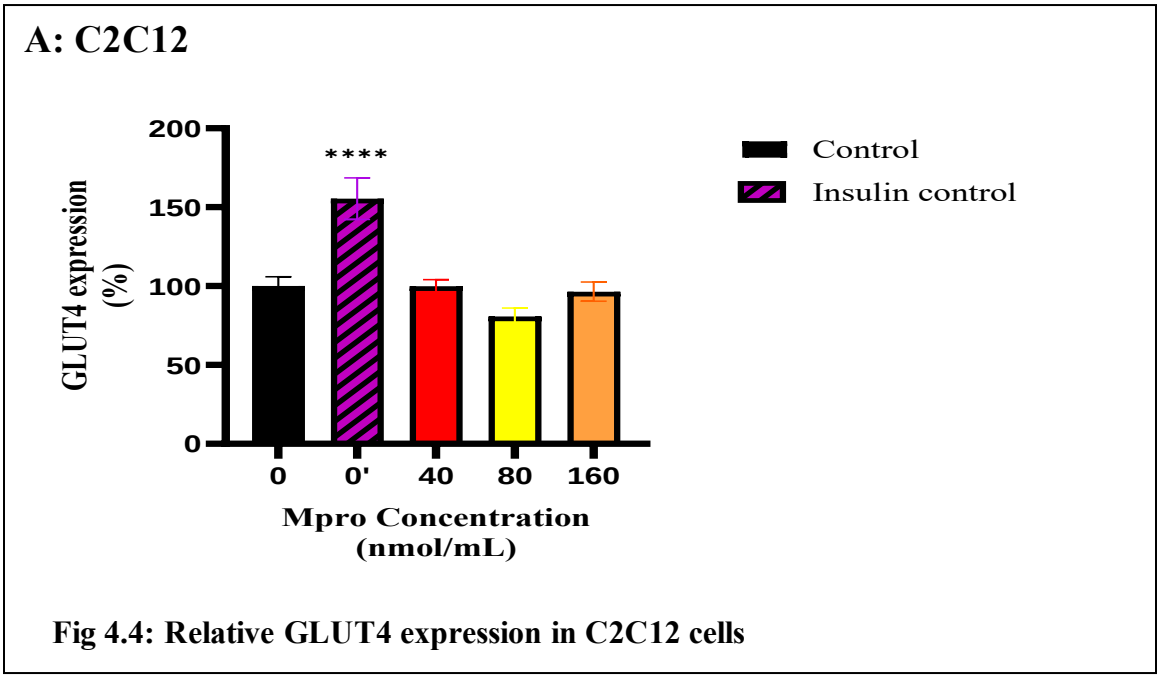

Fig 4.4: Relative GLUT4 expression in C2C12 cells

Figure 4.4: GLUT4 expression was estimated after treating the C2C12 cell with M^{pro} for 24 hours at the different concentrations of 40,80 and 160 nmol/mL. The values are expressed as mean ± SD represented with error bars, (n = 3). Results are expressed as a percentage.Untreated cells are presented as 0 while 0' represents insulin-treated cells. Untreated cells were used as the control

group. The asterisk (*) represents the statistical difference between the test compounds and the control at (****) $p < 0.0001$.

Figure 4.5 below depicts GLUT4 expression in C2C12 cells following insulin treatment. Insulin treatment failed to significantly elevate GLUT4 expression levels across all M^{pro}-treated cells. Statistical analysis revealed significant differences in GLUT4 expression between the insulin-treatment and M^{pro}-treated groups, ****$p<0.0001$.

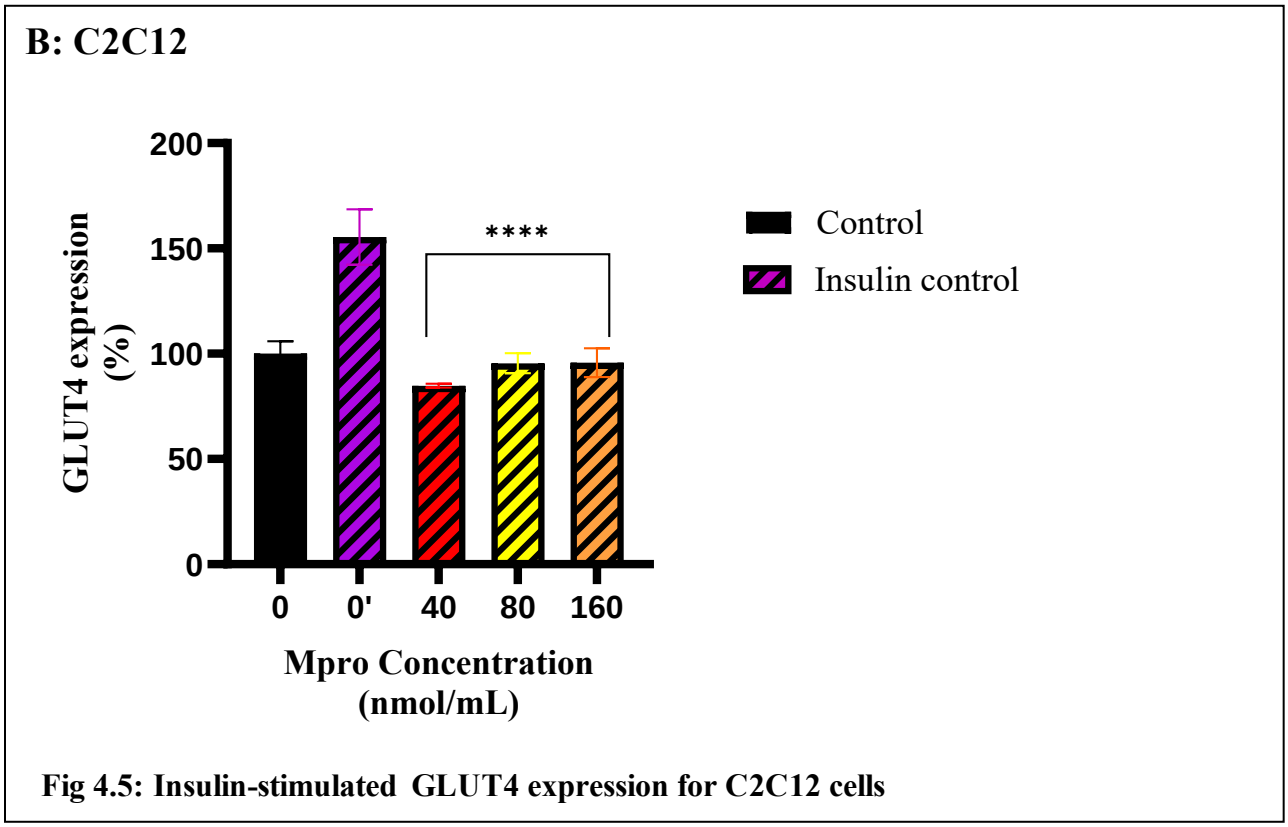

Fig 4.5: Insulin-stimulated GLUT4 expression for C2C12 cells

Figure 4.5: GLUT4 expression was estimated after treating the C2C12 cell with M^{pro} for 24 hours at the different concentrations of 40,80 and 160 nmol/mL. Following M^{pro} treatment, insulin was administered for 6 hours. The values are expressed as mean ± SD represented with error bars, (n = 3). Results are expressed as a percentage. Untreated cells are presented as 0 while 0' represents insulin-treated cells. The insulin group cells were used as the control group. The asterisk (*) represents the statistical difference between the test compounds and the control at (****) $p < 0.0001$.

4.3.2 Relative GLUT4 translocation

The relative appearance of GLUT4 at the surface of the cell was assessed following treatment with M^{pro} at different concentrations of 40 to 160 nmol/mL as shown in Figure 4.6. There is a slight decrease in the appearance of GLUT4 for 40 nmol/mL and 80 nmol/mL M^{pro} treatment groups, followed by a slight increase for the 160 nmol/mL concentration compared to the control (untreated) cells. There was no statistically significant difference between the control (untreated cells) and all treatment conditions. Overall, the results suggest that M^{pro} does not affect the availability of cell surface GLUT4.

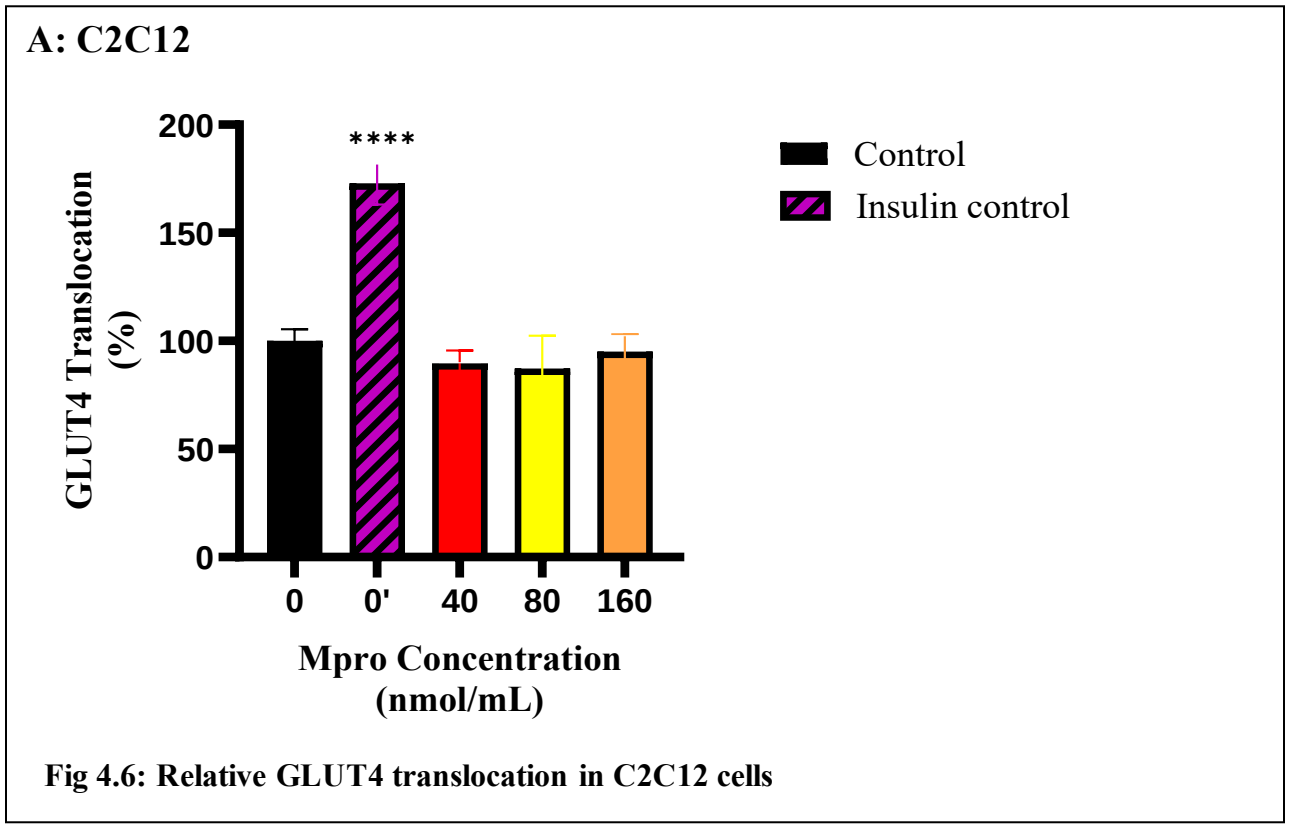

Fig 4.6: Relative GLUT4 translocation in C2C12 cells

Figure 4.6: GLUT4 translocation was estimated after treating the C2C12 cell line with M^{pro} for 24 hours at the different concentrations of 40, 80 and 160 nmol/mL. The values are expressed as mean ± SD represented with error bars, (n = 3). Results are expressed as a percentage. Untreated cells are presented as 0 while 0' represents insulin-treated cells. Untreated cells were used as the control group. The asterisk (*) represents the statistical difference between the test compounds and the control at (***) $p < 0.001$ and (****) $p < 0.0001$.

Following M^{pro} treatment, insulin treatment was done for 5 hours to activate GLUT4 translocation. Figure 4.7 below displays the percentage of the GLUT4 that translocated to the plasma membrane for the C2C12 cell line. Insulin-treated group (insulin only) showed a significant increase in GLUT4 translocation compared to the control (untreated) cells. Statistically significant differences were observed between the M^{pro} treatment +insulin compared to insulin-treated group. Overall, insulin was unable to effectively allow for GLUT4 translocation in the presence of M^{pro} at all concentrations.

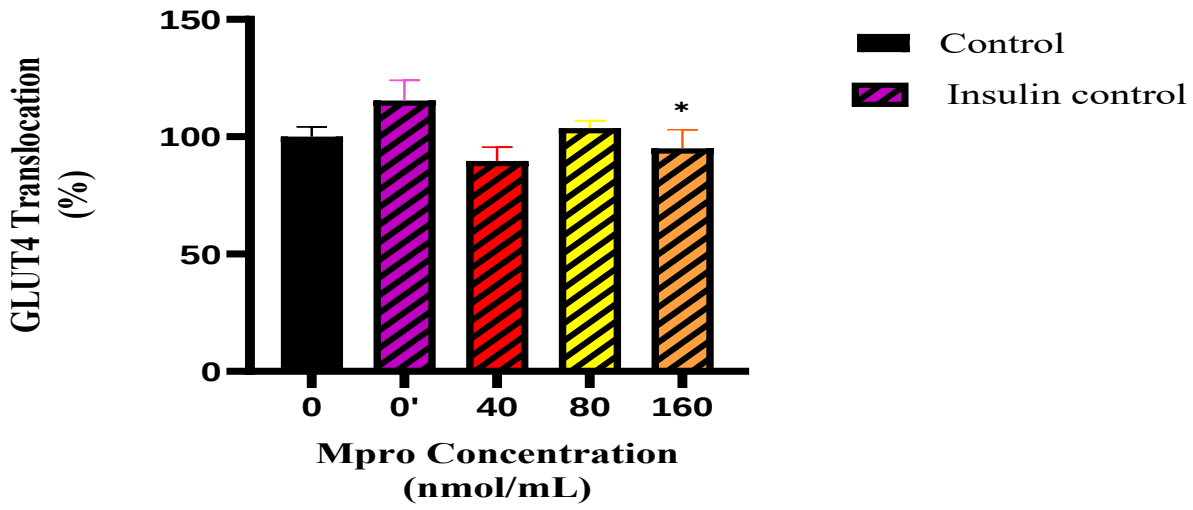

Fig 4.7 : Insulin-stimulated GLUT4 translocation in C2C12 cells

Figure 4.7: GLUT4 translocation was estimated after treating the C2C12 cell line with M^{pro} for 24 hours at the different concentrations of 40, 80 and 160 nmol/mL. The values are expressed as mean ± SD represented with error bars, (n = 3). Results are expressed as a percentage. Untreated cells are presented as 0 while 0' represents insulin-treated cells. Insulin-treated cells were used as the control group. The asterisk (*) represents the statistical difference between the test compounds and the control at (*) $p < 0.05$.

4.3.3 Effect on AKT expression

To assess any disturbances in the insulin signaling pathway, baseline expression of AKT production were analyzed in the C2C12 and HepG2 cell lines after M^{pro} treatment at concentrations of 40 to 160 nmol/mL as illustrated in Figures 4.8A and 4.8B, respectively. In the C2C12 cell line, Figure 4.8A shows a steady decline in AKT production levels, as the concentration of M^{pro} increased. The decrease suggests a dose-dependent relationship, with the highest concentration of M^{pro} showing the most significant reduction in baseline AKT expression when compared to the control (untreated) cells. At 80 and 160 nmol/mL, there is a slight decline in AKT expression, though this change is not statistically significant. This suggests that M^{pro} does not drastically alter baseline AKT expression in C2C12 cells. In contrast, the HepG2 cell line exhibits AKT levels maintained close to the control (untreated) cells, as shown in Figure 4.8B. For both cell lines, there was no statistically significant difference from the control.

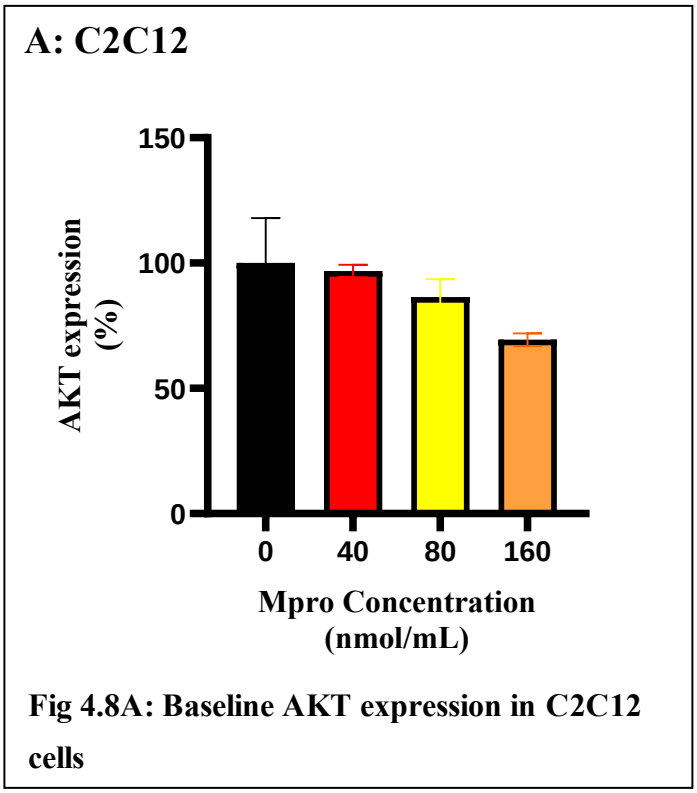

Fig 4.8A: Baseline AKT expression in C2C12 cells

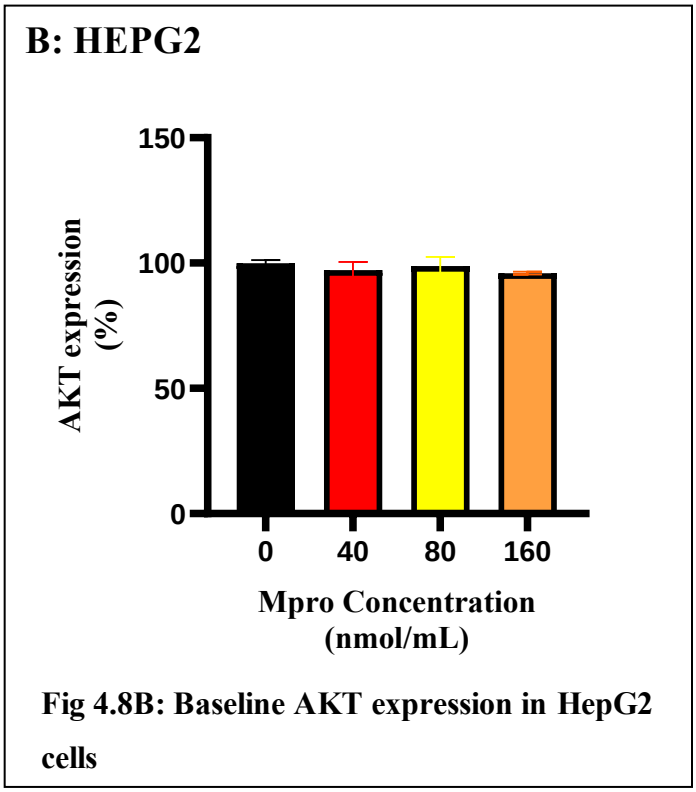

Fig 4.8B: Baseline AKT expression in HepG2 cells

Figure 4.8: The relative AKT expression was estimated after treating C2C12 and HepG2 cell lines with M^{pro} for 24 hours at 40 ,80 and 160 nmol/mL concentrations. The values are expressed as mean ± SD represented with error bars, (n = 3). Results are expressed as a percentage.

4.3.4 Effect on insulin stimulated AKT expression

Insulin is a known activator of the AKT pathway, making insulin-treated cells an effective positive control to confirm the robustness of the experimental setup and detection methods. To provide a comprehensive understanding of how treatments affect AKT expression under different conditions, a co-administration of insulin and M^{pro} was performed.

To assess the pathway-activated levels of AKT production, we analyzed the relative expression of AKT in the C2C12 and HepG2 cell lines after co-treatments of insulin and M^{pro}, as shown in Figures 4.9A and 4.9B, respectively. In the C2C12 cell line, the insulin control, showed that there was a significant enhancement of AKT expression, confirming the activation of the insulin pathway. Figure 4.9A shows that the AKT levels remain relatively consistent across all concentrations of M^{pro} (40, 80 and 160 nmol/mL) when co-administered with insulin-only control No significant change was observed compared to insulin control indicating that in C2C12 muscle cells, M^{pro} does not seem to significantly impair insulin's ability to activate the AKT pathway, even at higher concentrations. In contrast, Figure 4.9B shows a decrease in insulin-stimulated AKT production in the HepG2 cell line with increasing concentrations of M^{pro}. At 40 nmol/mL, AKT expression is significantly lower compared to insulin control ($p < 0.01$) and this reduction becomes even more pronounced at 80 and 160 nmol/mL, with the latter showing a highly significant decrease ($p < 0.0001$).

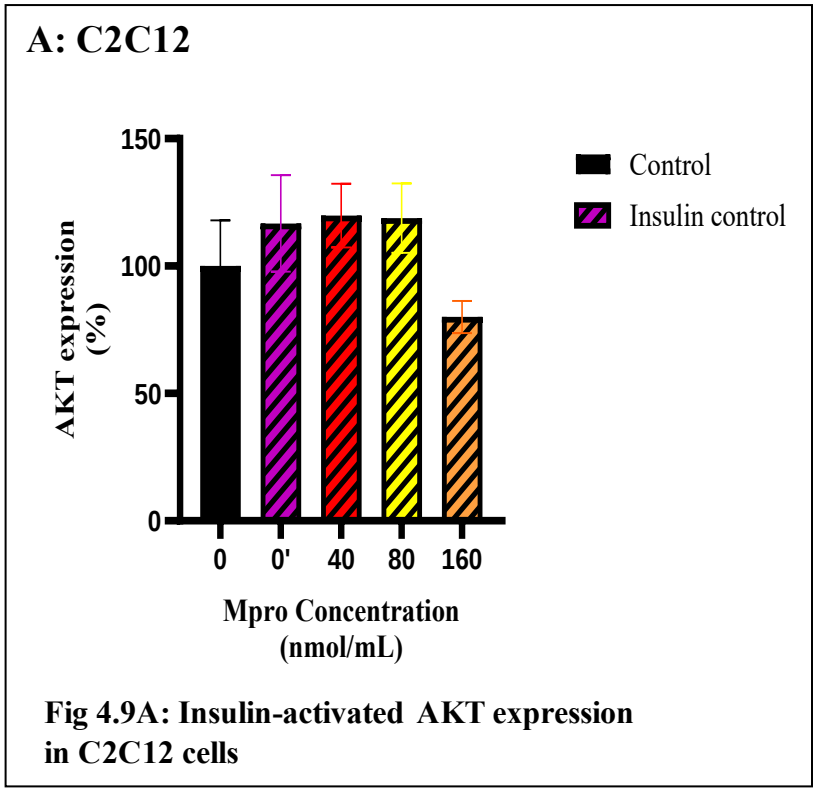

Fig 4.9A: Insulin-activated AKT expression in C2C12 cells

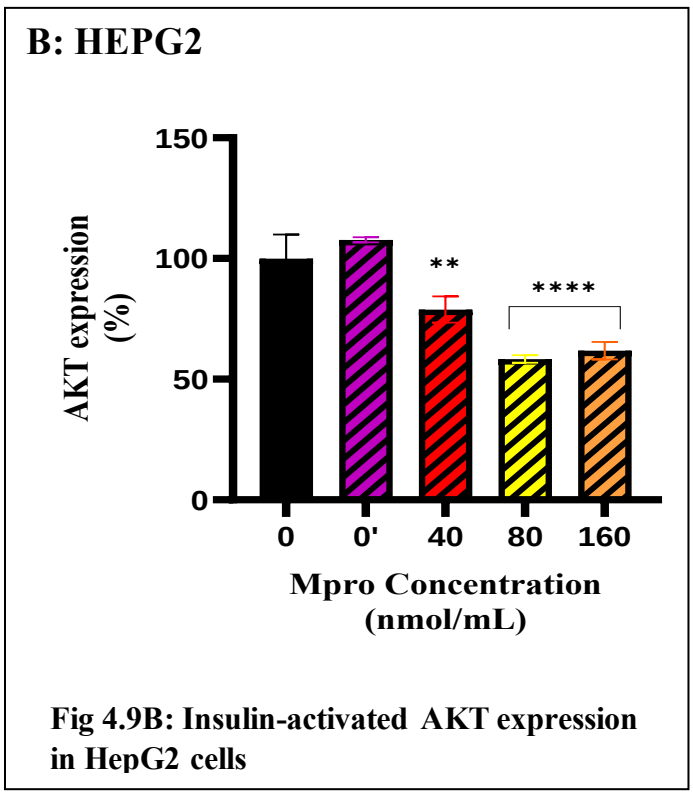

Fig 4.9B: Insulin-activated AKT expression in HepG2 cells

Figure 4.9: The relative expression of AKT was estimated after treating C2C12 and HepG2 cell lines with M^{pro} (40,80 and 160 nmol/mL). The values are expressed as mean ± SD represented with error bars, (n = 3). Results are expressed as a percentage. Untreated cells are presented as 0 while 0' represents insulin-treated cells. Insulin-treated cells were used as the control group. The asterisk (*) represents the statistical difference between the test compounds and the control at (**) $p < 0.01$ and (****) $p < 0.0001$.

4.3.5 Relative cellular DPP4 expression

Intracellular DPP4 levels were assessed in the C2C12 and HepG2 cell lines after 24-hour treatment with M^{pro} at the different concentrations of 40,80 and 160 nmol/mL, with the results presented in Figures 4.10A and 4.10B, respectively. In the C2C12 cell line, there is a decline in DPP4 expression as the concentration of M^{pro} increases by comparison to the control (untreated) cells. Statistically significant differences were observed between all the M^{pro} treatment and control groups at * $p< 0.05$ for 40 nmol/mL, **$p < 0.01$ for 80 nmol/mL and ***$p < 0.001$ for 160 nmol/mL

revealing a relatively more pronounced effect of M^{pro} with increasing concentrations. Conversely, in the HepG2 cell line, there is an increase in DPP4 expression with higher M^{pro} concentrations by comparison to the control (untreated) cells. Statistically significant differences were observed between all the treatment and control groups at ****p<0.0001.

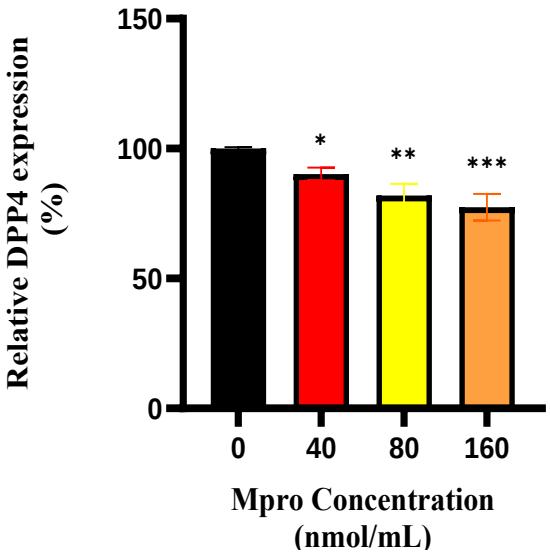

Fig 4.10A: DPP4 expression in C2C12 cells

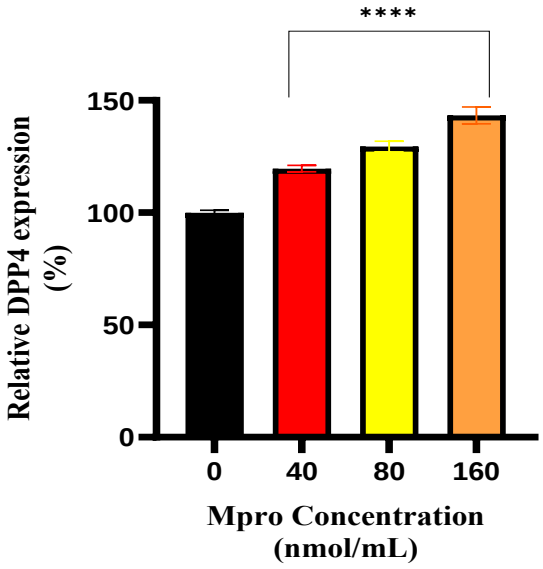

Fig 4.10B: DPP4 expression in HepG2 cells

Figure 4.10: The relative expression of DPP4 was estimated after treating C2C12 and HepG2 cell lines with M^{pro} for 24 hours at the different concentrations of 40, 80 and 160 nmol/mL. The values are expressed as mean ± SD represented with error bars, (n = 3). Results are expressed as a percentage. Untreated cells were used as the control group. The asterisk (*) represents the statistical difference between the test compounds and the control at (*) $p < 0.05$, (**) $p < 0.01$, (***) $p < 0.001$ and (****) $p < 0.0001$.

4.3.6 Relative medium DPP4 concentration

To further evaluate DPP4 shedding, cell culture media was collected and an ELISA was performed to assess the release of the membrane-bound form of DPP4 after treating with M^{pro}. Figures 4.11A

and 4.11B illustrate the relative percentage of DPP4 released into cell culture medium in the C2C12 and HepG2 cell lines, respectively. In the C2C12 cell line, there is a sharp increase in medium DPP4 levels at lower concentrations of M^{pro}, followed by a decline at higher concentrations which still above the control group. DPP4 release into the medium increases with the 40 nmol/mL concentration of M^{pro}, peaking at this point, although the difference is not statistically significant compared to the control.

For the HepG2 cell line, there is a decrease in DPP4 levels for all treatment concentrations when compared to the control. No statistically significant differences were found between the treatment and control groups.

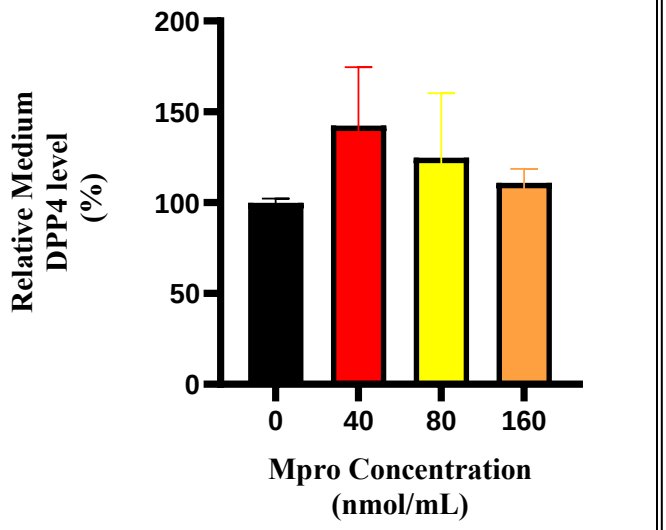

Fig 4.11A: Medium DPP4 level in C2C12 cells

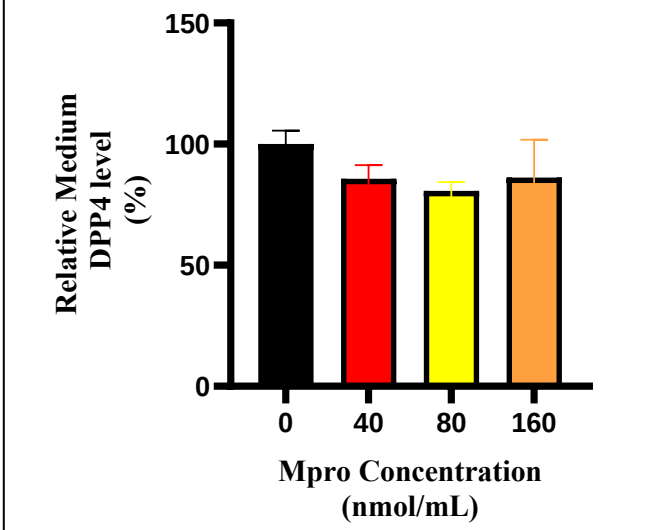

Fig 4.11B: Medium DPP4 level in HepG2 cells

Figure 4.11: The relative expression of medium DPP4 was estimated after treating C2C12 and HepG2 cell lines with M^{pro} for 24 hours at 40, 80 and 160 nmol/mL concentrations. The values are expressed as mean ± SD represented with error bars, (n = 3). Untreated cells were used as the control group.

4.3.7 Medium interleukin-6 (IL-6) concentration

Figures 4.12A and 4.12B depict the relative percentage medium expression of IL6 in C2C12 and HepG2 cell lines treated with M^{pro} at concentrations of 40, 80 and 160 nmol/mL, respectively. For the C2C12 cells, the results show an increase in the cellular expression of IL-6 compared to the control(untreated) cells with the highest peak being for the highest concentration of M^{pro}. No statistically significant difference was found between the control and treatment groups, except at the 160 nmol/mL concentration.

In HepG2 cells, the results show a dose-dependent increase in intracellular expression of IL-6 showing a substantial rise compared to the control (untreated) cells. Statistically significant differences were observed between the control and the higher treatment groups (80 and 160 nmol/mL) at ***($p<0.001$).

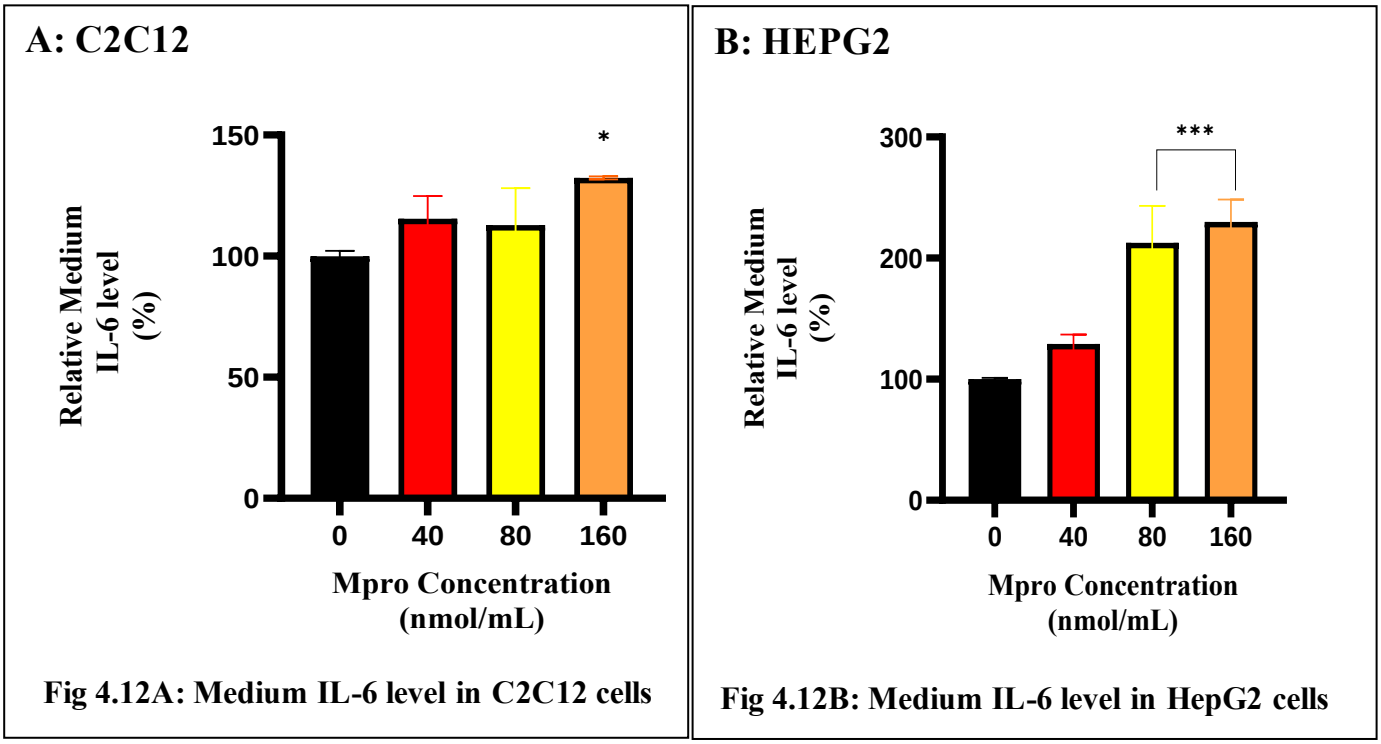

Fig 4.12A: Medium IL-6 level in C2C12 cells

Fig 4.12B: Medium IL-6 level in HepG2 cells

Figure 4.12: The relative expression of IL-6 in cell medium was estimated after treating C2C12 and HepG2 cell lines with M^{pro} for 24 hours at the different concentrations of 40, 80 and 160 nmol/mL respectively. The values are expressed as mean ± SD represented with error bars, (n = 3). Results are expressed as a percentage. Untreated cells were used as the control group. The

asterisk (*) represents the statistical difference between the test compounds and the control at (*) $p < 0.05$ and (***) $p < 0.001$.

4.3.8 Cellular interleukin-6 (IL-6) expression

An intracellular ELISA was conducted to gain insight into IL-6 expression within cells and understand cytokine production at the cellular level. Figures 4.13A and 4.13B illustrate the relative percentage in-cell expression of IL-6 in the C2C12 and HepG2 cell lines. In Figure 4.13A, a notable upregulation of IL-6 expression is observed in the C2C12 cells for all the different treatment concentrations compared to the control (untreated) cells. Statistically significant differences were observed between the treatment and control groups, ***$p<0.001$ suggesting that M^{pro} upregulates the expression of IL-6 in C2C12 cells. Conversely, the HepG2 cell line in Figure 4.13B exhibits a modest increase in IL-6 expression with the 80 and 160 nmol/mL concentrations showing a statistical difference compared to the control at ***$p<0.001$ and ****$p<0.0001$. However, the results show that M^{pro} does not result in a significant upregulation of IL-6 synthesis in HepG2 cells. Unlike in C2C12 cells, the expression of IL-6 in HepG2 cells is significantly lower, suggesting that even M^{pro} induces an inflammatory response differently in the different cell lines.

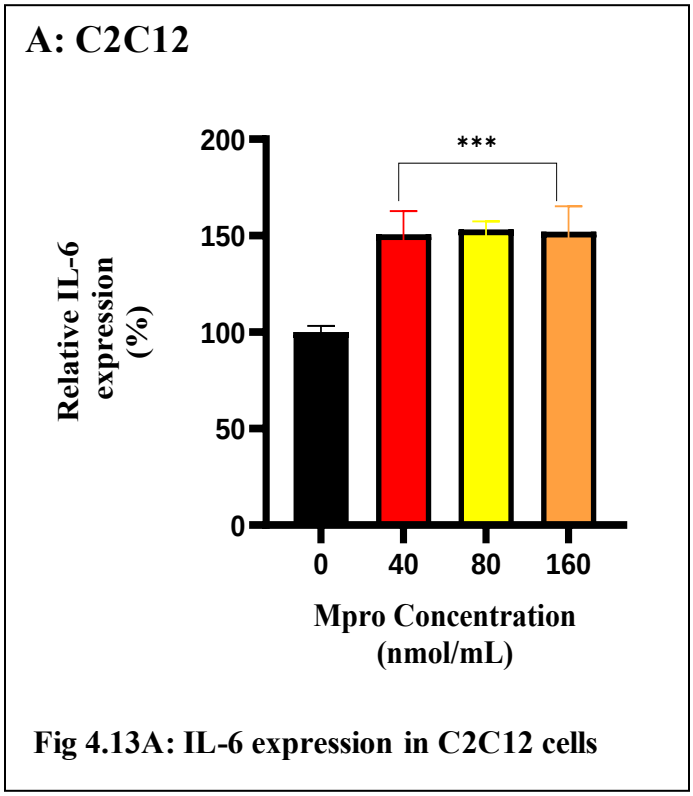

Fig 4.13A: IL-6 expression in C2C12 cells

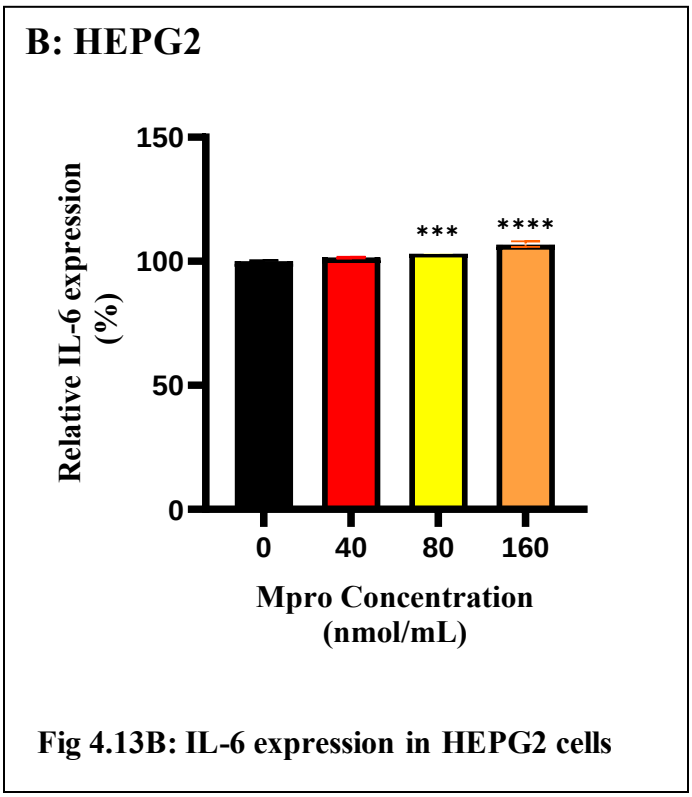

Fig 4.13B: IL-6 expression in HEPG2 cells

Figure 4.13: The relative cell expression of IL-6 was estimated after treating C2C12 and HepG2 cell lines with M^{pro} of 40, 80 and 160 nmol/mL respectively. The values are expressed as mean ± SD represented with error bars, (n = 3). Results are expressed as a percentage. Untreated cells were used as the control group. The asterisk (*) represents the statistical difference between the test compounds and the control at (***) $p < 0.001$ and (***) $p < 0.001$.

4.3.9 Relative cellular MMP1 expression

The relative expression of MMP1 was estimated after treating C2C12 and HepG2 cell lines with M^{pro} for 24 hours at the different concentrations of 40,80 and 160 nmol/mL as shown in Figures 4.14A and 4.14B, respectively. In the C2C12 cell line, Figure 4.14A depicts a decrease in MMP1 expression with increasing concentrations of M^{pro}. MMP1 expression remains close to the control level, showing a slight but non-significant reduction for the lowest M^{pro} concentration,40 nmol/mL. There is a significant decrease ($p < 0.01$) in MMP1 expression. A more pronounced reduction in MMP1 expression is observed for 160 nmol/mL (***$p < 0.001$), suggesting a strong effect of M^{pro} on MMP1 expression at high concentrations. Statistically significant differences

were observed between the treatment and control (untreated) cells at (**p<0.01) and (***p<0.001). In contrast, Figure 4.14B shows no significant change in MMP1 expression from the control in the HepG2 cell line for all concentrations of M^{pro}. No statistically significant difference was observed for the HepG2 cell line.

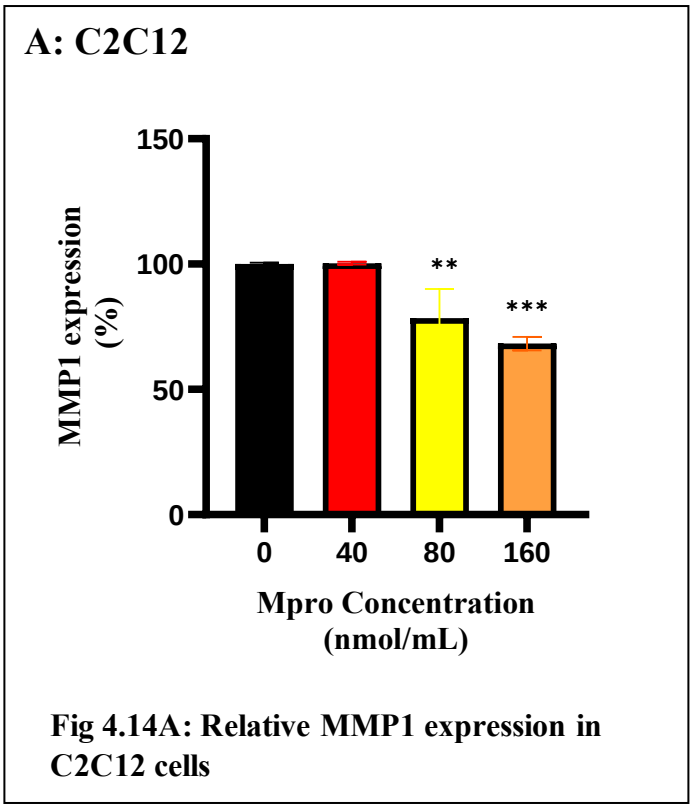

Fig 4.14A: Relative MMP1 expression in C2C12 cells

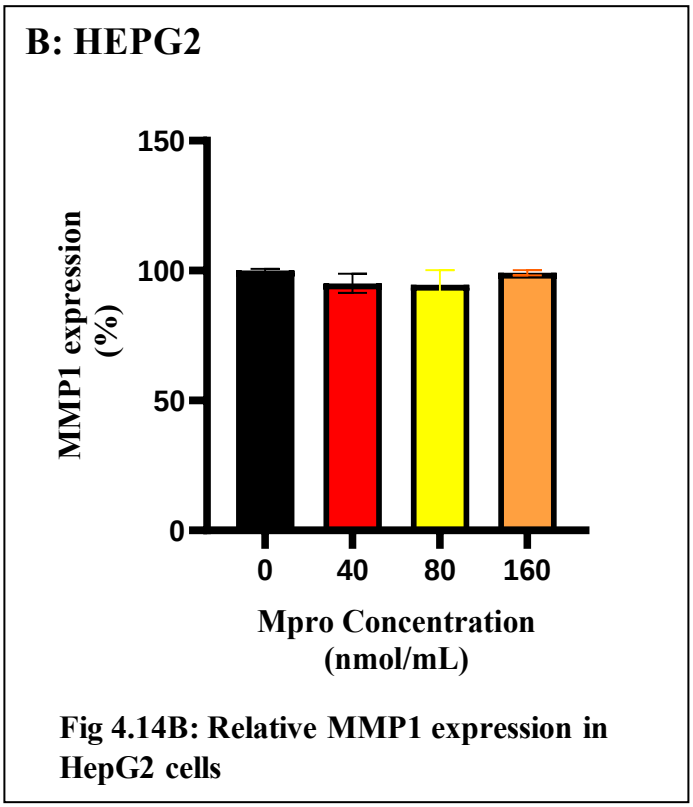

Fig 4.14B: Relative MMP1 expression in HepG2 cells

Figure 4.14: The relative expression of MMP1 was estimated after treating C2C12 and HepG2 cell lines with M^{pro} at the different concentrations of 40,80 and 160 nmol/mL. The values are expressed as mean ± SD represented with error bars, (n = 3). Results are expressed as a percentage. Untreated cells were used as the control group. The asterisk (*) represents the statistical difference between the test compounds and the control at (**) $p < 0.01$ and (***) $p < 0.001$.

4.3.10 Relative medium MMP1 concentration

To further evaluate extracellular MMP1, cell culture media was collected and an ELISA was performed to assess the release of the membrane-bound MMP1. Figures 4.15A and 4.15B illustrate the relative percentage expression of MMP1 in the media of C2C12 and HepG2 cell lines,

respectively. In the C2C12 cell line, there is a slight decrease in MMP1 levels for the treatments compared to the control (untreated) cells. In contrast, the HepG2 cell line shows a sharp increase in MMP1 levels, with the highest increase observed at 160 nmol/mL when compared to the control (untreated) cells. For the C2C12 cell line, no statistically significant differences were found between the treatment and control groups. However, for the HepG2 cell line, statistically significant differences were observed between the 160 nmol/mL treatment and control group at $p<0.05$.

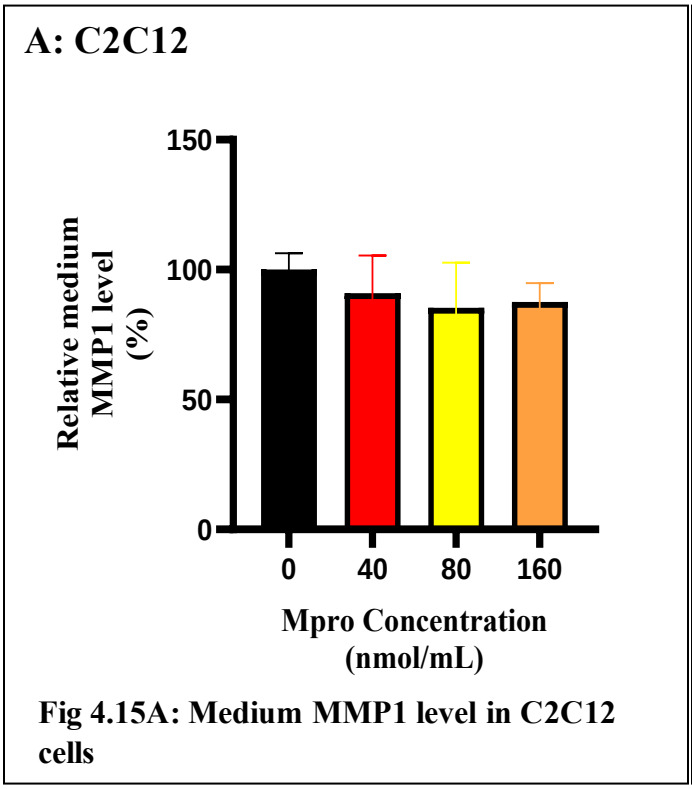

Fig 4.15A: Medium MMP1 level in C2C12 cells

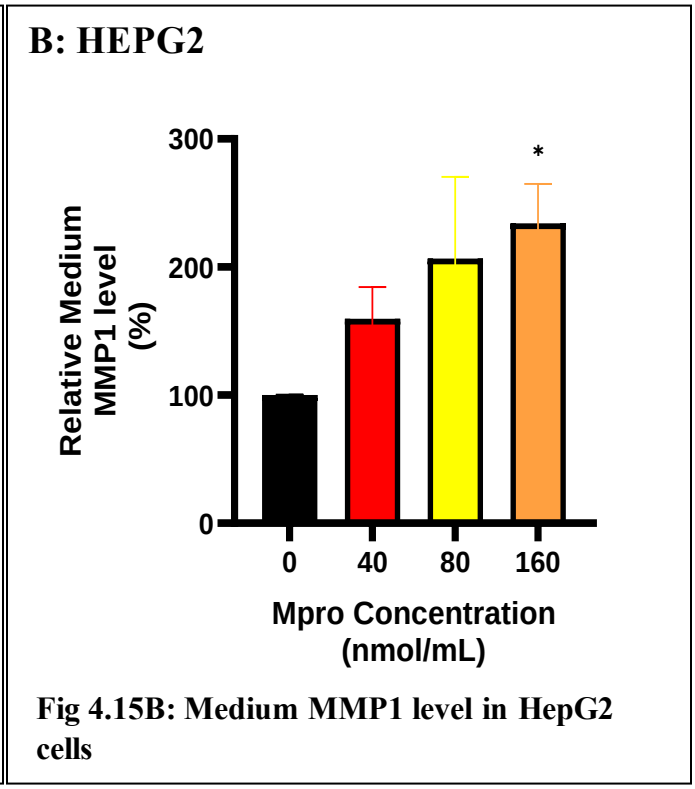

Fig 4.15B: Medium MMP1 level in HepG2 cells

Figure 4.15: The relative concentration of medium MMP1 was estimated after treating C2C12 and HepG2 cell lines with M^{pro} for 24 hours at the different concentrations of 40,80 and 160 nmol/mL. The values are expressed as mean ± SD represented with error bars, (n = 3). Results are expressed as a percentage. Untreated cells were used as the control group. The asterisk (*) represents the statistical difference between the test compounds and the control at *($p< 0.05$).

4.4 Relative MDA concentration

Figures 4.16A and 4.16B depict the relative percentage medium malondialdehyde (MDA) concentration in C2C12 and HepG2 cell lines treated with M^{pro} at concentrations of 40, 80 and 160 nmol/mL, respectively. In C2C12 cells, MDA levels in the medium increase with an increase in M^{pro} concentration with 40 nmol/mL M^{pro} resulting in a slight, non-significant increase. At 80 nmol/mL, MDA levels rose further, although not statistically significant, compared to the control (untreated) cells. The highest concentration of M^{pro} (160 nmol/mL) led to a statistically significant increase in MDA levels ($p < 0.01$), indicating enhanced oxidative stress at this concentration. This dose-dependent rise in MDA suggests that M^{pro} treatment induces oxidative stress in C2C12 cells, especially at higher concentrations.

A similar trend was observed in HepG2cells.The MDA levels also exhibit a dose-dependent increase with M^{pro} concentration. The findings for the HepG2 cell line showed no statistically significant differences between the treatment groups (40 and 80 nmol/mL) and the control group except at 160 nmol/mL* $p<0.05$.

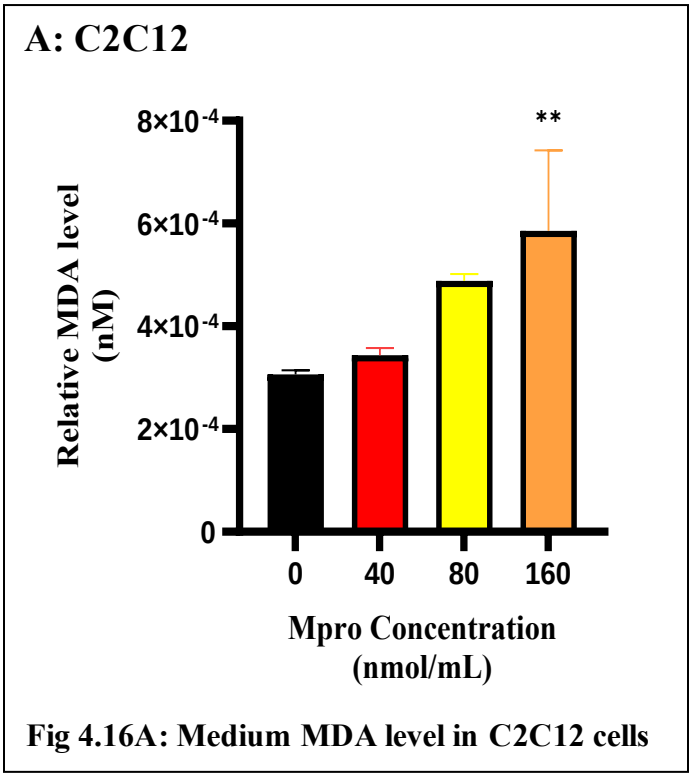

Fig 4.16A: Medium MDA level in C2C12 cells

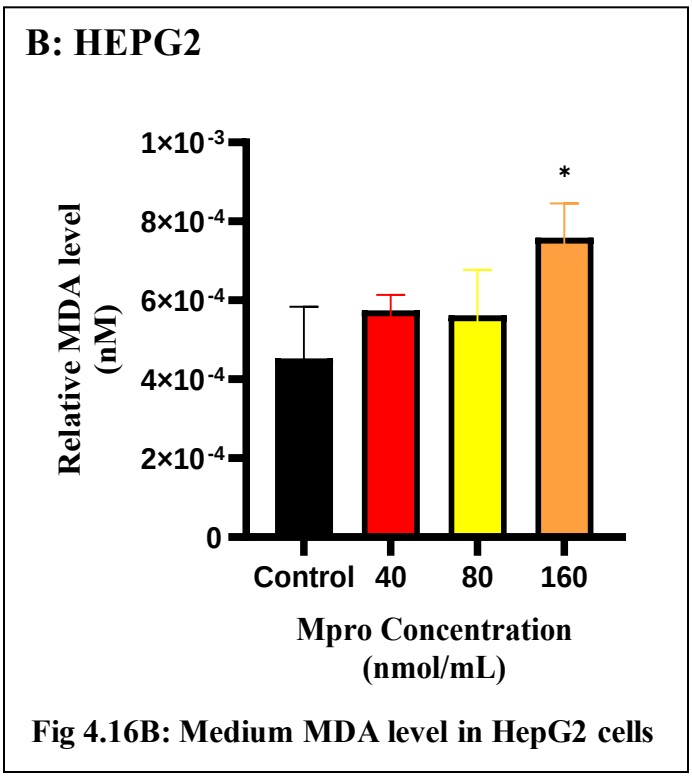

Fig 4.16B: Medium MDA level in HepG2 cells

Figure 4.16: The relative concentration of medium MDA was estimated after treating C2C12 and HepG2 cell lines with M^{pro} for 24 hours at the different concentrations of 40,80 and 160 nmol/mL. The values are expressed as mean ± SD represented with error bars, (n = 3). Results are expressed as a percentage. Untreated cells were used as the control group. The asterisk (*) represents the statistical difference between the test compounds and the control at *($p< 0.05$) and **($p<0.01$).

4.5 Relative fluorescence of ROS in C2C12

Figure 4.17 indicates a concentration-dependent increase in relative fluorescence in the C2C12 cell line. At the lowest concentration (40 nmol/mL), there is a modest increase in fluorescence compared to the control (untreated cells), though this increase is not statistically significant. However, at higher concentrations (80 and 160 nmol/mL), the fluorescence significantly increases, with statistical significance denoted by ** ($p < 0.01$) and **** ($p < 0.0001$), respectively when compared to the control (untreated cells).

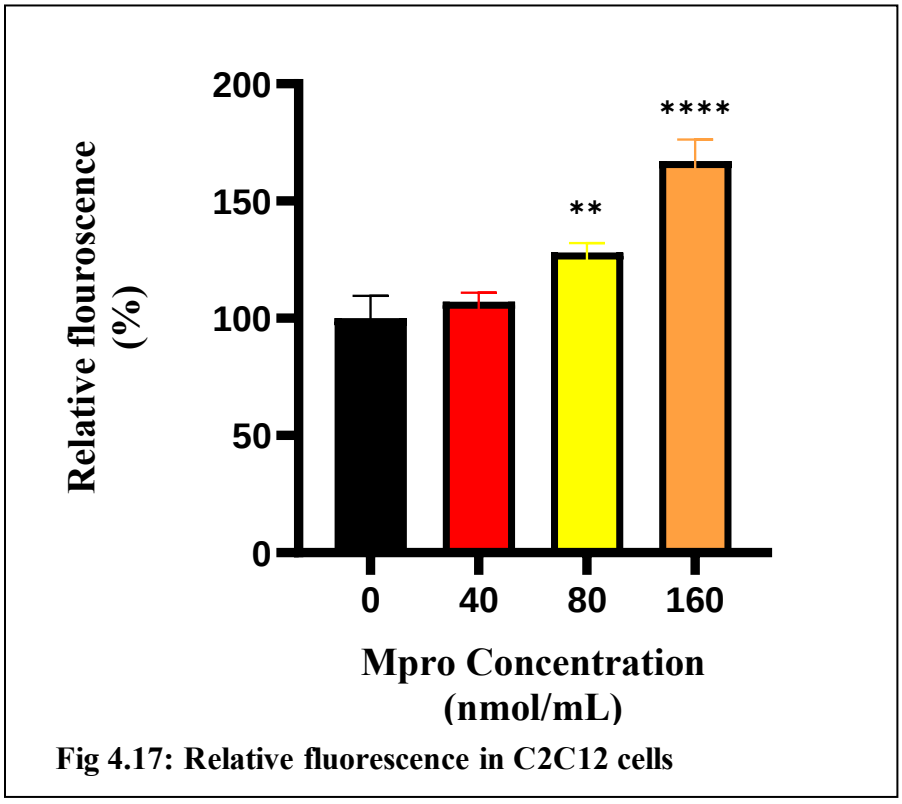

Fig 4.17: Relative fluorescence in C2C12 cells

Figure 4.17: The fluorescence level of the C2C12 cell line was estimated after treatment with M^{pro} for 24 hours at the different concentrations of 40,80 and 160 nmol/mL. The values are expressed as mean ± SD represented with error bars, (n = 3). Results are expressed as a percentage of the control group. The asterisk (*) represents the statistical difference between the test compounds and the control at **($p< 0.01$) and ****($p<0.0001$).

4.6 Relative insulin/M^{pro} Interaction

Figure 4.18 illustrates a solid-phase analysis designed to investigate potential interactions between M^{pro} and insulin. Two conditions were assessed: M^{pro}-only (solid bars) and M^{pro} in the presence of insulin (striped bars). The M^{pro}-only condition served as a form of a control to test whether the anti-insulin antibody non-specifically binds to M^{pro}. Across all concentrations tested (40, 80 and 160 nmol/mL), we see a relatively modest binding compared to the insulin-only control, although non-specific binding could be observed as the M^{pro} concentrations increase. There was no statistically significant difference between the insulin-only control solid bars, except at the 40 nmol/mL concentration, where a slight reduction in anti-insulin antibody non-specific interaction signal was observed. For the analysis of M^{pro}-insulin binding, insulin as introduced in plate coated with different M^{pro} concentration, followed by capturing the complex with an insulin antibody. The results (the stripped bars) suggest that the insulin could bind to M^{pro}. However, considering the observation was like the non-specific binding of insulin antibody on M^{pro}, the results can be interpreted as very minimal interaction took place between insulin-M^{pro}.

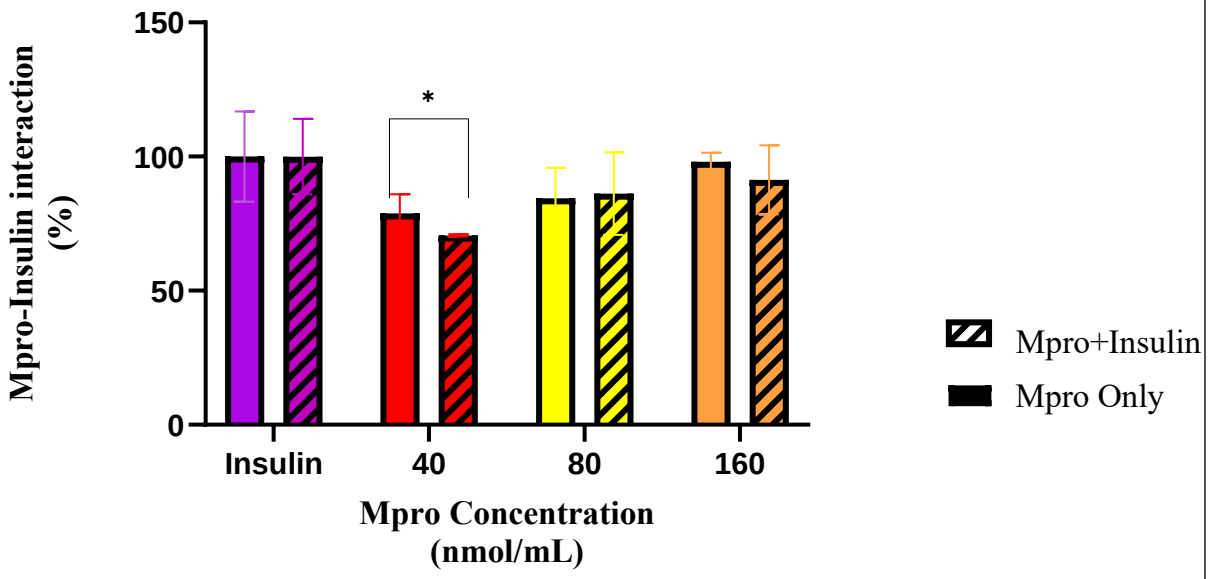

Fig 4.18: Solid phase analysis of M^{pro} and insulin

Figure 4.18*:* Solid-phase analysis of M^{pro}-insulin interaction at varying concentrations. The graph displays the interaction levels of M^{pro} with insulin at concentrations of 40, 80 and 160 nmol/mL. For the solid-phase analysis, the insulin only was the control. The asterisk (*) represents the statistical difference between the test compounds and the control at * $p<0.05$.

4.7 In-silico studies

Computational docking of PI3K, GLUT4, insulin receptor kinase domain and insulin yielded 30 different cluster conformations and binding strengths for each protein. The different clusters were ranked based on the number of poses per cluster. The interactions resulting in the lowest binding energy among the given model clusters were identified and visualized using the PyMOL tool. The structure of M^{pro} is shown in Figure 4.19 highlighting the near-native structure found physiologically. Fig 4.19 helps to aid the visualization of the different chains of M^{pro}.

Docking simulations between SARS-CoV-2 main protease (PDBID 7CAM) and insulin (PDBID 3I40) identified Cluster 0, the most populated cluster, containing 138 poses, reflecting high stability and consistency in the binding orientation. The cluster centre had a weighted score of -654.4, while the lowest energy pose recorded a weighted score of -795.9, indicating a strong and favourable binding interaction. The docking simulation between M^{pro} and insulin was the most favourable out of all the proteins tested. The interaction is shown in Figure 4.20 below.

The docking results for SARS-CoV-2 main protease (PDBID 7CAM) and the insulin receptor kinase domain (PDBID 1IRK) revealed that the top-ranked cluster, Cluster 0 contained 63 poses, indicating a relatively strong conformation. Weighted scores, reflecting binding energy, ranged from -794.0 for the cluster centre to -827.4 for the lowest-energy pose. The interaction is shown in Figure 4.21 below.

The docking results for SARS-CoV-2 main protease (PDBID 7CAM) and PI3K (PDBID 4JPS) yielded Cluster 0 which was characterized by 68 poses. The cluster centre had a weighted score of -804.6, while the lowest energy pose exhibited a significantly favourable binding energy of -1144.0. This suggests a relatively stable interaction between the two molecules. The interaction is shown in Figure 4.22 below.

Lastly, the docking analysis for SARS-CoV-2 main protease (PDBID 7CAM) and GLUT4 (PDBID 7WSM) revealed that Cluster 0 contained 52 poses, therefore representing the protein with the lowest probability of interaction with M^{pro}. The cluster centre had a weighted score of -1322.0, with the lowest energy pose achieving a weighted score of -1391.0, indicative of a strong and favourable interaction between M^{pro} and GLUT4.The interaction is shown in Figure 4.23 below. Table 4.1 provides a summary of the different protein-protein interactions as well as the binding energies.

Table 4.1: The binding energies of each protein-protein interaction

Protein (Receptor)	Protein (Ligand)	Binding energy
M^{pro}(7CAM)	Insulin(3I40)	-795.9

Insulin receptor(1IRK)	M^{pro}(7CAM)	-827.4
PI3K(4JPS)	M^{pro}(7CAM)	-1144.0
GLUT4(7WSM)	M^{pro}(7CAM)	-1391.0

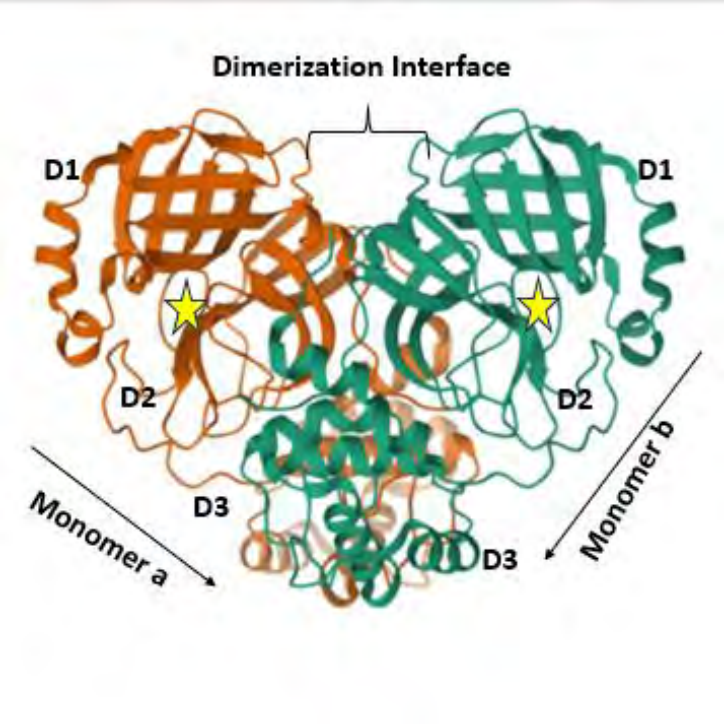

Figure 4.19: Dimer structure of the SARS-CoV-2 M^{pro} (PDB 7CAM) with the three domains shown. The black arrows and the dimerization interface labelled show the orientation of the two dimers. Yellow stars denote the catalytic site where the catalytic dyad residues (His41 and Cys145) are found. D1 represents domain 1, D2 represents domain 2 and D3 represents domain 3.

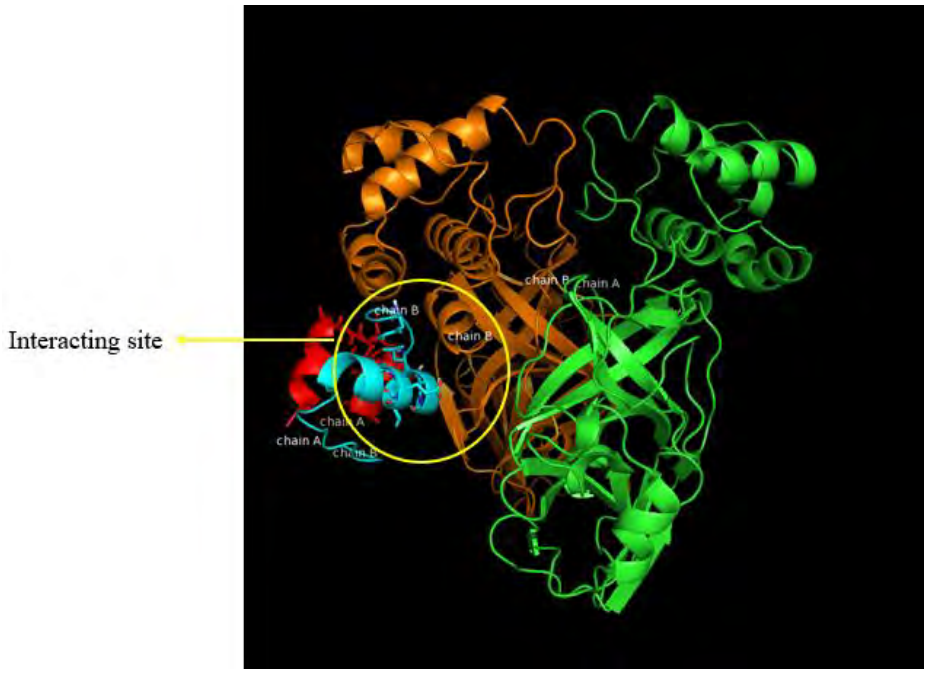

Figure 4.20: Protein-protein docking using ClusPro. Docking of human insulin domain (PDB ID:3I40) and SARS-CoV-2 M^{pro} (PDB ID:7CAM). The binding site of SARS-CoV-2 3CLpro (orange ribbons) with computationally docked insulin alpha (red chain) and beta chains (blue sticks).

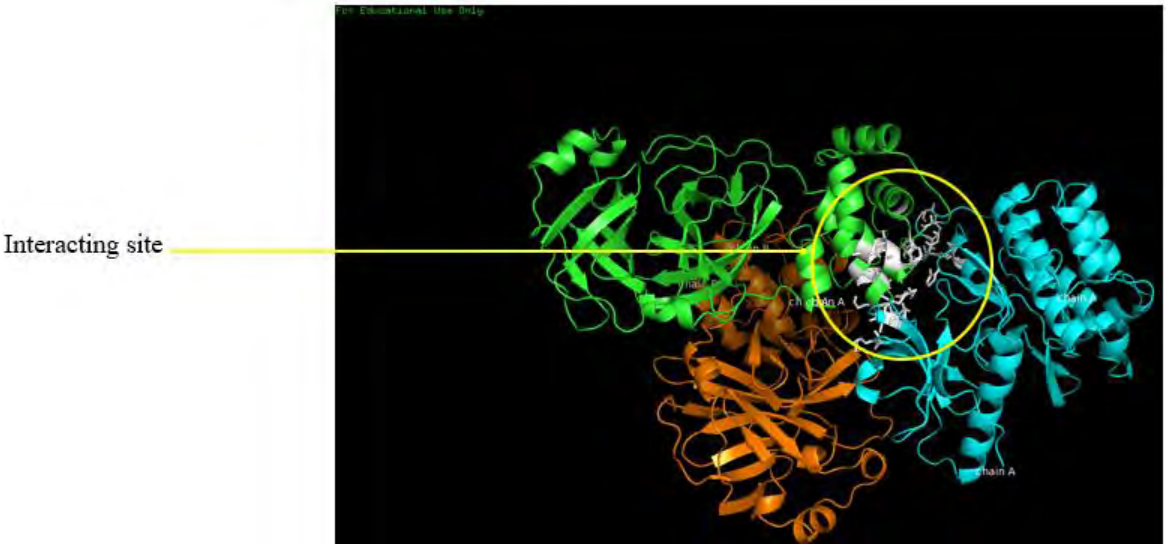

Figure 4.21: Protein-protein docking using ClusPro. Docking of the insulin receptor kinase domain (PDB ID:3I40) and SARS-CoV-2 M^{pro} (PDB ID:7CAM). The binding site of SARS-CoV-

2 M^{pro} (green ribbons) with the insulin receptor kinase domain (blue ribbons). The binding site of the complex is highlighted with grey-white sticks.

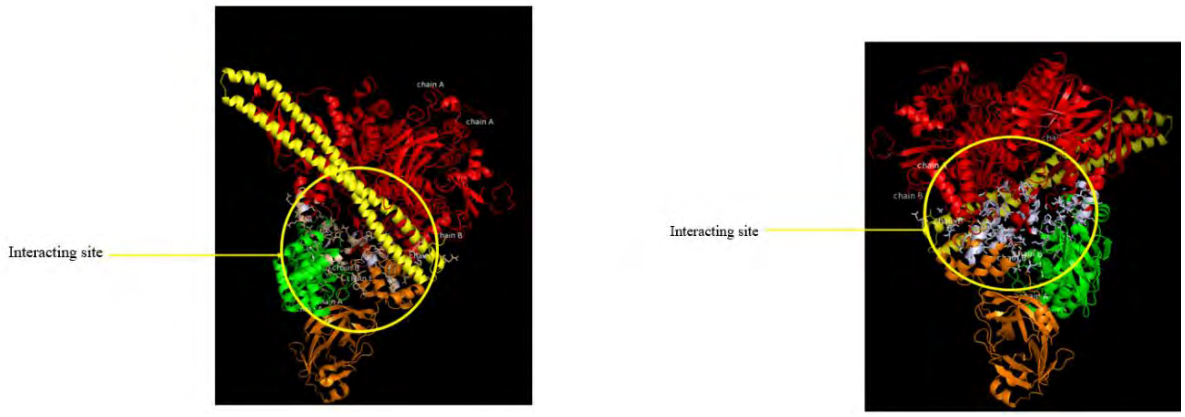

Figure 4.22: Front and back view docking of the PI3K and SARS-CoV-2 M^{pro}. The binding site of SARS-CoV-2 M^{pro} (green and orange surface) with computationally docked PI3K (red ribbons). The binding site of the complex is highlighted with grey-white sticks.

.

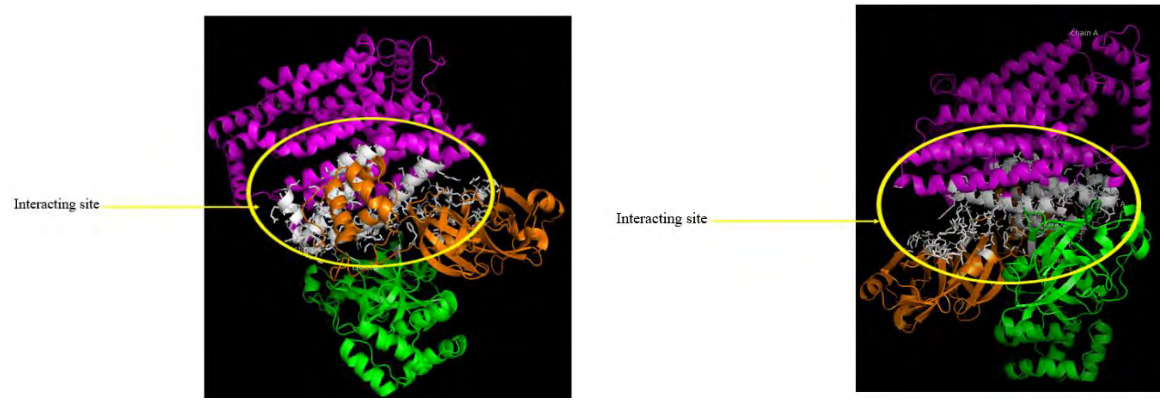

Figure 4.23: The front view and back view of the docking of GLUT4 and SARS-CoV-2 M^{pro}. The binding site of SARS-CoV-2 M^{pro} (green and orange ribbons) with computationally docked GLUT4 (purple ribbons). The binding site of the complex is highlighted with grey-white.

CHAPTER 5: DISCUSSION

Almost half of the COVID-19-related deaths occurred in patients with underlying metabolic and vascular disorders, especially metabolism and endocrine disorders (215). It has been suggested that COVID-19 may adversely affect survivors' endocrine and metabolic systems, including the brain, liver, skeletal muscle and adipose tissue, which could result in new-onset hyperglycaemia or insulin resistance (215). As of yet, COVID-19 remains controversial as to whether it can indirectly or directly lead to new-onset diabetes mellitus, undiagnosed diabetes mellitus, or prediabetes. The increase in diabetic cases, however, post the COVID-19 pandemic has prompted this research into the mechanistic pathways that the SARS-CoV-2 potentially utilizes in inducing DM. Research indicates a link between DM, inflammation and insulin resistance. This therefore makes it imperative to elucidate the mechanisms that are causing the rapid transition from prediabetes to DM in patients with a history of COVID-19 infection. Where such insights are shed, necessary steps and strategies could be employed to stop the transition. Furthermore, elucidating the exact mechanisms that the SARS-CoV-2 virus is utilizing to cause new-onset DM, will help researchers currently exploring new therapies to target DM in compound selection and target site selection. Therefore, this study aimed to assess the tissue-specific effects of SARS-CoV-2 M^{pro} on glucose handling *in vitro* and determine whether any factors would accelerate the transition from prediabetes to DM.

SARS-CoV-2 M^{pro} plays a crucial role in viral replication by proteolytically cleaving the overlapping pp1a and pp1ab into functional proteins. This process is essential for the virus to complete its replication cycle (216). Proteases are not only responsible for cleavage. The use of proteases as receptors, rather than for their proteolytic function is also observed in several other coronaviruses, therefore assessing M^{pro} binding interactions is key (217). From the cytotoxicity study, both cell lines resist M^{pro}-induced cytotoxicity, maintaining relatively high viability at low to moderate concentrations. HepG2 cells, on the other hand, showed a more pronounced dose-dependent decline in viability, particularly at moderate to high concentrations. Hepatic cells may be more vulnerable to protease-induced damage, likely because of their central role in metabolism and detoxification (151). Several theories have been proposed to potentially explain the mechanism of liver injury and failure in COVID-19 patients. One of the theories suggested by Tan

et al speaks to apoptosis of the liver cells via overexpression of one of the SARS-CoV-2 proteins, specifically protein 7a (218). Understanding how viral infections like COVID-19 affect specific tissues would help in guiding targeted therapeutic strategies to protect the more vulnerable organs like the liver. The differences in cytotoxic effects between C2C12 and HepG2 cells highlight how viral protease exposure impacts each tissue type uniquely.

Since DM is characterized by hyperglycaemia, assays to measure the glucose uptake by HepG2 cells and C2C12 were pertinent indicators of glucose handling. Glucose transport is widely regarded as the rate-limiting step in skeletal muscle glucose utilization (131). Skeletal muscles utilize approximately 80% of postprandial glucose from the circulation (192,194). A dose-dependent inhibition of baseline glucose uptake was evident in C2C12 cells with increasing concentrations of M^{pro}. Due to its primary localization on muscle cell surfaces, GLUT1 is considered the key glucose transporter isoform responsible for basal and non-insulin-stimulated glucose transport in skeletal muscle tissue (219). M^{pro} might directly or indirectly affect GLUT1 activity by interacting with GLUT1, altering its structure and function. This could impair the ability of GLUT1 to transport glucose into cells, leading to reduced glucose uptake. Alternatively, M^{pro} might affect signaling pathways that regulate GLUT1 expression or activity leading to downregulation of the transporter. Research has shown that DM is associated with a downregulation of GLUT1 expression in some tissues (220). Therefore, research would be warranted to explore the effect of M^{pro} on GLUT1.

In addition to understanding how M^{pro} affects glucose uptake in basal conditions, we assessed whether M^{pro} would affect insulin-stimulated glucose uptake. Insulin's primary physiological action is to enhance glucose disposal via skeletal muscle glucose transport therefore, it is imperative to understand the extent of the disturbance in the insulin signaling pathway. To investigate this phenomenon, insulin was administered in cells in the presence of M^{pro}. The observations suggest that insulin was unable to effectively mediate glucose uptake as expected, where cells we co-exposed to M^{pro}. As previously stated, the skeletal muscle is capable of reversing whole-body insulin resistance if the insulin resistance is brought on via skeletal muscles (192). Therefore, if M^{pro} is inducing an insulin-resistance state in C2C12 cells, this might be a precipitating factor in the induction of new-onset DM leading us to further evaluate the effect of M^{pro} on the insulin signaling pathway.

Insulin resistance in skeletal muscle has been shown to stem from issues early in the insulin signaling pathway, such as reduced activities of IRTK, IRS1, PI3K and AKT (94,221). Upon activation, the insulin receptor phosphorylates several intracellular substrates, triggering specific signaling pathways. Tyrosine phosphorylation of certain substrates activates PI3K, which generates polyphosphoinositides that interact with protein kinases and ultimately activates the kinase AKT (92,222). PI3K/AKT signaling downstream of insulin receptors plays an important role in glucose uptake and glycogen synthesis in skeletal muscles, according to research (93). Fröjdö et al reported that defects in IRS1-associated PI3K and IRS1 tyrosine phosphorylation activity occurred in insulin-resistant skeletal muscle (221). The results from our in-silico models showed relatively high binding between M^{pro} and PI3K with a binding energy of -1144.0 which could in part suggest that this virus protein could impair the activity of P13K, an important mediator in the insulin signaling pathway. Although detailed residue-specific interactions were not analyzed, the binding energy indicates that the interaction is thermodynamically favourable, potentially leading to functional consequences for PI3K activity. As previously noted, various steps of the insulin signaling pathway are essential for ensuring the correct biological responses to insulin across different tissues. Consequently, disruptions at any point in signal transduction play a significant role in the development of insulin resistance. As such, the M^{pro}-PI3K complex could possibly affect the activation of AKT, resulting in the poor glucose handling observed. As previously mentioned, Akt phosphorylation plays a crucial role in the insulin response mediated by PI3K. To explore this possibility, we evaluated AKT expression in the C2C12 cell line.

The reduction in insulin-stimulated glucose uptake in C2C12 cells could be attributed to various factors such as $M^{pro's}$ interference with the phosphorylation of the downstream effector, AKT in the insulin signaling cascade resulting in impaired translocation of GLUT4 to the plasma membrane or disruption in plasma GLUT4 (133). In the insulin signaling cascade, AKT phosphorylation leads to GSVs release, controlling various stages in the GLUT4 trafficking process such as approaching, tethering, docking and fusing vesicles with the cell membrane (132). Different molecules may help coordinate changes in GLUT4 trafficking when insulin is present, but we focused mainly on AKT for our cell-based assay as it is the upstream regulator of GLUT4 translocation. Researchers have reported that AKT activation alone, unlike other pathways, is enough to drive GLUT4 translocation to the cell membrane, mimicking insulin's effect (132).

The relative cellular expression of AKT in C2C12 cells showed a dose-dependent decrease in AKT expression with an increase in M^{pro} concentration. However, the results showed that M^{pro} has a minimum inhibitory effect on baseline AKT expression since there was no statistical significance. Observations of stable baseline levels of AKT allowed us to further explore $M^{pro's}$ effects in insulin-stimulated AKT expression to ascertain the exact disruption in the insulin signaling pathway. Insulin is also a known activator of AKT and the results for insulin-stimulated AKT expression revealed no significant differences compared to insulin control indicating that in C2C12 muscle cells, M^{pro} does not seem to significantly impair insulin's ability to activate AKT phosphorylation, even at higher concentrations. These findings suggest that the inhibitory effects in the insulin signaling pathway for C2C12 cells could not therefore be fully attributed to AKT. Our results are not surprising as insulin resistance has been documented even in the absence of reduced phosphorylation of AKT and its activation sites across various models, including insulin-resistant 3T3-L1 adipocytes, L6 myotubes and human muscle both *ex vivo* and *in vivo* (122,123,223). Secondly, research by Jaiswal and colleagues on 3T3-L1 adipocytes and mouse muscle has shown that only a small portion of the total cellular pool of AKT needs to be active to achieve maximal phosphorylation of its substrates (224). In other words, if one of the isoforms of AKT is still active, insulin signaling will not be affected. Jaiswal and colleagues further postulated that changes in signaling molecules beyond AKT in skeletal muscle are required to disrupt glucose tolerance and insulin sensitivity *in vivo* (224). Despite the observed interactions between PI3K and M^{pro}, the downstream effector AKT showed to be unaffected. Our results indicated that the poor glucose handling could not be attributed to the impairment of PI3K and AKT, leading us to speculate about a disruption at GLUT4 level.

Since the observed poor glucose handling in the C2C12 cell line remains unexplained, this prompted an investigation into the transporters responsible for facilitating glucose uptake. Several studies have demonstrated that the GLUT4 transporter mediates insulin-stimulated glucose transport in skeletal muscles (225–228). Stockli et al reported that identifying the main factors that cause problems with GLUT4 trafficking will bring significant benefits for treating metabolic diseases (132). The results for the baseline GLUT4 expression showed that there was no significant difference in GLUT4 between the control (untreated) cells and M^{pro}-treated cells. A plausible explanation for the reduction that was observed in insulin-stimulated glucose uptake in the face of relatively unaltered GLUT4 content is a reduction in the translocation of GLUT4. This distinction

between GLUT4 expression and translocation is critical. While expression refers to the total cellular content of GLUT4, translocation reflects the functional redistribution of GLUT4 to the plasma membrane, where it facilitates glucose uptake.

Early research in skeletal muscle showed that GLUT4 levels on the cell surface did not correspond to glucose transport rates, leading researchers to suggest that both GLUT4 translocation and its intrinsic activity regulate glucose transport (229). The idea was initially abandoned but has recently gained renewed attention. With this background, GLUT4 translocation was assessed in baseline and insulin-stimulated conditions. The baseline GLUT4 translocation showed a slight decrease compared to the control (untreated) cells with no statistical difference, suggesting that M^{pro} does not affect the basal translocation of GLUT4. However, upon insulin stimulation, there was no significant increase in GLUT4 presence at the membrane for M^{pro} treatments was observed in contrast with the insulin-only treatment. These observations therefore suggest that M^{pro} presence hindered insulin-stimulated GLUT4 translocation, which may explain reduced glucose uptake when the cells are exposed to the viral protein, M^{pro}.

Studies from as early as 1993 have observed that in both human skeletal muscle and adipose tissue, insulin resistance, characterized by impaired insulin-stimulated glucose transport, is believed to result from decreased delivery of GLUT4 to the cell surface (230,231). Additionally, Vannucci et al proposed that a decrease in glucose transport can be attributed to reduced effectiveness of translocated GLUT4 transporters caused by their reorientation (232). M^{pro} could potentially be affecting the orientation of the GLUT4 transporters or affecting any of the aforementioned factors. Insulin-stimulated GLUT4 levels on cell surfaces are generally reduced by impaired GLUT4 trafficking rather than a decrease in the total GLUT4 (122). This could be the case with our results as we observed a relatively unaltered GLUT4 expression and a decrease in GLUT4 translocation.

Van Gerwen however summarized a few issues from various studies that hypothesized what could lead to a decrease in GLUT4 translocation. Firstly, newly produced or internalized GLUT4 may end up directed away from glucose GSVs (230,231,233). Secondly, insulin's ability to move GSVs to the cell membrane could be impaired, meaning less GLUT4 would be available for insertion into the plasma membrane (234). Additionally, processes of tethering, docking and fusing GSVs could also be less efficient, resulting in a lower amount of GLUT4 making it into the cell membrane(235). Finally, the spread and concentration of GLUT4 within the membrane itself

might be diminished (122,236). Our findings align with the in silico docking studies as they revealed a strong binding interaction between the M^{pro} and the glucose transporter GLUT4, with a binding affinity suggesting the most stable complex out of all the proteins that underwent docking. This interaction was evidenced by the notable binding energy of -1391, suggesting potential interactions that could alter the transmembrane structure of GLUT4, thereby hindering glucose transport. This interaction could also be responsible for the decrease in GLUT4 available for glucose uptake. M^{pro} might potentially be inducing an insulin-resistant state which might be one of the precipitating factors of the new-onset DM seen in long COVID-19. As a therapeutic strategy to mitigate SARS-CoV-2-induced insulin resistance, researchers can potentially focus on novel drug designs to develop inhibitors of this interaction as this might help restore GLUT4 function and improve glucose metabolism.

Another plausible explanation for the decrease in insulin-stimulated glucose uptake is due to M^{pro}-induced dephosphorylation of insulin and its substrate. Research has shown that insulin action is weakened when the insulin receptor and its substrates are dephosphorylated (199). If we have M^{pro}, for instance, binding to one of the pockets of the insulin receptor, we will have diminished insulin action, leading to insulin resistance. Our in-silico models showed that there was binding between human insulin and M^{pro}. The binding energy of this interaction was -795.9. Furthermore, there is possibility that M^{pro} could interact or complex with insulin in the extracellular space, thus diminishing the amount of bioactive insulin. These changes might prevent insulin from binding to its receptor, effectively neutralizing its activity. The solid-phase analysis provided critical insights into the disturbances in the insulin signaling pathway that we have seen with our data thus far. The similarity in binding signals between the M^{pro}-only and M^{pro} + insulin conditions strongly suggests that M^{pro} does not directly bind with insulin at a significant level as seen with our in-silico work. The slight reduction observed at 40 nmol/mL in the M^{pro} + insulin condition may be attributed to 2 things: insulin and M^{pro} binding are favoured at lower concentrations of M^{pro} or experimental variability rather than a specific interaction occurring as the difference was not observed at higher concentrations. The findings show that M^{pro} unlikely disrupts insulin function directly through binding interactions, reinforcing the idea that any disturbances in insulin signaling caused by M^{pro} might occur through indirect mechanisms. However, given the absence of a positive control, such as an insulin-insulin receptor complex, these results should be interpreted with caution. These findings suggest the need to explore alternative pathways through which M^{pro} could impact insulin

signaling. Further research, including kinetic analyses, is essential to determine whether M^{pro} indirectly affects insulin-associated pathways, potentially contributing to the glucose metabolism dysregulation observed in COVID-19 and the insulin resistance that would lead to new-onset T2DM.

The disruption of insulin signaling was further corroborated by heightened oxidative stress, indicated by increased levels of intracellular ROS and MDA in the C2C12 cell lines. In skeletal muscles, it has been shown that elevated blood glucose concentrations and increased free fatty acids trigger substantial production of ROS in the mitochondria. This ROS buildup causes serine phosphorylation and degradation of the IRS1 protein, which weakens the insulin response and ultimately contributes to insulin resistance (137). Ding and colleagues showed that chronic oxidative stress could impair GLUT4 translocated to the cell surface in insulin-treated skeletal muscle cells (137). The mitochondrion is the main source of reactive oxygen species, as the respiratory chain generates a significant amount of free radicals during oxidative phosphorylation (237). Further chemical assays such as the assessment of ATP levels and mitochondrial depolarization would assist in investigating the cellular effects of oxidative stress and mitochondrial dysfunction. Any one of these issues, or a combination of them, could have led to the disruption in glucose uptake observed in the C2C12 cell line.

The liver also plays an important role in glucose metabolism. M^{pro} treatment showed a similar trend for baseline hepatic glucose uptake as in C2C12 cells, with a concentration-dependent reduction in glucose uptake across the different concentrations of M^{pro} (2.5 to 160 nmol/mL). However, the inhibitory effect of M^{pro} in HepG2 cells was less pronounced than in C2C12 cells. This inhibition indicates that M^{pro} may interfere with key pathways involved in glucose transporter regulation differently in different tissues. GLUT2 is the major glucose transporter in the plasma membrane of hepatocytes (238). In hepatocytes, GLUT2 is responsible for over 97% of glucose transport (238). Under normal conditions, GLUT2 is responsible for glucose uptake into the cell using glucokinase as a glucose sensor. This partnership ensures that the glucose concentration on both sides of the cell membrane is balanced (238). Research conducted on mice lacking GLUT2 revealed that GLUT2 was required for the bidirectional glucose uptake into and out of cells (239). We can therefore assume that M^{pro} induced a disturbance in GLUT2 availability or a disruption of the communication between glucokinase and GLUT2. Studies also suggest that when GLUT2 on

the liver cell surface is inactivated or expressed at lower levels, other transporters can compensate, making the impact on blood glucose balance less significant (238). This might explain why HepG2 cells experience a milder disruption in glucose uptake compared to C2C12 cells.

Similar to C2C12 cells, HepG2 cells also showed the disruption of the insulin signaling pathway especially at higher concentrations of M^{pro} (40-160 nmol/mL). Post-hoc tests revealed a statistically significant difference with the highest M^{pro} concentration, indicating that high M^{pro} concentrations potentially disrupt insulin-stimulated glucose uptake in HepG2 cells. In the liver, insulin activates IRTK, leading to the phosphorylation of IRS1, IRS2 and the activation of AKT2. This subsequently reduces hepatic glucose production, enhances glycogen synthesis and stimulates lipogenesis (94). Furthermore, insulin signaling, especially through the PI3K/AKT pathway, promotes GLUT2 activity and translocation in hepatocytes, enabling glucose uptake (240).

Individuals with T2DM usually have impaired, insulin signaling, including the activation of the insulin receptor tyrosine kinase. This disruption leads to insulin resistance, contributing to hyperglycaemia and other metabolic complications associated with the disease (241). In the absence of insulin, the IR adopts an inhibitory conformation that ensures a minimum distance between its two intracellular tyrosine kinases. This separation prevents the activation of the tyrosine kinase activation loop (242). Research has shown that people with obesity or DM often exhibit reduced insulin receptor kinase (IRK) activity and decreased surface expression of insulin receptors (243). As such by assessing the binding of M^{pro} to the insulin receptor kinase domain PDB ID(1IRK) and monomeric form of human insulin PDB ID (3I40), we can elucidate any disruptions that may result in insulin resistance. Studies have shown that insulin primarily exists in hexameric and dimeric forms during production, delivery and circulation; however, it interacts with its receptor in its monomeric form (243). By utilizing the monomeric form of insulin we obtained a more accurate insight into the binding interactions and mechanisms as it more closely represents the form of insulin that interacts with its receptor under physiological conditions (244).

Our in-silico models showed binding between the insulin receptor tyrosine kinase domain which would potentially have a profound impact on cellular signaling, glucose metabolism and overall metabolic health. The tyrosine kinase domain of the insulin receptor is essential for its activation (222). The receptor undergoes autophosphorylation on specific tyrosine residues in the kinase domain upon insulin binding therefore M^{pro} might prevent or reduce autophosphorylation,

inhibiting receptor activation. Considering the kinase domain's crucial role in insulin-regulated glucose control, the observed binding suggests that M^{pro} could disrupt phosphorylation processes, potentially contributing to metabolic issues like insulin resistance. This would have negative effects as an impairment of downstream signaling will occur. Key pathways such as the PI3K/AKT would be disrupted, reducing glucose uptake and metabolism.

Similar to the pattern observed in C2C12 cells, the baseline AKT expression in HepG2 cells showed no significant difference from the control (untreated) cells for all the treatment concentrations. This consistency across both cell lines suggests that M^{pro} does not affect AKT expression in baseline conditions. However, in contrast to C2C12 cells, we observed significant differences in insulin-stimulated AKT expression in the HepG2 cells. A significant reduction in AKT expression was seen with increasing M^{pro} concentrations suggesting an inhibitory effect of M^{pro} on insulin-stimulated AKT in HepG2 cells at higher concentrations. Ultimately, both cell lines demonstrate a clear dose-dependent reduction in glucose uptake with increasing M^{pro} concentrations, with a greater degree of inhibition in C2C12 cells. The differences in sensitivity might reflect tissue-specific roles in glucose metabolism, where the skeletal muscle plays a larger role in systemic glucose regulation and thus will be more severely impacted by disruptions in insulin signaling. Based on these findings, researchers may be able to investigate M^{pro} inhibitors as potential dual therapies to reduce both viral replication and metabolic disruptions. To validate the stability of these in-silico interactions and confirm whether they have a biological impact, future studies could include molecular dynamics simulations. We hypothesize that this could be one of the ways that M^{pro} might be affecting the insulin signaling pathway.

While the effects of M^{pro} on glucose uptake, AKT signaling, GLUT4 translocation and expression shed light on its metabolic implications, its role extends beyond these parameters. COVID-19 has been implicated in inflammatory processes, with potential crosstalk involving key players such as DPP4 and MMP1, which are known to mediate both tissue remodelling and systemic inflammation. Viruses can trigger chronic inflammation, which may lead to cellular transformation (162). Furthermore, a study by Queiroz and colleagues on cytokine profiles in acute and long-term COVID-19 syndrome highlighted IL-6 as a key cytokine influencing the outcome of COVID-19, including the disease's duration and severity (167). Inflammation has also been noted to induce insulin resistance hence this could be another potential mechanism in which M^{pro} is inducing glycaemic aberrations.

Our data shows that M^{pro} induces a dose-dependent increase in IL-6 expression in the C2C12 cells, with the highest levels observed at 160 nmol/mL. This means M^{pro} induced an increase in cytokine production at a cellular level. To assess whether IL-6 would have a role in systemic signaling, the extracellular level of IL-6 was measured. In C2C12 cells, the release into the medium was not as pronounced as expected. Skeletal muscles are localized producers of IL-6 under specific conditions such as injury or exercise (245), but they may not engage in the same aggressive inflammatory response under viral protease stress. Therefore, we can postulate that M^{pro}-induced inflammation was not contributing to the glycaemic dysregulation being observed in the C2C12 cell line. However, in contrast to C2C12 cells, M^{pro} did not induce an increase in intracellular IL-6 expression in HepG2 cells but there was a significant release of IL-6 into the medium. Our results corroborate literature as viruses have been shown to induce the production of IL-6 in the liver (175,246). Ulrich Spengler reported that in addition to viruses that are labelled as "hepatitis" viruses, other viruses such as influenza and coronaviruses can also cause hepatitis ranging from mild asymptomatic elevations of aminotransferases to liver failure (247). A study conducted by Lepiller and colleagues demonstrated that infection of HepG2 cells with HCMV caused the production of IL-6 in the supernatants of HepG2 cells starting as early as 2 hours post-infection (175). Carlquist et al. studied an *in vitro* induction of IL-6 by human lung fibroblasts in response to HCMV and found that both IL-6 gene transcription and IL-6 protein expression were similarly stimulated (246). This suggests that during viral infections, the liver may act as a cytokine producer, contributing to systemic inflammation without necessarily increasing intracellular cytokine levels.

In addition to its enzymatic role in glucose homeostasis, DPP4 exhibits diverse immunoregulatory properties, primarily mediated through protein-protein interactions (104). Research has shown that DPP4 associates with adenosine deaminase (ADA) on the T cell surface which in turn facilitates the interaction of ADA with adenosine receptors, forming a ternary complex. This complex is believed to play a crucial role as a co-stimulatory signal that promotes lymphocyte proliferation and cytokine production, leading to a significant increase in the production of pro-inflammatory cytokines, including IFN-γ, TNF-α and IL-6 (104). This in turn means that DPP4 can influence IL-6 levels by promoting its release, exacerbating muscle inflammation. The observed increase in both extracellular IL-6 and sDPP4 levels with M^{pro} exposure in C2C12 cells, suggests a connection between DPP4 and inflammation. Research has shown that there is a well-established relationship

between DPP4 and IL-6 (248). In C2C12 cells, M^{pro} gradually lowered intracellular DPP4 expression and increased sDPP4 shedding into the cell medium. Rohrborn and colleagues shed light on the enzymes involved in DPP4 shedding, identifying that MMP1, MMP2 and MMP14 play a role in regulating this process (106). Cell culture and rodent models have shown that DPP4 is shed from skeletal muscle membranes through the action of MMPs but the pathway for release of DPP4 and its function remains unclear (106). In C2C12 cells, we observed a decrease in both MMP1 and DPP4 intracellular expression, suggesting a potential regulatory relationship. Given that MMP1 is involved in extracellular matrix remodelling and DPP4 plays a role in metabolic regulation, one possibility is that the reduction in both proteins reflects a coordinated response to cellular stress or signaling alterations. M^{pro} might suppress MMP1 production and the consequence of this can be an impairment in the muscle's ability to remodel the ECM effectively resulting in pathophysiology of muscle-wasting conditions.

In contrast to C2C12 cells, M^{pro} could be inducing a stress response in HepG2 cells that triggers the downregulation of sDPP4 despite increased extracellular IL-6. In conditions such as inflammation or metabolic stress such as insulin resistance or liver injury, inflammatory mediators induce hepatic acute-phase protein synthesis (249). Upon M^{pro} exposure which has shown to increase the inflammatory mediator IL-6, HepG2 cells may prioritize acute-phase protein synthesis and the regulation of inflammation over the shedding of proteins like DPP4. This shift in cellular focus could lead to decreased DPP4 shedding despite increased IL-6 levels. In the liver, decreased sDPP4 might serve as a regulatory mechanism to limit excessive inflammation. Since sDPP4 is associated with immune activation, HepG2 cells may retain DPP4 to avoid exacerbating inflammation, especially if extracellular IL-6 is already elevated (104). Therefore, the increase in intracellular DPP4 in HepG2 cells could be a protective mechanism. By limiting DPP4 shedding, HepG2 cells may be attempting to control sustained systemic inflammation.

While no specific studies are focusing on viruses or proteases affecting enzymes that cause DPP4 shedding, research has shown that MMPs can regulate DPP4 shedding and activity (104). Our data showed high levels of extracellular MMP1 which should translate to high levels of sDPP4 in the HepG2 cell line. However, this was not the case, leading us to speculate that M^{pro} was affecting the cleavage process. Therefore, the observed decrease in sDPP4 in the medium could be due to altered cell-cell interactions, which could subsequently reduce the proteolytic activity of MMPs,

thereby affecting the production of sDPP4. Inflammatory or fibro genic stimuli like Transforming Growth Factor (TGF-β) or IL-6 can induce MMP1 expression in HepG2 cells (179). Given that our data assessing IL-6 expression in HepG2 cells showed low levels of the inflammatory mediator, this could also explain the low level of cellular MMP1 expression. The implications of this release of MMP1 into the extracellular matrix of the liver result in the promotion of extracellular matrix remodelling in the liver, possibly contributing to tissue restructuring. This would also further help explain why M^{pro} has had a less severe effect on HepG2 cells in terms of cell viability and glucose uptake. However, more studies need to be conducted to ascertain the degree of ECM remodelling occurring as excessive remodelling would lead to pathological conditions (180). In conclusion, these findings highlight the intricate interplay between inflammation and proteolysis, warranting further research to elucidate these pathways and their broader physiological and pathological impact on new-onset DM. Taken together, our study demonstrates that, SARS-CoV-2 M^{pro} presents itself as a risk factor for developing T2DM, possibly through the induction of insulin resistance. The potential mechanisms we have highlighted in the preceding sections should also bring into light the question of whether anti-hyperglycaemic are still as effective in managing hyperglycaemia during or after post-SARS-CoV-2 infection. With risks of pancreatic damage during SARS-CoV-2 infection, T2DM patient is at risk of losing the ability to produce and secrete insulin. In such a scenario, such patients would not benefit from sulphonyl urea-based therapy and in this case, insulin therapy would suffice as a substitute. Similarly, having highlighted the risk of developing insulin resistance, T1DM patients may have a challenge in affording tight glycaemic control using insulin alone; in such a case, an insulin sensitizer may be required. Indeed, in the prior section, we have alluded to cases where higher insulin doses were required to achieve glycaemic control. From what we have highlighted above, clinicians and authorities should consider SARS-CoV-2 infection as a risk factor for the ineffectiveness of anti-hyperglycaemic.

CHAPTER 6: CONCLUSION

The rise in the silent pandemic that is diabetes mellitus was already expected without COVID-19-induced DM. COVID-19, despite its devastating impact on human life, has, however, provided several lessons and has further accelerated our understanding of the aetiology and pathogenesis of DM. It has further solidified the impact of viral infections and their role in metabolic reprogramming in inducing glycaemic aberrations. Understanding the cellular and molecular mechanical insights pertaining to glucose metabolism is crucial as it consolidates the links between the diseases, therefore allowing us to contemplate preventative therapeutic interventions, not only for preventing DM but also for combating the virus itself. This study highlights the potential impact of COVID-19 M^{pro} on glucose metabolism which appears to disrupt the insulin signaling pathways in both skeletal muscle and hepatic cell lines to different degrees. Collectively our observations reveal the impairment of glucose uptake, downregulation of GLUT4 translocation and increased DPP4 shedding coupled with alterations in the AKT pathway, suggesting that COVID-19 may exacerbate insulin resistance, a key factor in the development of DM and other metabolic disorders. Additionally, the observed increase in inflammatory markers like IL-6 provides further evidence that systemic inflammation contributes to these metabolic disturbances. These findings highlight the importance of gaining a deeper understanding of how viral infections, such as COVID-19, may impact metabolic processes and potentially elevate the risk of the transition from prediabetes to DM. While there is currently insufficient evidence in this study and the literature to conclusively state that M^{pro} is responsible for hyperglycaemia observed in long-COVID-19 patients, we can effectively state that M^{pro} is causing some disturbances to the insulin signaling pathway. Given the disturbances seen in glucose handling, GLUT4 and inflammatory markers only in the data, it is reasonable to propose that $M^{pro's}$ effect is predominantly indirect. M^{pro} likely disrupts intracellular signaling proteins and pathways critical for insulin signaling rather than directly interacting with insulin itself, as supported by the minimal binding observed in the solid-phase analysis. While extensive progress has been made, numerous gaps remain in our understanding of the precise molecular events involved in new-onset DM post-COVID-19 infection. Additional research is needed to validate these in vitro results and investigate therapeutic approaches to alleviate these effects in COVID-19 patients.

6.1 Study limitations and recommendations for future work

The present study provided valuable insights into the extent to which M^{pro} affects glycaemic regulation. However, there were limitations to this study. *In vitro* and *in vivo* results differ considerably, highlighting the importance of extreme caution when comparing laboratory results with clinical outcomes. These studies typically involve continuously growing, tumour-like cells that differ substantially from normal, resting, non-neoplastic cells derived from patients. C2C12 and HepG2 cell lines are commonly used to assess the pathogenesis of T2DM. However, these models have significant limitations, as they cannot fully replicate the intricate genetic profiles and metabolic dysfunctions characteristic of human conditions. Furthermore, the study did not include long-term observations to evaluate the sustained effects of treatments on insulin signaling, glucose uptake, or oxidative stress, potentially overlooking delayed or cumulative effects. We therefore recommend conducting *in vivo* studies (animal studies) as well to provide a complete picture of the effect of M^{pro} and thus understand the clinical implications while offering a more comprehensive insight into the development of T2DM.

A key limitation of this research was the utilization of M^{pro} rather than using the SARS-CoV-2, which might not fully replicate the complexity of SARS-CoV-2's effects on the insulin signaling pathway. Future studies utilizing live or inactivated virus models could provide a more accurate understanding of how the virus impacts cellular mechanisms. Additionally, exploring whether insulin-sensitizers could help manage the disruptions in the insulin signaling pathway is an exciting direction for future research. This could shed light on their potential as therapeutic options to counteract the metabolic disturbances linked to SARS-CoV-2 infection.

Due to the unavailability of Triton X, a key positive control used for validating cytotoxicity in the assay, its absence may have affected the interpretation of results. This reagent is commonly used to assess maximum toxicity levels, providing a baseline to compare the effects of M^{pro} and without it, the full scope of cytotoxicity may not have been accurately captured in this experiment. Incorporating a robust positive control in future experiments will help validate the results and provide a reference for maximum cytotoxicity.

Proteomic techniques can be utilized in the future to analyze the broader effects on the insulin signaling pathway. Changes in phosphorylation states of multiple pathway components beyond Akt were not utilized. This may have missed potential mechanistic insights.

Furthermore, studies have shown that high glucose concentrations (25 mM) in the medium can desensitize insulin-dependent signaling, leading to reduced glucose uptake in C2C12 cells (250). This underscores the necessity of conducting *in vivo* assays to fully understand the role of skeletal muscles in insulin resistance. Notably, the medium used in our study contained a high glucose concentration, which may have influenced the results.

The inclusion of M^{pro}-only controls was crucial in confirming that the anti-insulin antibody non-specifically binds to M^{pro}. However, we observed interactions between M^{pro} and the anti-insulin body making the control less robust. Future studies could employ an insulin receptor control to ensure higher accuracy. This approach would provide a more precise assessment of antibody specificity and minimize potential confounding interactions with M^{pro}.

This study faced significant financial constraints, limiting the scope of biochemical analyses. For example, intracellular ROS analysis was performed only for C2C12 cells. Furthermore, the assay for intracellular ROS could not be repeated thrice. Assays such as ATP bioluminescence, mitochondrial depolarization and lactate assessment would have provided critical insights into M^{pro}-induced disturbances. Additionally, several studies have suggested a potential role of TNF-α in insulin resistance, highlighting the importance of including this marker in future investigations (91,170,251).

Quantitatively measuring proteins is challenging because of their varied size, interactions with other molecules, length, amino acid sequences and post-translational modifications therefore the exact binding regions could not be stated. Detailed analysis of the docking poses would have revealed whether M^{pro} interacts with critical residues within the catalytic domain of our proteins and assess whether M^{pro}, potentially obstructs the active site or disrupts substrate binding. Future advancements in proteomics, such as the use of more refined mass spectrometry techniques or advanced computational modelling, may help address these limitations and provide more precise insights into protein interactions and binding regions. Despite these advancements, challenges still remain in accounting for protein flexibility, dynamic conformational changes and the effects of

the cellular environment, which may limit the translatability of in silico predictions to biological systems(252).

Funding

The study was funded by the National Research Foundation (NRF) South Africa: TTK220318196 and Rhodes University Postgraduate funding.

REFERENCES

1. Abegunde DO, Mathers CD, Adam T, Ortegon M, Strong K. The burden and costs of chronic diseases in low-income and middle-income countries. The Lancet. 2007 Dec 8;370(9603):1929–38.

2. Kiernan K, MacIver NJ. Viral Infection "Interferes" with Glucose Tolerance. Immunity. 2018 Jul 17;49(1):6–8.

3. American Diabetes Association. 2. Classification and Diagnosis of Diabetes: Standards of Medical Care in Diabetes—2018. Diabetes Care. 2017 Nov 24;41(Supplement_1):S13–27.

4. Abegunde DO, Mathers CD, Adam T, Ortegon M, Strong K. The burden and costs of chronic diseases in low-income and middle-income countries. The Lancet. 2007 Dec 8;370(9603):1929–38.

5. Khetan AK, Rajagopalan S. Prediabetes. Canadian Journal of Cardiology. 2018 May 1;34(5):615–23.

6. Jeong SU, Kang DG, Lee DH, Lee KW, Lim DM, Kim BJ, et al. Clinical Characteristics of Type 2 Diabetes Patients according to Family History of Diabetes. Korean Diabetes J. 2010 Aug;34(4):222–8.

7. Rey-Reñones C, Martinez-Torres S, Martín-Luján FM, Pericas C, Redondo A, Vilaplana-Carnerero C, et al. Type 2 Diabetes Mellitus and COVID-19: A Narrative Review. Biomedicines. 2022 Sep;10(9):2089.

8. Alam U, Asghar O, Azmi S, Malik RA. Chapter 15 - General aspects of diabetes mellitus. In: Zochodne DW, Malik RA, editors. Handbook of Clinical Neurology [Internet]. Elsevier; 2014 [cited 2023 Jun 28]. p. 211–22. (Diabetes and the Nervous System; vol. 126). Available from: https://www.sciencedirect.com/science/article/pii/B9780444534804000151

9. Leslie RD, Palmer J, Schloot NC, Lernmark A. Diabetes at the crossroads: relevance of disease classification to pathophysiology and treatment. Diabetologia. 2016 Jan 1;59(1):13–20.

10. Abdul-Ghani MA, DeFronzo RA. Pathophysiology of prediabetes. Curr Diab Rep. 2009 Jun 1;9(3):193–9.

11. Sibiya N, Mzimela N, Mbatha B, Ngubane P, Khathi A. The Insights on Why Diabetes Prevalence May Increase Amid or Post COVID-19 Pandemic. Curr Diabetes Rev. 2023 Jan 1;19(4):37–45.

12. Šestan M, Marinović S, Kavazović I, Cekinović Đ, Wueest S, Turk Wensveen T, et al. Virus-Induced Interferon-γ Causes Insulin Resistance in Skeletal Muscle and Derails Glycemic Control in Obesity. Immunity. 2018 Jul 17;49(1):164-177.e6.

13. Metwally AA, Mehta P, Johnson BS, Nagarjuna A, Snyder MP. COVID-19–Induced New-Onset Diabetes: Trends and Technologies. Diabetes. 2021 Oct 22;70(12):2733–44.

14. Pal R, Banerjee M. COVID-19 and the endocrine system: exploring the unexplored. J Endocrinol Invest. 2020 Jul;43(7):1027–31.

15. Coppelli A, Giannarelli R, Aragona M, Penno G, Falcone M, Tiseo G, et al. Hyperglycemia at Hospital Admission Is Associated With Severity of the Prognosis in Patients Hospitalized for COVID-19: The Pisa COVID-19 Study. Diabetes Care. 2020 Aug 11;43(10):2345–8.

16. Iacobellis G, Penaherrera CA, Bermudez LE, Bernal Mizrachi E. Admission hyperglycemia and radiological findings of SARS-CoV2 in patients with and without diabetes. Diabetes Research and Clinical Practice. 2020 Jun 1;164:108185.

17. Baidya A, Singh SK, Bajaj S, Zargar AH, Singh P, Das S, et al. Diabetes and COVID-19: A Review. Journal of the ASEAN Federation of Endocrine Societies. 2020 May 22;35(1):40–8.

18. WHO Coronavirus (COVID-19) Dashboard [Internet]. [cited 2023 Jun 27]. Available from: https://covid19.who.int

19. Yin JX, Agbana YL, Sun ZS, Fei SW, Zhao HQ, Zhou XN, et al. Increased interleukin-6 is associated with long COVID-19: a systematic review and meta-analysis. Infectious Diseases of Poverty. 2023 Apr 24;12(1):43.

20. Kaul D. An overview of coronaviruses including the SARS-2 coronavirus – Molecular biology, epidemiology and clinical implications. Current Medicine Research and Practice. 2020 Mar 1;10(2):54–64.

21. Sharma S, Deep S. In-silico drug repurposing for targeting SARS-CoV-2 main protease (Mpro). Journal of Biomolecular Structure and Dynamics. 2022 May 3;40(7):3003–10.

22. Dallavalasa S, Tulimilli SV, Prakash J, Ramachandra R, Madhunapantula SV, Veeranna RP. COVID-19: Diabetes Perspective—Pathophysiology and Management. Pathogens. 2023 Feb;12(2):184.

23. Yuki K, Fujiogi M, Koutsogiannaki S. COVID-19 pathophysiology: A review. Clinical Immunology. 2020 Jun;215:108427.

24. Gangadharan C, Ahluwalia R, Sigamani A. Diabetes and COVID-19: Role of insulin resistance as a risk factor for COVID-19 severity. World J Diabetes. 2021 Sep 15;12(9):1550–62.

25. Malkova A, Kudlay D, Kudryavtsev I, Starshinova A, Yablonskiy P, Shoenfeld Y. Immunogenetic Predictors of Severe COVID-19. Vaccines. 2021 Mar;9(3):211.

26. Kathiravan MK, Radhakrishnan S, Namasivayam V, Palaniappan S. An Overview of Spike Surface Glycoprotein in Severe Acute Respiratory Syndrome–Coronavirus. Frontiers in

Molecular Biosciences [Internet]. 2021 [cited 2023 Oct 4];8. Available from: https://www.frontiersin.org/articles/10.3389/fmolb.2021.637550

27. Ferreira JC, Fadl S, Villanueva AJ, Rabeh WM. Catalytic Dyad Residues His41 and Cys145 Impact the Catalytic Activity and Overall Conformational Fold of the Main SARS-CoV-2 Protease 3-Chymotrypsin-Like Protease. Frontiers in Chemistry [Internet]. 2021 [cited 2023 Sep 13];9. Available from: https://www.frontiersin.org/articles/10.3389/fchem.2021.692168

28. Narayanan A, Narwal M, Majowicz SA, Varricchio C, Toner SA, Ballatore C, et al. Identification of SARS-CoV-2 inhibitors targeting Mpro and PLpro using in-cell-protease assay. Commun Biol. 2022 Feb 25;5(1):1–17.

29. Vuong W, Khan MB, Fischer C, Arutyunova E, Lamer T, Shields J, et al. Feline coronavirus drug inhibits the main protease of SARS-CoV-2 and blocks virus replication. Nat Commun. 2020 Aug 27;11(1):1–8.

30. Huff S, Kummetha IR, Tiwari SK, Huante MB, Clark AE, Wang S, et al. Discovery and Mechanism of SARS-CoV-2 Main Protease Inhibitors. J Med Chem. 2022 Feb 24;65(4):2866–79.

31. Roe MK, Junod NA, Young AR, Beachboard DC, Stobart CC. Targeting novel structural and functional features of coronavirus protease nsp5 (3CLpro, Mpro) in the age of COVID-19. Journal of General Virology. 2021;102(3):001558.

32. Suryawanshi RK, Koganti R, Agelidis A, Patil CD, Shukla D. Dysregulation of Cell Signaling by SARS-CoV-2. Trends in Microbiology. 2021 Mar 1;29(3):224–37.

33. Fehr AR, Perlman S. Coronaviruses: An Overview of Their Replication and Pathogenesis. In: Coronaviruses [Internet]. Humana Press, New York, NY; 2015 [cited 2023 Oct 4]. p. 1–23. Available from: https://0-link.springer.com.wam.seals.ac.za/protocol/10.1007/978-1-4939-2438-7_1

34. Neuman BW, Kiss G, Kunding AH, Bhella D, Baksh MF, Connelly S, et al. A structural analysis of M protein in coronavirus assembly and morphology. J Struct Biol. 2011 Apr;174(1):11–22.

35. Zhou S, Lv P, Li M, Chen Z, Xin H, Reilly S, et al. SARS-CoV-2 E protein: Pathogenesis and potential therapeutic development. Biomed Pharmacother. 2023 Mar;159:114242.

36. Iketani S, Hong SJ, Sheng J, Bahari F, Culbertson B, Atanaki FF, et al. Functional map of SARS-CoV-2 3CL protease reveals tolerant and immutable sites. Cell Host & Microbe. 2022 Oct 12;30(10):1354-1362.e6.

37. Anand K, Ziebuhr J, Wadhwani P, Mesters JR, Hilgenfeld R. Coronavirus Main Proteinase (3CLpro) Structure: Basis for Design of Anti-SARS Drugs. Science. 2003 Jun 13;300(5626):1763–7.

38. Pillaiyar T, Manickam M, Namasivayam V, Hayashi Y, Jung SH. An Overview of Severe Acute Respiratory Syndrome–Coronavirus (SARS-CoV) 3CL Protease Inhibitors: Peptidomimetics and Small Molecule Chemotherapy. J Med Chem. 2016 Jul 28;59(14):6595–628.

39. Ksiazek TG, Erdman D, Goldsmith CS, Zaki SR, Peret T, Emery S, et al. A Novel Coronavirus Associated with Severe Acute Respiratory Syndrome. New England Journal of Medicine. 2003 May 15;348(20):1953–66.

40. Bzówka M, Mitusińska K, Raczyńska A, Samol A, Tuszyński JA, Góra A. Structural and Evolutionary Analysis Indicate That the SARS-CoV-2 Mpro Is a Challenging Target for Small-Molecule Inhibitor Design. International Journal of Molecular Sciences. 2020 Jan;21(9):3099.

41. Estrada E. Topological analysis of SARS CoV-2 main protease. Chaos: An Interdisciplinary Journal of Nonlinear Science. 2020 Jun 9;30(6):061102.

42. Kneller DW, Phillips G, O'Neill HM, Jedrzejczak R, Stols L, Langan P, et al. Structural plasticity of SARS-CoV-2 3CL Mpro active site cavity revealed by room temperature X-ray crystallography. Nat Commun. 2020 Jun 24;11(1):3202.

43. Hu Q, Xiong Y, Zhu GH, Zhang YN, Zhang YW, Huang P, et al. The SARS-CoV-2 main protease (Mpro): Structure, function, and emerging therapies for COVID-19. MedComm. 2022 Sep 1;3(3):e151.

44. Su H, Yao S, Zhao W, Zhang Y, Liu J, Shao Q, et al. Identification of pyrogallol as a warhead in design of covalent inhibitors for the SARS-CoV-2 3CL protease. Nat Commun. 2021 Jun 15;12(1):1–12.

45. Flynn JM, Samant N, Schneider-Nachum G, Barkan DT, Yilmaz NK, Schiffer CA, et al. Comprehensive fitness landscape of SARS-CoV-2 Mpro reveals insights into viral resistance mechanisms. Ogbunugafor CB, Barkai N, Fraser JS, Weinreich D, editors. eLife. 2022 Jun 20;11:e77433.

46. Wenzel J, Lampe J, Müller-Fielitz H, Schuster R, Zille M, Müller K, et al. The SARS-CoV-2 main protease Mpro causes microvascular brain pathology by cleaving NEMO in brain endothelial cells. Nat Neurosci. 2021;24(11):1522–33.

47. Katsarou A, Gudbjörnsdottir S, Rawshani A, Dabelea D, Bonifacio E, Anderson BJ, et al. Type 1 diabetes mellitus. Nat Rev Dis Primers. 2017 Mar 30;3(1):1–17.

48. Roep BO, Thomaidou S, van Tienhoven R, Zaldumbide A. Type 1 diabetes mellitus as a disease of the β-cell (do not blame the immune system?). Nat Rev Endocrinol. 2021 Mar;17(3):150–61.

49. Van Belle TL, Coppieters KT, Von Herrath MG. Type 1 Diabetes: Etiology, Immunology, and Therapeutic Strategies. Physiological Reviews. 2011 Jan;91(1):79–118.

50. Gardner KE. "The Art of Insulin Treatment:" Diabetes, Insulin, and the 1920s. J Med Humanit. 2019 Jun;40(2):171–80.

51. Silver B, Ramaiya K, Andrew SB, Fredrick O, Bajaj S, Kalra S, et al. EADSG Guidelines: Insulin Therapy in Diabetes. Diabetes Ther. 2018 Apr 1;9(2):449–92.

52. McCall AL. Insulin Therapy and Hypoglycemia. Endocrinology and Metabolism Clinics. 2012 Mar 1;41(1):57–87.

53. Donnor T, Sarkar S. Insulin- Pharmacology, Therapeutic Regimens and Principles of Intensive Insulin Therapy. In: Feingold KR, Anawalt B, Blackman MR, Boyce A, Chrousos

G, Corpas E, et al., editors. Endotext [Internet]. South Dartmouth (MA): MDText.com, Inc.; 2000 [cited 2024 Dec 10]. Available from: http://www.ncbi.nlm.nih.gov/books/NBK278938/

54. Cavaghan MK, Ehrmann DA, Polonsky KS. Interactions between insulin resistance and insulin secretion in the development of glucose intolerance. J Clin Invest. 2000 Aug 1;106(3):329–33.

55. Fazakerley DJ, Krycer JR, Kearney AL, Hocking SL, James DE. Muscle and adipose tissue insulin resistance: malady without mechanism? J Lipid Res. 2019 Oct;60(10):1720–32.

56. Banerjee M, Chakraborty S, Pal R. Diabetes self-management amid COVID-19 pandemic. Diabetes & Metabolic Syndrome: Clinical Research & Reviews. 2020 Jul 1;14(4):351–4.

57. Khetan AK, Rajagopalan S. Prediabetes. Canadian Journal of Cardiology. 2018 May 1;34(5):615–23.

58. Schroeder EB. Management of Type 2 Diabetes: Selecting Amongst Available Pharmacological Agents. In: Feingold KR, Anawalt B, Blackman MR, Boyce A, Chrousos G, Corpas E, et al., editors. Endotext [Internet]. South Dartmouth (MA): MDText.com, Inc.; 2000 [cited 2024 Dec 10]. Available from: http://www.ncbi.nlm.nih.gov/books/NBK425702/

59. Bell DSH. Do sulfonylurea drugs increase the risk of cardiac events? CMAJ. 2006 Jan 17;174(2):185–6.

60. Proks P, Reimann F, Green N, Gribble F, Ashcroft F. Sulfonylurea stimulation of insulin secretion. Diabetes. 2002 Dec;51 Suppl 3:S368-376.

61. Chaudhury A, Duvoor C, Reddy Dendi VS, Kraleti S, Chada A, Ravilla R, et al. Clinical Review of Antidiabetic Drugs: Implications for Type 2 Diabetes Mellitus Management. Front Endocrinol (Lausanne). 2017 Jan 24;8:6.

62. Harrigan RA, Nathan MS, Beattie P. Oral agents for the treatment of type 2 diabetes mellitus: pharmacology, toxicity, and treatment. Ann Emerg Med. 2001 Jul;38(1):68–78.

63. Lebovitz HE. Thiazolidinediones: the Forgotten Diabetes Medications. Curr Diab Rep. 2019 Nov 27;19(12):151.

64. Poudel RR. Renal glucose handling in diabetes and sodium glucose cotransporter 2 inhibition. Indian J Endocrinol Metab. 2013;17(4):588–93.

65. Barnett A. DPP-4 inhibitors and their potential role in the management of type 2 diabetes. Int J Clin Pract. 2006 Nov;60(11):1454–70.

66. Trujillo JM, Nuffer W, Ellis SL. GLP-1 receptor agonists: a review of head-to-head clinical studies. Ther Adv Endocrinol Metab. 2015 Feb;6(1):19–28.

67. Pathak R, Bridgeman MB. Dipeptidyl Peptidase-4 (DPP-4) Inhibitors In the Management of Diabetes. P T. 2010 Sep;35(9):509–13.

68. Nauck M. Incretin therapies: highlighting common features and differences in the modes of action of glucagon-like peptide-1 receptor agonists and dipeptidyl peptidase-4 inhibitors. Diabetes Obes Metab. 2016 Mar;18(3):203–16.

69. Yki-Järvinen H. Thiazolidinediones. N Engl J Med. 2004 Sep 9;351(11):1106–18.

70. Yang X, Yu Y, Xu J, Shu H, Xia J, Liu H, et al. Clinical course and outcomes of critically ill patients with SARS-CoV-2 pneumonia in Wuhan, China: a single-centered, retrospective, observational study. The Lancet Respiratory Medicine. 2020 May 1;8(5):475–81.

71. Wu Z, McGoogan JM. Characteristics of and Important Lessons From the Coronavirus Disease 2019 (COVID-19) Outbreak in China: Summary of a Report of 72 314 Cases From the Chinese Center for Disease Control and Prevention. JAMA. 2020 Apr 7;323(13):1239–42.

72. Yang JK, Lin SS, Ji XJ, Guo LM. Binding of SARS coronavirus to its receptor damages islets and causes acute diabetes. Acta Diabetol. 2010 Sep 1;47(3):193–9.

73. Lim S, Bae JH, Kwon HS, Nauck MA. COVID-19 and diabetes mellitus: from pathophysiology to clinical management. Nat Rev Endocrinol. 2021 Jan;17(1):11–30.

74. Lui GCY, Yip TCF, Wong VWS, Chow VCY, Ho THY, Li TCM, et al. Significantly Lower Case-fatality Ratio of Coronavirus Disease 2019 (COVID-19) than Severe Acute Respiratory Syndrome (SARS) in Hong Kong—A Territory-Wide Cohort Study. Clinical Infectious Diseases. 2021 May 15;72(10):e466–75.

75. Yu B, Li C, Sun Y, Wang DW. Insulin Treatment Is Associated with Increased Mortality in Patients with COVID-19 and Type 2 Diabetes. Cell Metabolism. 2021 Jan 5;33(1):65-77.e2.

76. Riahi S, Sombra LRS, Lo KB, Chacko SR, Neto AGM, Azmaiparashvili Z, et al. Insulin Use, Diabetes Control, and Outcomes in Patients with COVID-19. Endocrine Research. 2021 Apr 3;46(2):45–50.

77. Wang W, Sun Y, Wang S, Sun Y. The Relationship Between Insulin Use And Increased Mortality In Patients With COVID-19 And Diabetes: A Meta-Analysis. Endocrine Research. 2022 Jan 2;47(1):32–8.

78. Yang Y, Cai Z, Zhang J. Insulin Treatment May Increase Adverse Outcomes in Patients With COVID-19 and Diabetes: A Systematic Review and Meta-Analysis. Frontiers in Endocrinology [Internet]. 2021 [cited 2023 Oct 30];12. Available from: https://www.frontiersin.org/articles/10.3389/fendo.2021.696087

79. Sardu C, D'Onofrio N, Balestrieri ML, Barbieri M, Rizzo MR, Messina V, et al. Outcomes in Patients With Hyperglycemia Affected by COVID-19: Can We Do More on Glycemic Control? Diabetes Care. 2020 May 19;43(7):1408–15.

80. Nakrani MN, Wineland RH, Anjum F. Physiology, Glucose Metabolism. In: StatPearls [Internet]. Treasure Island (FL): StatPearls Publishing; 2023 [cited 2023 Nov 22]. Available from: http://www.ncbi.nlm.nih.gov/books/NBK560599/

81. Girdhar K, Powis A, Raisingani A, Chrudinová M, Huang R, Tran T, et al. Viruses and Metabolism: The Effects of Viral Infections and Viral Insulins on Host Metabolism. Annu Rev Virol. 2021 Sep 29;8(1):373–91.

82. Navale AM, Paranjape AN. Glucose transporters: physiological and pathological roles. Biophys Rev. 2016 Mar 1;8(1):5–9.

83. Huang S, Czech MP. The GLUT4 Glucose Transporter. Cell Metabolism. 2007 Apr 4;5(4):237–52.

84. Diehl N, Schaal H. Make Yourself at Home: Viral Hijacking of the PI3K/Akt Signaling Pathway. Viruses. 2013 Dec;5(12):3192–212.

85. Cheng ML, Chien KY, Lai CH, Li GJ, Lin JF, Ho HY. Metabolic Reprogramming of Host Cells in Response to Enteroviral Infection. Cells. 2020 Feb;9(2):473.

86. Fontaine KA, Sanchez EL, Camarda R, Lagunoff M. Dengue Virus Induces and Requires Glycolysis for Optimal Replication. Journal of Virology. 2015 Jan 26;89(4):2358–66.

87. Dippe SE, Miller M, Bennett PH, Maynard JE, Berquist KR. LACK OF CAUSAL ASSOCIATION BETWEEN COXSACKIE B4 VIRUS INFECTION AND DIABETES. The Lancet. 1975 Jun 14;305(7920):1314–7.

88. Yoon JW, Onodera T, Notkins AL. Virus-induced diabetes mellitus. XV. Beta cell damage and insulin-dependent hyperglycemia in mice infected with coxsackie virus B4. Journal of Experimental Medicine. 1978 Oct 1;148(4):1068–80.

89. Honeyman MC, Coulson BS, Stone NL, Gellert SA, Goldwater PN, Steele CE, et al. Association between rotavirus infection and pancreatic islet autoimmunity in children at risk of developing type 1 diabetes. Diabetes. 2000 Aug 1;49(8):1319–24.

90. Dotta F, Censini S, van Halteren AGS, Marselli L, Masini M, Dionisi S, et al. Coxsackie B4 virus infection of β cells and natural killer cell insulitis in recent-onset type 1 diabetic patients. Proceedings of the National Academy of Sciences. 2007 Mar 20;104(12):5115–20.

91. Govender N, Khaliq OP, Moodley J, Naicker T. Insulin resistance in COVID-19 and diabetes. Primary Care Diabetes. 2021 Aug 1;15(4):629–34.

92. Li M, Chi X, Wang Y, Setrerrahmane S, Xie W, Xu H. Trends in insulin resistance: insights into mechanisms and therapeutic strategy. Sig Transduct Target Ther. 2022 Jul 6;7(1):1–25.

93. Saltiel AR, Kahn CR. Insulin signalling and the regulation of glucose and lipid metabolism. Nature. 2001 Dec;414(6865):799–806.

94. Lee SH, Park SY, Choi CS. Insulin Resistance: From Mechanisms to Therapeutic Strategies. Diabetes Metab J. 2022 Jan;46(1):15–37.

95. Duvnjak L, Duvnjak M. The metabolic syndrome - an ongoing story. J Physiol Pharmacol. 2009 Dec;60 Suppl 7:19–24.

96. Fasipe OJ, Ayoade OG, Enikuomehin AC. Severity Grade Assessment Classifications for Both Insulin Resistance Syndrome and Status of Pancreatic Beta Cell Function in Clinical Practice Using Homeostasis Model Assessment Method Indices. Canadian Journal of Diabetes. 2020 Oct 1;44(7):663–9.

97. Seino S, Shibasaki T, Minami K. Dynamics of insulin secretion and the clinical implications for obesity and diabetes. J Clin Invest. 2011 Jun 1;121(6):2118–25.

98. Fridlyand LE, Philipson LH. Glucose sensing in the pancreatic beta cell: a computational systems analysis. Theor Biol Med Model. 2010 Dec;7(1):1–44.

99. Hiriart M, Aguilar-Bryan L. Channel regulation of glucose sensing in the pancreatic β-cell. American Journal of Physiology-Endocrinology and Metabolism [Internet]. 2008 Dec 1 [cited 2023 Dec 29]; Available from: https://0-journals.physiology.org.wam.seals.ac.za/doi/10.1152/ajpendo.90493.2008

100. Vilsbøll T, Holst JJ. Incretins, insulin secretion and Type 2 diabetes mellitus. Diabetologia. 2004 Mar;47(3):357–66.

101. Holst JJ, Gromada J. Role of incretin hormones in the regulation of insulin secretion in diabetic and nondiabetic humans. American Journal of Physiology-Endocrinology and Metabolism. 2004 Aug;287(2):E199–206.

102. Neidert LE, Mobley CB, Kephart WC, Roberts MD, Kluess HA. The serine protease, dipeptidyl peptidase IV as a myokine: dietary protein and exercise mimetics as a stimulus for transcription and release. Physiological Reports. 2016 Jun 1;4(12):e12827.

103. Lamers D, Famulla S, Wronkowitz N, Hartwig S, Lehr S, Ouwens DM, et al. Dipeptidyl Peptidase 4 Is a Novel Adipokine Potentially Linking Obesity to the Metabolic Syndrome. Diabetes. 2011 Jun 20;60(7):1917–25.

104. Sebastián-Martín A, Sánchez BG, Mora-Rodríguez JM, Bort A, Díaz-Laviada I. Role of Dipeptidyl Peptidase-4 (DPP4) on COVID-19 Physiopathology. Biomedicines. 2022 Aug;10(8):2026.

105. Richter B, Bandeira-Echtler E, Bergerhoff K, Lerch C. Emerging role of dipeptidyl peptidase-4 inhibitors in the management of type 2 diabetes. Vasc Health Risk Manag. 2008 Aug;4(4):753–68.

106. Röhrborn D, Eckel J, Sell H. Shedding of dipeptidyl peptidase 4 is mediated by metalloproteases and up-regulated by hypoxia in human adipocytes and smooth muscle cells. FEBS Letters. 2014 Nov 3;588(21):3870–7.

107. Raschke S, Eckardt K, Holven KB, Jensen J, Eckel J. Identification and Validation of Novel Contraction-Regulated Myokines Released from Primary Human Skeletal Muscle Cells. PLOS ONE. 2013 Apr 24;8(4):e62008.

108. Peck KM, Scobey T, Swanstrom J, Jensen KL, Burch CL, Baric RS, et al. Permissivity of Dipeptidyl Peptidase 4 Orthologs to Middle East Respiratory Syndrome Coronavirus Is Governed by Glycosylation and Other Complex Determinants. Journal of Virology. 2017 Sep 12;91(19):10.1128/jvi.00534-17.

109. Gęca T, Wojtowicz K, Guzik P, Góra T. Increased Risk of COVID-19 in Patients with Diabetes Mellitus—Current Challenges in Pathophysiology, Treatment and Prevention. International Journal of Environmental Research and Public Health. 2022 Jan;19(11):6555.

110. Kelesidis T, Mantzoros CS. Cross-talk between SARS-CoV-2 infection and the insulin/IGF signaling pathway: Implications for metabolic diseases in COVID-19 and for post-acute sequelae of SARS-CoV-2 infection. Metabolism. 2022 Sep 1;134:155267.

111. Liu F, Long X, Zhang B, Zhang W, Chen X, Zhang Z. ACE2 Expression in Pancreas May Cause Pancreatic Damage After SARS-CoV-2 Infection. Clinical Gastroenterology and Hepatology. 2020 Aug 1;18(9):2128-2130.e2.

112. Müller JA, Groß R, Conzelmann C, Krüger J, Merle U, Steinhart J, et al. SARS-CoV-2 infects and replicates in cells of the human endocrine and exocrine pancreas. Nat Metab. 2021 Feb;3(2):149–65.

113. Morris A. Effects of pancreatic SARS-CoV-2 infection identified. Nat Rev Endocrinol. 2021 Apr;17(4):192–192.

114. Qadir MMF, Bhondeley M, Beatty W, Gaupp DD, Doyle-Meyers LA, Fischer T, et al. SARS-CoV-2 infection of the pancreas promotes thrombofibrosis and is associated with new-onset diabetes. JCI Insight. 2021 Aug 23;6(16):e151551.

115. Wagenknecht LE, Roseman JM, Herman WH. Increased Incidence of Insulin-Dependent Diabetes Mellitus Following an Epidemic of Coxsackievirus B5. American Journal of Epidemiology. 1991 May 15;133(10):1024–31.

116. Sioofy-Khojine AB, Lehtonen J, Nurminen N, Laitinen OH, Oikarinen S, Huhtala H, et al. Coxsackievirus B1 infections are associated with the initiation of insulin-driven autoimmunity that progresses to type 1 diabetes. Diabetologia. 2018 May 1;61(5):1193–202.

117. Ducluzeau PH, Perretti N, Laville M, Andreelli F, Vega N, Riou JP, et al. Regulation by Insulin of Gene Expression in Human Skeletal Muscle and Adipose Tissue: Evidence for Specific Defects in Type 2 Diabetes. Diabetes. 2001 May 1;50(5):1134–42.

118. Sibiya N. The effects of oxidovanadium complexes on glucose metabolism in liver and skeletal muscle cell lines. 2014; Available from: https://www.semanticscholar.org/paper/The-effects-of-oxidovanadium-complexes-on-glucose-Sibiya/1d2701fa785e4c499132c38c31fdaa959bddbc5c

119. Lizcano JM, Alessi DR. The insulin signalling pathway. Curr Biol. 2002 Apr 2;12(7):R236-238.

120. Saltiel AR, Pessin JE. Insulin Signaling in Microdomains of the Plasma Membrane. Traffic. 2003 Sep;4(11):711–6.

121. Chang L, Chiang SH, Saltiel AR. Insulin Signaling and the Regulation of Glucose Transport. Mol Med. 2004 Jul;10(7):65–71.

122. van Gerwen J, Shun-Shion AS, Fazakerley DJ. Insulin signalling and GLUT4 trafficking in insulin resistance. Biochemical Society Transactions. 2023 May 30;51(3):1057–69.

123. Fazakerley DJ, Minard AY, Krycer JR, Thomas KC, Stöckli J, Harney DJ, et al. Mitochondrial oxidative stress causes insulin resistance without disrupting oxidative phosphorylation. Journal of Biological Chemistry. 2018 May 11;293(19):7315–28.

124. Luo J, Sobkiw CL, Hirshman MF, Logsdon MN, Li TQ, Goodyear LJ, et al. Loss of class IA PI3K signaling in muscle leads to impaired muscle growth, insulin response, and hyperlipidemia. Cell Metabolism. 2006 May 1;3(5):355–66.

125. Sechi LA, Griffin CA, Giacchetti G, Zingaro L, Catena C, Bartoli E, et al. Abnormalities of Insulin Receptors in Spontaneously Hypertensive Rats. Hypertension. 1996 Apr;27(4):955–61.

126. Shin J, Toyoda S, Nishitani S, Onodera T, Fukuda S, Kita S, et al. SARS-CoV-2 infection impairs the insulin/IGF signaling pathway in the lung, liver, adipose tissue, and pancreatic cells via IRF1. Metabolism. 2022 Aug 1;133:155236.

127. Petersen MC, Shulman GI. Mechanisms of Insulin Action and Insulin Resistance. Physiol Rev. 2018 Oct 1;98(4):2133–223.

128. Wilcox G. Insulin and insulin resistance. Clin Biochem Rev. 2005 May;26(2):19–39.

129. Montgomery MK, Turner N. Mitochondrial dysfunction and insulin resistance: an update. Endocr Connect. 2014 Dec 9;4(1):R1–15.

130. Teff KL, Rickels MR, Grudziak J, Fuller C, Nguyen HL, Rickels K. Antipsychotic-induced insulin resistance and postprandial hormonal dysregulation independent of weight gain or psychiatric disease. Diabetes. 2013 Sep;62(9):3232–40.

131. Han XX, Bonen A. Epinephrine translocates GLUT-4 but inhibits insulin-stimulated glucose transport in rat muscle. American Journal of Physiology-Endocrinology and Metabolism. 1998 Apr;274(4):E700–7.

132. Stöckli J, Fazakerley DJ, James DE. GLUT4 exocytosis. Journal of Cell Science. 2011 Dec 15;124(24):4147.

133. Wong CY, Al-Salami H, Dass CR. C2C12 cell model: its role in understanding of insulin resistance at the molecular level and pharmaceutical development at the preclinical stage. J Pharm Pharmacol. 2020 Dec;72(12):1667–93.

134. Henriksen EJ, Diamond-Stanic MK, Marchionne EM. Oxidative Stress and the Etiology of Insulin Resistance and Type 2 Diabetes. Free Radic Biol Med. 2011 Sep 1;51(5):993–9.

135. Georgescu SR, Mitran CI, Mitran MI, Caruntu C, Sarbu MI, Matei C, et al. New Insights in the Pathogenesis of HPV Infection and the Associated Carcinogenic Processes: The Role of Chronic Inflammation and Oxidative Stress. Journal of Immunology Research. 2018;2018(1):5315816.

136. Ito F, Sono Y, Ito T. Measurement and Clinical Significance of Lipid Peroxidation as a Biomarker of Oxidative Stress: Oxidative Stress in Diabetes, Atherosclerosis, and Chronic Inflammation. Antioxidants (Basel). 2019 Mar 25;8(3):72.

137. Ding H, Heng B, He W, Shi L, Lai C, Xiao L, et al. Chronic reactive oxygen species exposure inhibits glucose uptake and causes insulin resistance in C2C12 myotubes. Biochemical and Biophysical Research Communications. 2016 Sep 16;478(2):798–803.

138. Maddux BA, See W, Lawrence JC Jr, Goldfine AL, Goldfine ID, Evans JL. Protection Against Oxidative Stress—Induced Insulin Resistance in Rat L6 Muscle Cells by Micromolar Concentrations of α-Lipoic Acid. Diabetes. 2001 Feb 1;50(2):404–10.

139. Turner N, Kowalski GM, Leslie SJ, Risis S, Yang C, Lee-Young RS, et al. Distinct patterns of tissue-specific lipid accumulation during the induction of insulin resistance in mice by high-fat feeding. Diabetologia. 2013 Jul;56(7):1638–48.

140. Chueire VB, Muscelli E. Effect of free fatty acids on insulin secretion, insulin sensitivity and incretin effect – a narrative review. Arch Endocrinol Metab. 2020 Dec 15;65(1):24–31.

141. Cusi K. The Role of Adipose Tissue and Lipotoxicity in the Pathogenesis of Type 2 Diabetes. Curr Diab Rep. 2010 Aug 1;10(4):306–15.

142. Giacca A, Xiao C, Oprescu AI, Carpentier AC, Lewis GF. Lipid-induced pancreatic β-cell dysfunction: focus on in vivo studies. American Journal of Physiology-Endocrinology and Metabolism. 2011 Feb;300(2):E255–62.

143. Yu C, Chen Y, Cline GW, Zhang D, Zong H, Wang Y, et al. Mechanism by Which Fatty Acids Inhibit Insulin Activation of Insulin Receptor Substrate-1 (IRS-1)-associated Phosphatidylinositol 3-Kinase Activity in Muscle *. Journal of Biological Chemistry. 2002 Dec 27;277(52):50230–6.

144. Kruszynska YT, Worrall DS, Ofrecio J, Frias JP, Macaraeg G, Olefsky JM. Fatty Acid-Induced Insulin Resistance: Decreased Muscle PI3K Activation But Unchanged Akt Phosphorylation. The Journal of Clinical Endocrinology & Metabolism. 2002 Jan 1;87(1):226–34.

145. Hurrle S, Hsu WH. The etiology of oxidative stress in insulin resistance. Biomedical Journal. 2017 Oct 1;40(5):257–62.

146. Ayala A, Muñoz MF, Argüelles S. Lipid Peroxidation: Production, Metabolism, and Signaling Mechanisms of Malondialdehyde and 4-Hydroxy-2-Nonenal. Oxid Med Cell Longev. 2014;2014:360438.

147. Esterbauer H, Eckl P, Ortner A. Possible mutagens derived from lipids and lipid precursors. Mutation Research/Reviews in Genetic Toxicology. 1990 May 1;238(3):223–33.

148. Caturano A, D'Angelo M, Mormone A, Russo V, Mollica MP, Salvatore T, et al. Oxidative Stress in Type 2 Diabetes: Impacts from Pathogenesis to Lifestyle Modifications. Curr Issues Mol Biol. 2023 Aug 12;45(8):6651–66.

149. Georgieva E, Ananiev J, Yovchev Y, Arabadzhiev G, Abrashev H, Abrasheva D, et al. COVID-19 Complications: Oxidative Stress, Inflammation, and Mitochondrial and Endothelial Dysfunction. Int J Mol Sci. 2023 Oct 4;24(19):14876.

150. Protzer U, Maini MK, Knolle PA. Living in the liver: hepatic infections. Nat Rev Immunol. 2012 Mar;12(3):201–13.

151. MALHI H, GUICCIARDI ME, GORES GJ. Hepatocyte Death: A Clear and Present Danger. Physiol Rev. 2010 Jul;90(3):1165–94.

152. Hanley B, Naresh KN, Roufosse C, Nicholson AG, Weir J, Cooke GS, et al. Histopathological findings and viral tropism in UK patients with severe fatal COVID-19: a post-mortem study. The Lancet Microbe. 2020 Oct 1;1(6):e245–53.

153. Barreto EA, Cruz AS, Veras FP, Martins R, Bernardelli RS, Paiva IM, et al. COVID-19-related hyperglycemia is associated with infection of hepatocytes and stimulation of gluconeogenesis. Proc Natl Acad Sci U S A. 2023 May 23;120(21):e2217119120.

154. Mercado-Gómez M, Prieto-Fernández E, Goikoetxea-Usandizaga N, Vila-Vecilla L, Azkargorta M, Bravo M, et al. The spike of SARS-CoV-2 promotes metabolic rewiring in hepatocytes. Commun Biol. 2022 Aug 17;5(1):1–13.

155. Icard P, Lincet H, Wu Z, Coquerel A, Forgez P, Alifano M, et al. The key role of Warburg effect in SARS-CoV-2 replication and associated inflammatory response. Biochimie. 2021 Jan;180:169–77.

156. Codo AC, Davanzo GG, Monteiro L de B, de Souza GF, Muraro SP, Virgilio-da-Silva JV, et al. Elevated Glucose Levels Favor SARS-CoV-2 Infection and Monocyte Response through a HIF-1α/Glycolysis-Dependent Axis. Cell Metab. 2020 Sep 1;32(3):437-446.e5.

157. Kumar V. How could we forget immunometabolism in SARS-CoV2 infection or COVID-19? Int Rev Immunol. 2021;40(1–2):72–107.

158. Santos AF, Póvoa P, Paixão P, Mendonça A, Taborda-Barata L. Changes in Glycolytic Pathway in SARS-COV 2 Infection and Their Importance in Understanding the Severity of COVID-19. Frontiers in Chemistry [Internet]. 2021 [cited 2024 Jan 26];9. Available from: https://www.frontiersin.org/articles/10.3389/fchem.2021.685196

159. Chen XY, Huang MY, Xiao Z wei, Yang S, Chen XQ. Lactate dehydrogenase elevations is associated with severity of COVID-19: a meta-analysis. Critical Care. 2020 Jul 24;24(1):459.

160. Choi CS, Kim YB, Lee FN, Zabolotny JM, Kahn BB, Youn JH. Lactate induces insulin resistance in skeletal muscle by suppressing glycolysis and impairing insulin signaling. Am J Physiol Endocrinol Metab. 2002 Aug;283(2):E233-240.

161. Alfano G, Fontana F, Mori G, Giaroni F, Ferrari A, Giovanella S, et al. Acid base disorders in patients with COVID-19. Int Urol Nephrol. 2022 Feb;54(2):405–10.

162. Tay MZ, Poh CM, Rénia L, MacAry PA, Ng LFP. The trinity of COVID-19: immunity, inflammation and intervention. Nat Rev Immunol. 2020 Jun;20(6):363–74.

163. Pickup JC. Inflammation and Activated Innate Immunity in the Pathogenesis of Type 2 Diabetes. Diabetes Care. 2004 Mar 1;27(3):813–23.

164. Bhaskar S, Sinha A, Banach M, Mittoo S, Weissert R, Kass JS, et al. Cytokine Storm in COVID-19—Immunopathological Mechanisms, Clinical Considerations, and Therapeutic Approaches: The REPROGRAM Consortium Position Paper. Front Immunol. 2020 Jul 10;11:1648.

165. Rotter V, Nagaev I, Smith U. Interleukin-6 (IL-6) Induces Insulin Resistance in 3T3-L1 Adipocytes and Is, Like IL-8 and Tumor Necrosis Factor-α, Overexpressed in Human Fat Cells from Insulin-resistant Subjects *. Journal of Biological Chemistry. 2003 Nov 14;278(46):45777–84.

166. Chen T, Wu D, Chen H, Yan W, Yang D, Chen G, et al. Clinical characteristics of 113 deceased patients with coronavirus disease 2019: retrospective study. BMJ. 2020 Mar 26;368:m1091.

167. Queiroz MAF, Neves PFM das, Lima SS, Lopes J da C, Torres MK da S, Vallinoto IMVC, et al. Cytokine Profiles Associated With Acute COVID-19 and Long COVID-19 Syndrome. Frontiers in Cellular and Infection Microbiology [Internet]. 2022 [cited 2023 Aug 28];12. Available from: https://www.frontiersin.org/articles/10.3389/fcimb.2022.922422

168. Wellen KE, Hotamisligil GS. Inflammation, stress, and diabetes [Internet]. American Society for Clinical Investigation; 2005 [cited 2023 Apr 7]. Available from: https://www.jci.org/articles/view/25102/cite

169. Steinberg GR, Michell BJ, van Denderen BJW, Watt MJ, Carey AL, Fam BC, et al. Tumor necrosis factor α-induced skeletal muscle insulin resistance involves suppression of AMP-kinase signaling. Cell Metabolism. 2006 Dec 1;4(6):465–74.

170. Plomgaard P, Bouzakri K, Krogh-Madsen R, Mittendorfer B, Zierath JR, Pedersen BK. Tumor Necrosis Factor-α Induces Skeletal Muscle Insulin Resistance in Healthy Human Subjects via Inhibition of Akt Substrate 160 Phosphorylation. Diabetes. 2005 Oct 1;54(10):2939–45.

171. Freeman AM, Acevedo LA, Pennings N. Insulin Resistance. In: StatPearls [Internet]. Treasure Island (FL): StatPearls Publishing; 2024 [cited 2024 Dec 6]. Available from: http://www.ncbi.nlm.nih.gov/books/NBK507839/

172. de Luca C, Olefsky JM. Inflammation and insulin resistance. FEBS Lett. 2008 Jan 9;582(1):97–105.

173. Rehman K, Akash MSH. Mechanisms of inflammatory responses and development of insulin resistance: how are they interlinked? J Biomed Sci. 2016 Dec 3;23(1):87.

174. Pickup JC, Mattock MB, Chusney GD, Burt D. NIDDM as a disease of the innate immune system: association of acute-phase reactants and interleukin-6 with metabolic syndrome X. Diabetologia. 1997 Nov;40(11):1286–92.

175. Lepiller Q, Abbas W, Kumar A, Tripathy MK, Herbein G. HCMV Activates the IL-6-JAK-STAT3 Axis in HepG2 Cells and Primary Human Hepatocytes. PLOS ONE. 2013 Mar 26;8(3):e59591.

176. Santos A, Magro DO, Evangelista-Poderoso R, Saad MJA. Diabetes, obesity, and insulin resistance in COVID-19: molecular interrelationship and therapeutic implications. Diabetol Metab Syndr. 2021 Dec;13(1):1–14.

177. Burhans MS, Hagman DK, Kuzma JN, Schmidt KA, Kratz M. Contribution of adipose tissue inflammation to the development of type 2 diabetes mellitus. Compr Physiol. 2018 Dec 13;9(1):1–58.

178. Death AK, Fisher EJ, McGrath KCY, Yue DK. High glucose alters matrix metalloproteinase expression in two key vascular cells: potential impact on atherosclerosis in diabetes. Atherosclerosis. 2003 Jun 1;168(2):263–9.

179. Hemmann S, Graf J, Roderfeld M, Roeb E. Expression of MMPs and TIMPs in liver fibrosis – a systematic review with special emphasis on anti-fibrotic strategies. Journal of Hepatology. 2007 May 1;46(5):955–75.

180. Duarte S, Baber J, Fujii T, Coito AJ. Matrix metalloproteinases in liver injury, repair and fibrosis. Matrix Biology. 2015 May 1;44–46:147–56.

181. Parks WC, Wilson CL, López-Boado YS. Matrix metalloproteinases as modulators of inflammation and innate immunity. Nat Rev Immunol. 2004 Aug;4(8):617–29.

182. Nagase H. Matrix metalloproteinases. In: Zinc Metalloproteases In Health And Disease. CRC Press; 1996.

183. Uemura S, Matsushita H, Li W, Glassford AJ, Asagami T, Lee KH, et al. Diabetes Mellitus Enhances Vascular Matrix Metalloproteinase Activity. Circulation Research. 2001 Jun 22;88(12):1291–8.

184. Mclennan SV, Fisher E, Martell SY, Death AK, Williams PF, Lyons JG, et al. Effects of glucose on matrix metalloproteinase and plasmin activities in mesangial cells: Possible role in diabetic nephropathy. Kidney International. 2000 Sep 1;58:S81–7.

185. Reinboldt S, Wenzel F, Rauch BH, Hohlfeld T, Grandoch M, Fischer JW, et al. Preliminary evidence for a matrix metalloproteinase-2 (MMP-2)-dependent shedding of soluble CD40 ligand (sCD40L) from activated platelets. Platelets. 2009 Jan 1;20(6):441–4.

186. Unsworth R, Wallace S, Oliver NS, Yeung S, Kshirsagar A, Naidu H, et al. New-Onset Type 1 Diabetes in Children During COVID-19: Multicenter Regional Findings in the U.K. Diabetes Care. 2020 Nov;43(11):e170–1.

187. Fadini GP, Morieri ML, Boscari F, Fioretto P, Maran A, Busetto L, et al. Newly-diagnosed diabetes and admission hyperglycemia predict COVID-19 severity by aggravating respiratory deterioration. Diabetes Research and Clinical Practice. 2020 Oct 1;168:108374.

188. Singh AK, Khunti K. COVID-19 and Diabetes. Annual Review of Medicine. 2022;73(1):129–47.

189. Bode B, Garrett V, Messler J, McFarland R, Crowe J, Booth R, et al. Glycemic Characteristics and Clinical Outcomes of COVID-19 Patients Hospitalized in the United States. J Diabetes Sci Technol. 2020 Jul 1;14(4):813–21.

190. Drucker DJ. Diabetes, obesity, metabolism, and SARS-CoV-2 infection: the end of the beginning. Cell Metabolism. 2021 Mar;33(3):479–98.

191. Ibrahim S, Monaco GSF, Sims EK. Not so sweet and simple: impacts of SARS-CoV-2 on the β cell. Islets. 2021 Jul 4;13(3–4):66–79.

192. Merz KE, Thurmond DC. Role of Skeletal Muscle in Insulin Resistance and Glucose Uptake. In: Comprehensive Physiology [Internet]. John Wiley & Sons, Ltd; 2020 [cited 2023 Sep 5]. p. 785–809. Available from: https://onlinelibrary.wiley.com/doi/abs/10.1002/cphy.c190029

193. Florin A, Lambert C, Sanchez C, Zappia J, Durieux N, Tieppo AM, et al. The secretome of skeletal muscle cells: A systematic review. Osteoarthritis and Cartilage Open. 2020 Jan 2;2(1):100019.

194. Chadt A, Al-Hasani H. Glucose transporters in adipose tissue, liver, and skeletal muscle in metabolic health and disease. Pflugers Arch - Eur J Physiol. 2020 Sep 1;472(9):1273–98.

195. Arzumanian VA, Kiseleva OI, Poverennaya EV. The Curious Case of the HepG2 Cell Line: 40 Years of Expertise. International Journal of Molecular Sciences. 2021 Jan;22(23):13135.

196. Sharabi K, Tavares CDJ, Rines AK, Puigserver P. Molecular Pathophysiology of Hepatic Glucose Production. Mol Aspects Med. 2015 Dec;46:21–33.

197. Kammerer S, Küpper JH. Human hepatocyte systems for in vitro toxicology analysis. Journal of Cellular Biotechnology. 2018 Jan 1;3(2):85–93.

198. Guo L, Dial S, Shi L, Branham W, Liu J, Fang JL, et al. Similarities and Differences in the Expression of Drug-Metabolizing Enzymes between Human Hepatic Cell Lines and Primary Human Hepatocytes. Drug Metab Dispos. 2011 Mar 1;39(3):528–38.

199. Pillay Y, Nagiah S, Chuturgoon A. Patulin Alters Insulin Signaling and Metabolic Flexibility in HepG2 and HEK293 Cells. Toxins. 2023 Apr;15(4):244.

200. Doostdar H, Duthie SJ, Burke MD, Melvin WT, Grant MH. The influence of culture medium composition on drug metabolising enzyme activities of the human liver derived Hep G2 cell line. FEBS Letters. 1988 Dec 5;241(1):15–8.

201. Braun P, Gingras AC. History of protein–protein interactions: From egg-white to complex networks. PROTEOMICS. 2012;12(10):1478–98.

202. Rao VS, Srinivas K, Sujini GN, Kumar GNS. Protein-Protein Interaction Detection: Methods and Analysis. International Journal of Proteomics. 2014 Feb 17;2014:1–12.

203. Nooren IMA, Thornton JM. Diversity of protein–protein interactions. The EMBO Journal. 2003 Jul 15;22(14):3486–92.

204. Vickery HB. The Origin of the Word Protein. Yale J Biol Med. 1950 May;22(5):387–93.

205. Northrup SH, Erickson HP. Kinetics of protein-protein association explained by Brownian dynamics computer simulation. Proc Natl Acad Sci U S A. 1992 Apr 15;89(8):3338–42.

206. Kozakov D, Hall DR, Xia B, Porter KA, Padhorny D, Yueh C, et al. The ClusPro web server for protein–protein docking. Nat Protoc. 2017 Feb;12(2):255–78.

207. Jones G, Jindal A, Ghani U, Kotelnikov S, Egbert M, Hashemi N, et al. Elucidation of protein function using computational docking and hotspot analysis by ClusPro and FTMap. Acta Cryst D. 2022 Jun 1;78(6):690–7.

208. Lensink MF, Brysbaert G, Nadzirin N, Velankar S, Chaleil RAG, Gerguri T, et al. Blind prediction of homo- and hetero-protein complexes: The CASP13-CAPRI experiment. Proteins: Structure, Function, and Bioinformatics. 2019;87(12):1200–21.

209. Biesiadecki BJ, Jin JP. A High-Throughput Solid-Phase Microplate Protein-Binding Assay to Investigate Interactions between Myofilament Proteins. J Biomed Biotechnol. 2011;2011:421701.

210. Mould PA. Solid Phase Assays for Studying ECM Protein–Protein Interactions. In: Extracellular Matrix Protocols [Internet]. Humana Press; 2009 [cited 2024 Dec 10]. p. 195–200. Available from: https://0-link.springer.com.wam.seals.ac.za/protocol/10.1007/978-1-59745-413-1_13

211. Mosmann T. Rapid colorimetric assay for cellular growth and survival: Application to proliferation and cytotoxicity assays. Journal of Immunological Methods. 1983 Dec 16;65(1):55–63.

212. Farooq S, Mazhar A, Haq I, Ullah N. One-Pot Multicomponent Synthesis and Bioevaluation of Tetrahydroquinoline Derivatives as Potential Antioxidants, α-Amylase Enzyme Inhibitors, Anti-Cancerous and Anti-Inflammatory Agents. Molecules. 2020 Jun 11;25.

213. van de Venter M, Roux S, Bungu LC, Louw J, Crouch NR, Grace OM, et al. Antidiabetic screening and scoring of 11 plants traditionally used in South Africa. Journal of Ethnopharmacology. 2008 Sep 2;119(1):81–6.

214. Nagiah S, Phulukdaree A, Chuturgoon A. Mitochondrial and Oxidative Stress Response in HepG2 Cells Following Acute and Prolonged Exposure to Antiretroviral Drugs. J Cell Biochem. 2015 Sep;116(9):1939–46.

215. Steenblock C, Schwarz PEH, Ludwig B, Linkermann A, Zimmet P, Kulebyakin K, et al. COVID-19 and metabolic disease: mechanisms and clinical management. Lancet Diabetes Endocrinol. 2021 Nov;9(11):786–98.

216. Ullrich S, Nitsche C. The SARS-CoV-2 main protease as drug target. Bioorganic & Medicinal Chemistry Letters. 2020 Sep 1;30(17):127377.

217. Lubinski B, Whittaker GR. Host Cell Proteases Involved in Human Respiratory Viral Infections and Their Inhibitors: A Review. Viruses. 2024 Jun;16(6):984.

218. Tan YJ, Fielding BC, Goh PY, Shen S, Tan THP, Lim SG, et al. Overexpression of 7a, a Protein Specifically Encoded by the Severe Acute Respiratory Syndrome Coronavirus, Induces Apoptosis via a Caspase-Dependent Pathway. Journal of Virology [Internet]. 2004 Dec 15 [cited 2024 Oct 25]; Available from: https://journals.asm.org/doi/10.1128/jvi.78.24.14043-14047.2004

219. Marette A, Richardson JM, Ramlal T, Balon TW, Vranic M, Pessin JE, et al. Abundance, localization, and insulin-induced translocation of glucose transporters in red and white muscle. American Journal of Physiology-Cell Physiology. 1992 Aug;263(2):C443–52.

220. Badr GA, Tang J, Ismail-Beigi F, Kern TS. Diabetes downregulates GLUT1 expression in the retina and its microvessels but not in the cerebral cortex or its microvessels. Diabetes. 2000 Jun 1;49(6):1016–21.

221. Fröjdö S, Vidal H, Pirola L. Alterations of insulin signaling in type 2 diabetes: A review of the current evidence from humans. Biochimica et Biophysica Acta (BBA) - Molecular Basis of Disease. 2009 Feb 1;1792(2):83–92.

222. Saltiel AR. Insulin signaling in health and disease. J Clin Invest [Internet]. 2021 Jan 4 [cited 2024 Nov 28];131(1). Available from: https://www.jci.org/articles/view/142241

223. Ramos PA, Lytle KA, Delivanis D, Nielsen S, LeBrasseur NK, Jensen MD. Insulin-Stimulated Muscle Glucose Uptake and Insulin Signaling in Lean and Obese Humans. The Journal of Clinical Endocrinology & Metabolism. 2021 Apr 1;106(4):1631–46.

224. Jaiswal N, Gavin MG, Quinn WJ, Luongo TS, Gelfer RG, Baur JA, et al. The role of skeletal muscle Akt in the regulation of muscle mass and glucose homeostasis. Molecular Metabolism. 2019 Oct 1;28:1–13.

225. James DE, Brown R, Navarro J, Pilch PF. Insulin-regulatable tissues express a unique insulin-sensitive glucose transport protein. Nature. 1988 May 12;333(6169):183–5.

226. Zorzano A, Sevilla L, Tomàs E, Camps M, Gumà A, Palacín M. Trafficking pathway of GLUT4 glucose transporters in muscle (review). Int J Mol Med. 1998 Sep;2(3):263–71.

227. Rea S, James DE. Moving GLUT4: the biogenesis and trafficking of GLUT4 storage vesicles. Diabetes. 1997 Nov;46(11):1667–77.

228. Evans PL, McMillin SL, Weyrauch LA, Witczak CA. Regulation of Skeletal Muscle Glucose Transport and Glucose Metabolism by Exercise Training. Nutrients. 2019 Oct 12;11(10):2432.

229. Alkhateeb H, Chabowski A, Glatz JFC, Luiken JFP, Bonen A. Two phases of palmitate-induced insulin resistance in skeletal muscle: impaired GLUT4 translocation is followed by a reduced GLUT4 intrinsic activity. American Journal of Physiology-Endocrinology and Metabolism. 2007 Sep;293(3):E783–93.

230. Garvey WT, Maianu L, Zhu JH, Hancock JA, Golichowski AM. Multiple defects in the adipocyte glucose transport system cause cellular insulin resistance in gestational diabetes. Heterogeneity in the number and a novel abnormality in subcellular localization of GLUT4 glucose transporters. Diabetes. 1993 Dec;42(12):1773–85.

231. Garvey WT, Maianu L, Zhu JH, Brechtel-Hook G, Wallace P, Baron AD. Evidence for defects in the trafficking and translocation of GLUT4 glucose transporters in skeletal muscle as a cause of human insulin resistance. J Clin Invest. 1998 Jun 1;101(11):2377–86.

232. Vannucci SJ, Nishimura H, Satoh S, Cushman SW, Holman GD, Simpson IA. Cell surface accessibility of GLUT4 glucose transporters in insulin-stimulated rat adipose cells. Modulation by isoprenaline and adenosine. Biochem J. 1992 Nov 15;288 (Pt 1)(Pt 1):325–30.

233. Maianu L, Keller SR, Garvey WT. Adipocytes Exhibit Abnormal Subcellular Distribution and Translocation of Vesicles Containing Glucose Transporter 4 and Insulin-Regulated Aminopeptidase in Type 2 Diabetes Mellitus: Implications Regarding Defects in Vesicle Trafficking. The Journal of Clinical Endocrinology & Metabolism. 2001 Nov 1;86(11):5450–6.

234. Xiong W, Jordens I, Gonzalez E, McGraw TE. GLUT4 Is Sorted to Vesicles Whose Accumulation Beneath and Insertion into the Plasma Membrane Are Differentially Regulated by Insulin and Selectively Affected by Insulin Resistance. MBoC. 2010 Apr 15;21(8):1375–86.

235. Lizunov VA, Lee JP, Skarulis MC, Zimmerberg J, Cushman SW, Stenkula KG. Impaired Tethering and Fusion of GLUT4 Vesicles in Insulin-Resistant Human Adipose Cells. Diabetes. 2013 Aug 15;62(9):3114–9.

236. Gao L, Chen J, Gao J, Wang H, Xiong W. Super-resolution microscopy reveals the insulin-resistance-regulated reorganization of GLUT4 on plasma membranes. Journal of Cell Science. 2017 Jan 15;130(2):396–405.

237. Scialò F, Fernández-Ayala DJ, Sanz A. Role of Mitochondrial Reverse Electron Transport in ROS Signaling: Potential Roles in Health and Disease. Front Physiol [Internet]. 2017 Jun 27 [cited 2024 Nov 28];8. Available from: https://www.frontiersin.org/journals/physiology/articles/10.3389/fphys.2017.00428/full

238. Sun B, Chen H, Xue J, Li P, Fu X. The role of GLUT2 in glucose metabolism in multiple organs and tissues. Mol Biol Rep. 2023 Aug 1;50(8):6963–74.

239. Thorens B. GLUT2, glucose sensing and glucose homeostasis. Diabetologia. 2015 Feb 1;58(2):221–32.

240. Szablewski L. Blood Glucose Levels. BoD – Books on Demand; 2020. 140 p.

241. James DE, Stöckli J, Birnbaum MJ. The aetiology and molecular landscape of insulin resistance. Nat Rev Mol Cell Biol. 2021 Nov;22(11):751–71.

242. Belfiore A, Frasca F, Pandini G, Sciacca L, Vigneri R. Insulin Receptor Isoforms and Insulin Receptor/Insulin-Like Growth Factor Receptor Hybrids in Physiology and Disease. Endocrine Reviews. 2009 Oct 1;30(6):586–623.

243. DeFelippis MR, Chance RE, Frank BH. Insulin Self-Association and the Relationship to Pharmacokinetics and Pharmacodynamics. CRT [Internet]. 2001 [cited 2024 Nov 21];18(2). Available from: https://www.dl.begellhouse.com/journals/3667c4ae6e8fd136,3481482215006254,242b58293466d539.html

244. Busto-Moner L, Feng CJ, Antoszewski A, Tokmakoff A, Dinner AR. Structural Ensemble of the Insulin Monomer. Biochemistry. 2021 Oct 26;60(42):3125–36.

245. Pedersen BK, Steensberg A, Schjerling P. Muscle-derived interleukin-6: possible biological effects. J Physiol. 2001 Oct 15;536(Pt 2):329–37.

246. Carlquist JF, Edelman L, Bennion DW, Anderson JL. Cytomegalovirus Induction of Interleukin-6 in Lung Fibroblasts Occurs Independently of Active Infection and Involves a G Protein and the Transcription Factor, NF-κB. The Journal of Infectious Diseases. 1999 May 1;179(5):1094–100.

247. Spengler U. Liver Disease Associated with Non-Hepatitis Viruses. Encyclopedia of Gastroenterology. 2019 Nov 1;363.

248. Wronkowitz N, Görgens SW, Romacho T, Villalobos LA, Sánchez-Ferrer CF, Peiró C, et al. Soluble DPP4 induces inflammation and proliferation of human smooth muscle cells via protease-activated receptor 2. Biochimica et Biophysica Acta (BBA) - Molecular Basis of Disease. 2014 Sep 1;1842(9):1613–21.

249. Ehlting C, Wolf SD, Bode JG. Acute-phase protein synthesis: a key feature of innate immune functions of the liver. Biological Chemistry. 2021 Aug 1;402(9):1129–45.

250. Nedachi T, Kanzaki M. Regulation of glucose transporters by insulin and extracellular glucose in C2C12 myotubes. Am J Physiol Endocrinol Metab. 2006 Oct;291(4):E817-828.

251. Steinberg GR, Michell BJ, van Denderen BJW, Watt MJ, Carey AL, Fam BC, et al. Tumor necrosis factor α-induced skeletal muscle insulin resistance involves suppression of AMP-kinase signaling. Cell Metabolism. 2006 Dec 1;4(6):465–74.

252. Huang SY, Zou X. Advances and Challenges in Protein-Ligand Docking. Int J Mol Sci. 2010 Aug 18;11(8):3016–34.

APPENDICES

Appendix 1: Abstract of a peer-reviewed article published in the Multidisciplinary Digital Publishing Institute Journals (MDPI)

ISP *pathophysiology*

MDPI

Review

COVID-19-Induced Diabetes Mellitus: Comprehensive Cellular and Molecular Mechanistic Insights

Praise Tatenda Nhau [1], Mlindeli Gamede [2] and Ntethelelo Sibiya [1,*]

[1] Pharmacology Division, Faculty of Pharmacy, Rhodes University, Makhanda 6139, South Africa; tatenhau@gmail.com
[2] Human Physiology Department, University of Pretoria, Pretoria 0028, South Africa; mlindeli.gamede@up.ac.za
* Correspondence: n.sibiya@ru.ac.za

Abstract: Despite evidence demonstrating the risks of developing diabetes mellitus because of SARS-CoV-2, there is, however, insufficient scientific data available to elucidate the relationship between diabetes mellitus and COVID-19. Research indicates that SARS-CoV-2 infection is associated with persistent damage to organ systems due to the systemic inflammatory response. Since COVID-19 is known to induce these conditions, further investigation is necessary to fully understand its long-term effects on human health. Consequently, it is essential to consider the effect of the COVID-19 pandemic when predicting the prevalence of diabetes mellitus in the future, especially since the incidence of diabetes mellitus was already on the rise before the pandemic. Additional research is required to fully comprehend the impact of SARS-CoV-2 infection on glucose tolerance and insulin sensitivity. Therefore, this article delves deeper into the current literature and links the perceived relationship between SARS-CoV-2 and diabetes. In addition, the article highlights the necessity for further research to fully grasp the mechanisms that SARS-CoV-2 utilises to induce new-onset diabetes. Where understanding and consensus are reached, therapeutic interventions to prevent the onset of diabetes could be proposed. Lastly, we propose advocating for the regular screening of diabetes and pre-diabetes, particularly for the high-risk population with a history of COVID-19 infection.

Appendix 2: Certificate of participation for poster presentation at the FIP Conference, Cape Town, September 1-5, 2024

CERTIFICATE OF POSTER PRESENTATION

82ND FIP WORLD CONGRESS OF PHARMACY AND PHARMACEUTICAL SCIENCES

CAPE TOWN, SOUTH AFRICA
1-4 SEPTEMBER 2024

fip CAPE TOWN 2024 FIP WORLD CONGRESS 1-4 September

THE INTERNATIONAL PHARMACEUTICAL FEDERATION (FIP) HEREBY DECLARES THAT

Ms Praise Tatenda Nhau

HAS PRESENTED THE FOLLOWING ABSTRACT

"HMI-036 - Investigating the effects of COVID-19 main protease on glucose handling in C2C12 skeletal muscle cell lines and hepatic cell lines, in vitro"

AS A POSTER PRESENTATION DURING THE 82ND FIP WORLD CONGRESS

Paul Sinclair
President
International Pharmaceutical Federation (FIP)

Mariet Eksteen

Dr Mariet Eksteen
Professional Development and Support
Pharmaceutical Society of South Africa (PSSA)

Appendix 3: Certificate awarded for the oral presentation of research findings at the Postgraduate Conference 2024, showcasing original contributions, held at Rhodes University on from 13-14 September 2024.

CERTIFICATE

OF PRESENTATION

This is to proudly acknowledge and honour

Tatenda Nhau

for presenting at the 6th Annual

Rhodes University Postgraduate Conference

Building Bridges: Unleashing the Potential of Scholarship

13-14 September 2024

Professor Sybert Mutereko
Director: Centre for Postgraduate Studies

Dr Nomakwezi Mzilikazi
DVC: Research, Innovation & Strategic Partnerships

CPGS

Appendix 5: The poster presentation from the Rhodes University Annual Research Day at Eden Groove Red from 21-22nd of November 2024

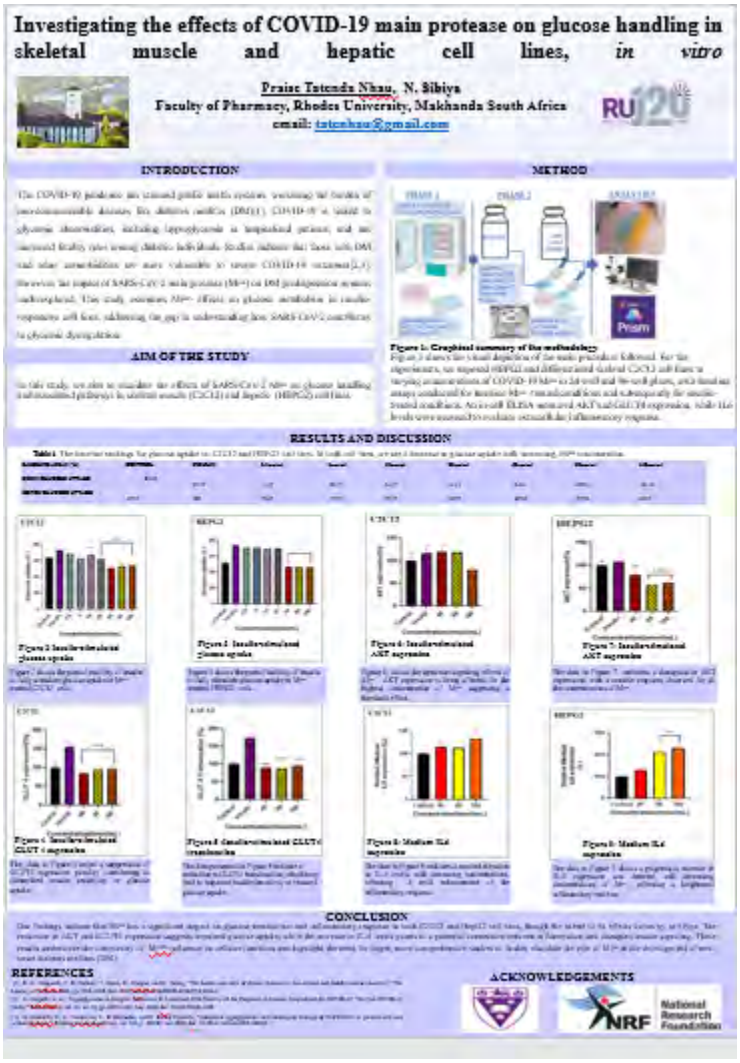

Appendix 6: Certificate of participation for the oral presentation of my results during the 56th Annual Conference of South African Society for Basic and Clinical Pharmacology at Rhodes University, 24-27 August 2023.

South African Society for Basic and Clinical Pharmacology

Certificate of Participation

This is to confirm that

Ms Tatenda Nhau

Has attended the 2023 Conference
of
The South African Society for Basic and Clinical Pharmacology
at Rhodes University
on the 24th - 27th August 2023

(accredited for 18 CPD Points)

56th ANNUAL CONFERENCE

"Pharmacology celebrating resilience: Current and Future strategies"

Prof Mamza Mothibe
Chairperson: 2023 Organising Committee

Ms Tanusha Dukhan
Secretary: 2023 Organising Committee

Appendix 7: Abstract for a presentation that was presented during the faculty of Pharmacy postgraduate research day at Rhodes University on the 20th of October 2023.

Tatenda Nhau

INVESTIGATING THE EFFECTS OF COVID-19 MAIN PROTEASE ON SKELETAL MUSCLE CELL LINES: RELATIONSHIP BETWEEN PROTEASE CONCENTRATION AND GLUCOSE UPTAKE

Tatenda Nhau, Dr. Nsithelelo Sibya

Division of Pharmacology, Faculty of Pharmacy, Rhodes University, South Africa

E-mail-address tnnhau@gmail.com

Background: The SARS-CoV-2 virus has affected various organ systems in the body and thus has raised concerns regarding its long-term impact. Skeletal muscle cells play an important role in maintaining glucose homeostasis. Insulin resistance throughout the body is driven by skeletal muscle. It is sufficient to restore whole -body glucose balance by resolving insulin resistance in skeletal muscle alone. It becomes crucial to understand the effects of viral proteins, such as the main protease (Mpro), on skeletal muscles to enable us to comprehend any disease pathogenesis that, may result. In this study, we aim to elucidate the effects of COVID-19 Mpro on skeletal muscle cell lines and examine the association between protease activity and glucose handling.

Methods: To address this knowledge gap, we exposed differentiated and non-differentiated skeletal muscle cell (C2C12) lines to varying concentrations of COVID-19 Mpro in 24 well plates. After 24 hours of exposure, the glucose readings were measured. The cells were then left for another 24 hours and then the media glucose readings were taken.

Results: Our results revealed a dose-dependent relationship between COVID-19 Mpro concentration and glucose detection within skeletal muscle cells. The higher the concentration of COVID-19 Mpro, the higher the glucose levels detected in the cell culture medium. Interestingly, the highest concentration of the Mpro revealed an increase in glucose level than the initial media concentration. This finding suggests a potential disruption of glucose metabolism pathways induced by the viral protease. Further investigations are required to elucidate the underlying mechanisms responsible for these results and evaluate the subsequent effects such as insulin resistance.

Conclusion: In conclusion, our study highlights the effects of COVID-19 Mpro on skeletal muscle cell lines and reveals the possibility of SARS-CoV-2-induced skeletal muscle complications. More research needs to be conducted to elucidate if any insulin resistance has been induced.